



Analytical and Numerical Investigation of Detachable Short Links with Flush and Extended-End Plate Connections

Candidate name: Lourey May Saflor

Supervisors: Prof. Ph.D. Raffaele Landolfo, Asst. Prof. Ph.D Mario D'Aniello

Co-Supervisor: Engr. Mariana Zimbru



Thesis submitted in partial fulfilment of the requirements for the degree SUSCOS_M European Master in Sustainable Constructions under natural hazards and catastrophic events

University of Naples “Federico II”

Date: January 2018

STATEMENT OF THESIS APPROVAL

This thesis prepared by **Lourey May Saflor**, entitled “**Analytical and Numerical Investigation of Detachable Short Links with Flush and Extended-End Plate Connections**”, is approved in partial fulfilment of the requirements for the degree of Master of Science by the following faculty members who served as the supervisory committee chair and members.

_____, Chair _____
Date approved _____

_____, Member _____
Date approved _____

_____, Member _____
Date approved _____

Student's signature _____

Date of submission _____

ABSTRACT

Along with the increasing utilization of steel in -capacity design of structures, an eccentrically-braced frame (EBF) is one of the structural typologies introduced with links acting in bending and/or shear to resist horizontal forces. With efficiency considerations in post-seismic repair of structures, detachable seismic links have also been introduced. With these devices, only the links need to be replaced while the other members continue to be structurally appropriate to function.

Studies have shown that there is significant development of axial force in links, but they are not considered in established design procedures. Considering this gap, this parametric study aims to achieve a more thorough grasp of shear overstrength and axial force as influenced by different parameters such as length ratio, strength of connection, stiffness, and boundary conditions.

Twenty-five flush-end plate (FEP) and 15 extended-end plate (EEP) connections for short links are designed using the component method until Method 1 of link verifications are satisfied. The same configurations are also verified according to Methods 2 and 3. Numerical analyses are performed on the 40 models using FE software Abaqus 6.14 considering two boundary conditions: with fully rigid restraints and with deformable springs.

From the analytical perspective, FEP connections have design limitations and cannot be used for all length ratios of HEB profiles, nor for $0.75e_s$ and e_s of HEA profiles. On the other hand, EEP connections have a wider range of application. For all analyses of assemblies performed, the values of shear overstrength at 0.08 rad link rotation are consistently close to 1.5 (1.4 to 1.66). The shear overstrength is also observed to decrease along with the increase of profile depth and/or length ratio. Moreover, wide-flange profiles have higher shear overstrength than narrow-flange profiles.

In terms of axial force, there are also several parameters that affect the behavior of its development. The imposed boundary conditions that represent the stiffness of the frame has significant effect on the level of axial forces, with higher forces for fully rigid BC and lower values for deformable springs. Short length ratio, low strength of connection, and high stiffness have been observed to affect the level catenary action in links, resulting to large compressive arches and lower tensile force (if the tension zone is reached). Lastly, tensile forces are found to be more detrimental than compressive forces in terms of bending resistance of the link-connection assembly.

TABLE OF CONTENTS

Abstract	2
Table of Contents	3
Acknowledgments	4
Chapter 1. Introduction	5
1.1 Motivation.....	5
1.2 Objectives.....	8
1.3 Scope and Limitations.....	9
Chapter 2. State of the Art	10
Chapter 3. Analytical Background	22
3.1 Component method according to Eurocode 1993 Part 1-8.....	22
3.1.1 Joint classification.....	22
3.1.2 Basis of component method.....	24
3.1.3 Characterization of the components.....	24
3.1.4 Assembly of the components.....	25
3.1.5 Resistance of the joint.....	25
3.1.6 Rotational stiffness of the joint.....	26
3.1.7 T-stub behavior of an end plate in bending.....	27
3.2 Analytical methods to verify resistance of link connections	31
3.3 Calculation of design forces on links.....	33
3.4 Evaluation of the axial and flexural stiffness of the frame.....	34
Chapter 4. The Numerical Model Assumptions and Validation	37
Chapter 5. Parametric Study	49
5.1 Investigation on the Flush-end plate connections.....	51
5.1.1 Analytical Analysis.....	51
5.1.2 Numerical Analysis.....	58
5.2 Investigation on the Extended-end plate connections.....	76
5.2.1 Analytical Analysis.....	76
5.2.2 Numerical Analysis.....	80
Chapter 6. Final Conclusions	90
References	92

ACKNOWLEDGMENTS

It is with high respect and appreciation that I acknowledge my supervisor, Asst. Professor Mario D'ANIELLO, for his guidance, support, and encouragement that enabled me to complete this master thesis. Also, this wouldn't be possible without the continuous supervision of Engr. Mariana ZIMBRU. I would like to thank her for sharing her time and knowledge that helped me in learning the software, understanding the principles, and solving the problems I encountered during my study period.

I extend my gratitude to Professor Raffaele LANDOLFO and Professor Federico MAZZOLANI for accepting us three SUSCOS_M students in the Department of Structures for Engineering at the University of Naples "Federico II".

To the members of the department especially to Engr. Roberto TARTAGLIA, thank you for making me feel welcomed during my stay, and for your contribution to my work.

I also offer my appreciation to the SUSCOS_M coordinators – Professor František WALD, Professor Raffaele LANDOLFO, Professor Dan DUBINA, Professor Jean-Pierre JASPART, and Professor Luis Simões DA SILVA for arranging this course, and for all other professors who shared their knowledge and expertise to us. It is truly an honour to learn under your distinguished names.

A vital component of the time I spent here in Europe is spent with my SUSCOS_M colleagues and I will be forever grateful for having the opportunity to be friends with them during our three semesters together. The bond we have truly spans across continents and cultures and I appreciate how my world perspectives have broadened.

I would like to thank the European Commission and Erasmus Mundus Organization for placing high importance on continuous learning and global integration, and for providing me an opportunity to study under a full scholarship.

I am also deeply grateful for my family and friends in the Philippines, for their unwavering support and words of encouragement that truly know no distance; and for my friends here in Naples for being with me during this challenging period.

Above all, I offer my praise to the Divine Almighty for His blessings and guidance.

CHAPTER I. INTRODUCTION

1. 1 Motivation

Earthquakes pose a great risk to lives and properties. It is a challenge commonly faced by countries especially those located in the Pacific Ring of Fire. In 2011, an earthquake in Japan caused an economic damage of 201 billion USD while the one that occurred in Szechuan, China in 2007 had more than 87,500 fatalities. These events, along with other earthquakes worldwide, fuel further advancement in seismic engineering. In Europe, the development of seismic codes started in 1980s and since then, provisions are made to protect human lives and limit the damage to structures.

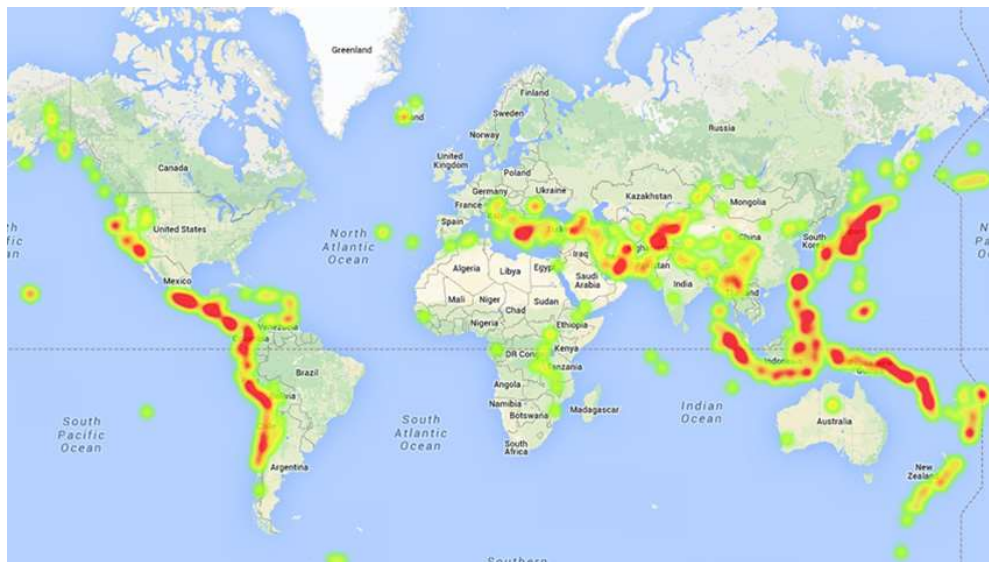


Figure 1. Seismic map of the world [28]

The main principle used in the seismic design of structures is capacity design. This principle allows the design of dissipative members, where the energy dissipation will be concentrated during a seismic event, while the non-dissipative members are protected from failure by providing them with a level of over-strength such that they can resist the maximum force developed by the plastification in the dissipative zones.

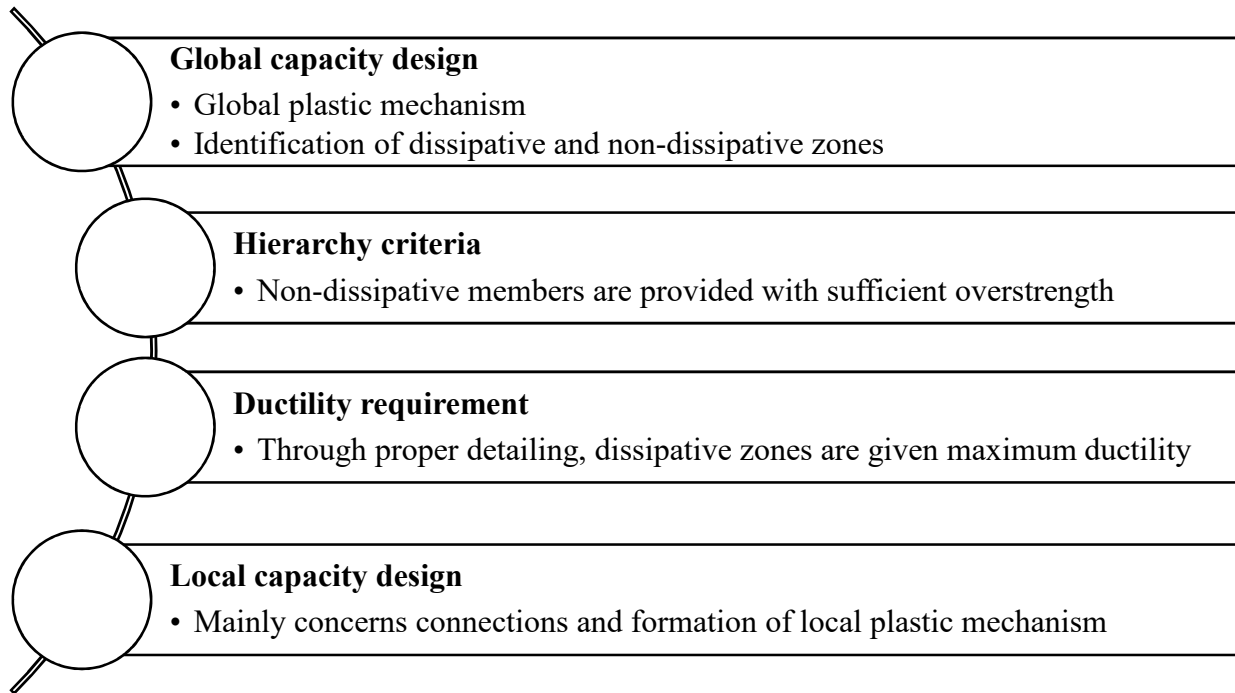


Figure 2. Capacity design principles

With the development of earthquake-resistant design, steel in structures is becoming increasingly employed. Experiences from the past earthquakes have demonstrated that steel structures exhibit high performances even in the case of strong ground motion. An eccentrically-braced frame (EBF) is one of the structural typologies for steel building where horizontal forces are resisted by seismic links acting in bending and/or shear. The idea of EBF systems originated in Japan with the aim of designing a structure with both high elastic stiffness and high energy dissipation during seismic events. Essentially, it combines the features of a moment frame and a concentrically braced frame while minimizing their disadvantages. In contrast with the conventional diagonal bracing in which the centerline of the bracing intersects with the center of beam-column joints, eccentric braces are placed with an off-set from the joint center. The links are the dissipative elements and therefore serve as the fuse of the structure. Energy is dissipated through plastic bending or plastic shear mechanisms before failure of the connections and the connected members (yielding or buckling of beams, columns, and bracings).

Shown in *Fig.3* are some of the configurations of an EBF system, with their expected plastic mechanisms. The segments in the frame marked by *e* are the links.

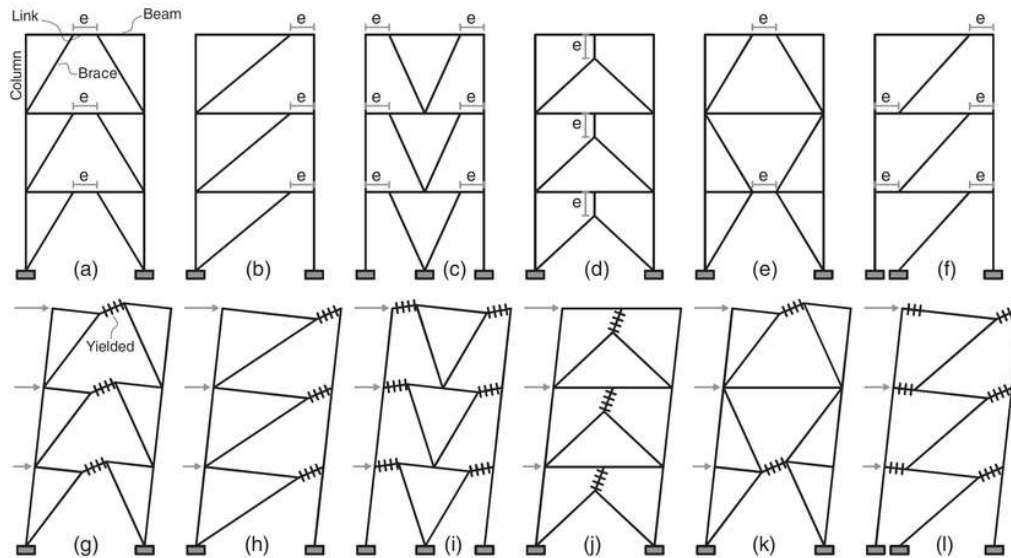


Figure 3. Different configurations of eccentrically braced frame (EBF) [1]

Links are classified into three categories, according to the plastic mechanism:

- (i) Short links – yield through shear plastic mechanism and dissipate energy through cyclic plastic deformation along with some hardening
- (ii) Intermediate links – the plastic mechanism involves both bending and shear
- (iii) Long links – dissipation of energy occurs mainly through bending

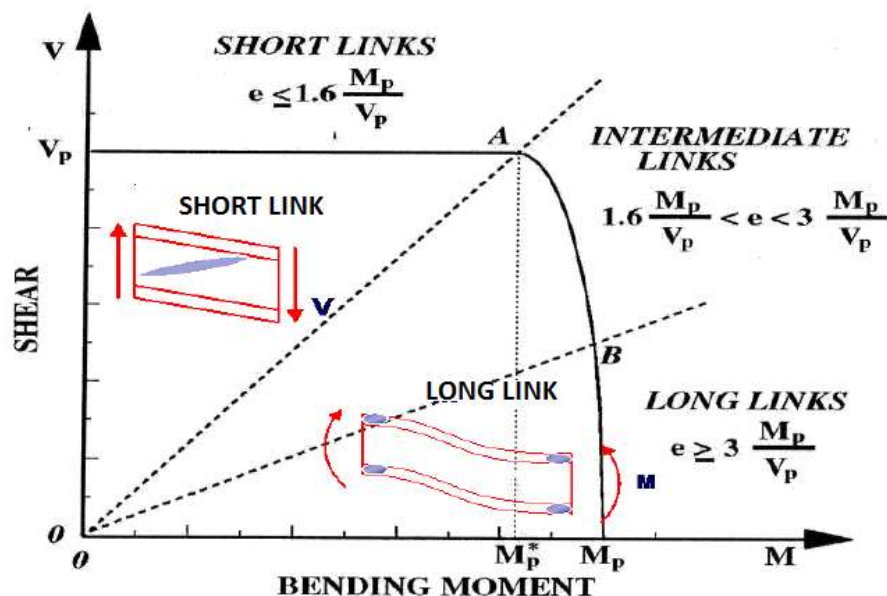


Figure 4. Classification of seismic links [10]

With the advancement of research in the field of seismic engineering, detachable seismic links have also been introduced. Replaceability of links reduces the repair time and costs of a

structure after a seismic event. With capacity design, plastification is concentrated in the dissipative zones, which in the case of EBFs are the seismic links, by designing the links as the weakest points while the other members are designed to remain elastic. By doing so, only the links need to be replaced while the other members continue to be structurally appropriate to function.

The use of bolted connections enables the links to be replaceable. Both the link and its connection need to be carefully designed as they are crucial in how effective the structural performance of an EBF will be. Recent studies have shown that for short links subjected to large deformation and with end restraints, shear overstrength may be smaller or larger than the Eurocode's value of 1.5. Along with this, significant axial force that is not taken into account by the current design codes may also develop. Lack of understanding of these forces may affect the design of the connections and lead to premature failure that can prevent the desired failure mechanism (yielding of the link).

In light of these considerations, numerous analytical, numerical, and experimental studies are now being conducted to provide an improved design and detailing guidelines of seismic links. Researchers aim to understand the behavior of these forces in further detail and integrate them into the current design practices. The current research work covers some of these aspects as it includes a comprehensive parametric analyses of detachable links detailed with flush end-plate (FEP) and extended end-plate (EEP) assemblies using analytical and numerical methods.

1.2 Objectives

Since yielding of the link is governed by either shear or bending, established design procedures have focused on this, neglecting the effect of axial forces. However, significant development of axial forces in links have been observed, albeit with limited depth.

The result of the parametric study aims to serve as a guide in the design of seismic links by developing a more thorough grasp of shear overstrength and axial force. It will also identify the influence of the observed parameters such as link length, strength of connection, stiffness, and frame's deformability on the development of axial force.

This study, with the following objectives, focuses on the investigation of short links:

1. Perform a critical review of relevant literature in order to gauge the extent of studies performed and identify the gap that needs to be addressed

2. Design connections for seismic links according to Method 1 i.e. applying the Component method in Eurocode and perform analytical checks using other methods available
3. Using the Abaqus FE software, investigate relevant parameters of the link-connection assembly such as strength, stiffness, length ratio, and boundary conditions and their correlation to the development of axial force within the links.

1.3 Scope and Limitations

The study focuses on short links with length ratio of 0.5, 0.75, and $1.0e_s$ (where e_s is the maximum shear length for short links) with two types of end-plates connections – flush-end (FEP) and extended-end (EEP). Due to time and technical limitations, a total of 40 assemblies are used: 25 for flush-end plates and 15 for extended-end plates. One assembly consists of the link and connections on both ends (bolts, end plates). They are all initially designed to satisfy Method 1 of link verification and therefore, they have varying strength and stiffness. Models of the same assemblies are created and analyzed using Abaqus with the modelling assumptions and simplifications discussed in further detail in Chapter IV. During the analyses, additional models were created by modifying the initial configuration in order to single out the influence of a specific parameter. Lastly, the analysis and interpretation of results from the analytical and numerical investigation concentrates on the development of shear overstrength and axial forces within the links.

CHAPTER II. STATE OF THE ART

All steel buildings shall be assigned to one structural typology depending on the behavior of their primary resisting structure under seismic actions. In moment-resisting frames (MRF), members act primarily in flexure to resist the horizontal forces thus dissipating energy through cyclic bending. On the other hand, concentrically-braced frames (CBF) have diagonal braces that act in tension to resist horizontal forces. In eccentrically-braced frame (EBF), these forces are resisted by “seismic links” that act in bending and/or shear.

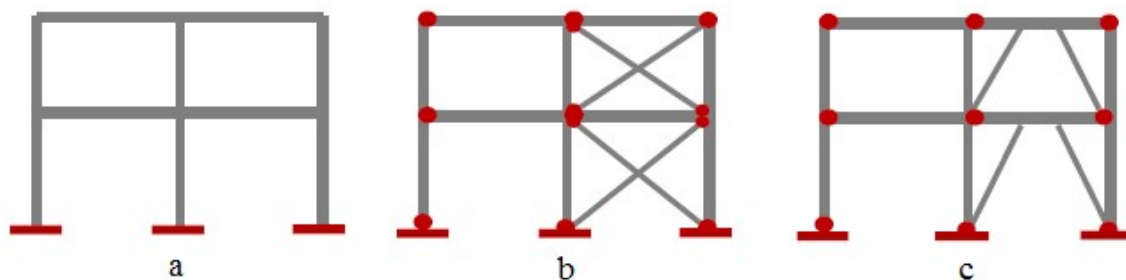


Figure 5. Three of the structural typologies for steel structures (a) MRF (b) CBF (c) EBF [10]

Each structural typology has its own structural features and application, but the seismic design must adhere to two basic criteria: (1) sufficient stiffness to satisfy the serviceability limits and avoid damage to non-structural elements during events of low seismicity and (2) sufficient ductility to prevent collapse in the case of major seismic events. MRFs and CBFs have been dominantly implemented in the past, but they do not satisfy both of the mentioned requirements. With further considerations in efficiency and possible repair, EBFs have been the concentration of several studies as an alternative to the conventional framing system. A properly designed EBF offers more economical solutions for drift compared with MRFs. Additionally, it demonstrates higher ductility and better design versatility than CBFs. **Khademi and Rezaie [23]** recently performed a comparison study of CBFs and EBFs bracing in steel structures using nonlinear time history analysis. The study made use of four fifteen-storey models: (1) two-storey X-braced, (2) single-storey X-braced, (3) inverted V-braced, and (4) EBF-braced. A notable result of their analysis is presented in the figure below. EBF shows good seismic behavior under shaking ground motion. It has the maximum displacement value on the horizontal direction and has the minimum in the vertical direction. Additionally, EBF has a higher energy absorption capacity that reached 25,000 KJ for the experiment, while the CBF is limited to 800 KJ.

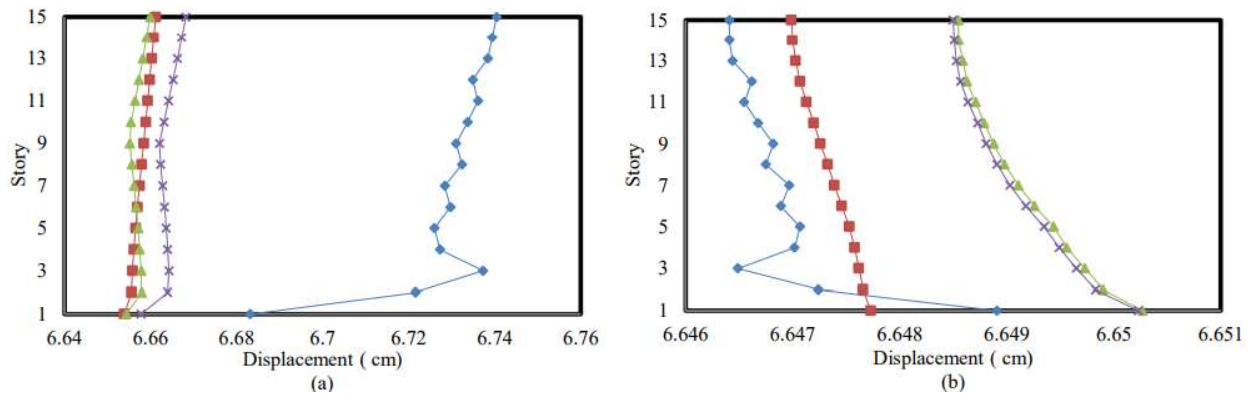


Figure 6. Horizontal (a) and vertical (b) displacement values [23]

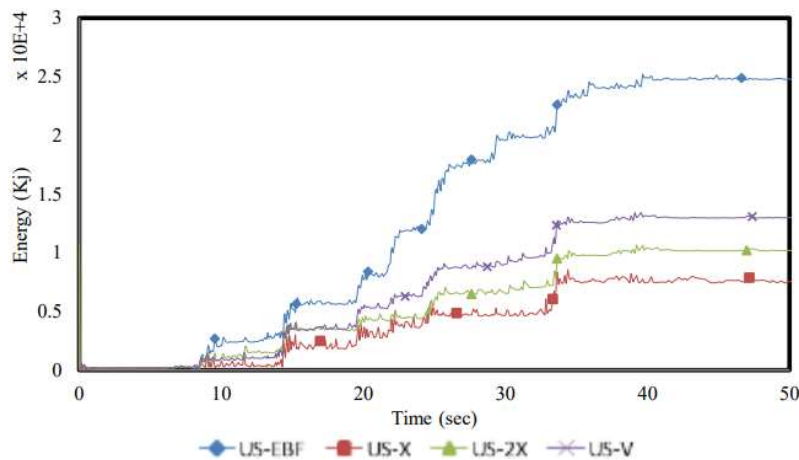


Figure 7. Energy dissipation of the frames [23]

As an overview of the design procedure, **Han [16]** explained that the ductile performance of EBFs is based on the yielding of links while other members are designed to remain elastic. The link develops shearing force in proportion to the storey shear and this will cause yielding. A beam is then chosen to carry the force in the link with a limited strength factor α to avoid overdesign. To account for the strain of the link, a factor K is further considered. Members that need to remain in the elastic range are designed with forces from the storey shear force, magnified by αK . **Mansour et al [25]** outlined the basic design philosophy of EBF in three steps: (1) size the link to provide the required strength, (2) detail the link to satisfy the required ductility (3) design the other members to be stronger than the forces developed upon yielding of the link and to satisfy drift requirements.

Bosco et al [2] summarized the criticisms of researchers on the effectiveness of the rules of Eurocode 8 for the design of EBFs. The objections raised are:

- (i) There should be restrictions on the use of lateral force method in highly ductile EBF to limit the errors in the evaluation of the overstrength factor in links.

- (ii) The provisions are conservative as it neglects the structural overstrength in considering the P- Δ effects
- (iii) Eurocode 8 evaluates the overstrength factor of links with regard to the ultimate internal forces of these members. This is not in accordance with the proposal of Popov [29] and does not ensure a reliable control over the dissipative behavior of the structure
- (iv) The link overstrength factor is discontinuous at a value of the mechanical length of links and neglects the presence of gravity loads
- (v) The design procedure does not seem adequate for structures with intermediate or long links. The rules for the application of the capacity design principles to braces, columns, and beam segments outside links are unconservative because of the underestimate of the bending moment

The importance of seismic links in the seismic design of structure has been a focus of numerical and experimental studies for a few decades.

The link in equilibrium shown below is simultaneously subjected to shear and flexure. For a theoretical balanced failure to occur, the link length ratio is 2.0. When the length ratio is less than this value, the link reaches its maximum plastic shear capacity prior to its maximum plastic moment capacity and therefore yields in shear. However, links in actuality experience interaction between shear and moment and they are significantly affected by strain hardening. This reason fueled further studies on the range of link ratios in which link failure transitions from shear to flexure. The succeeding studies performed by **Popov** and his colleagues [29] developed the limit of $1.6M_{pl}/V_{pl}$ for short links.

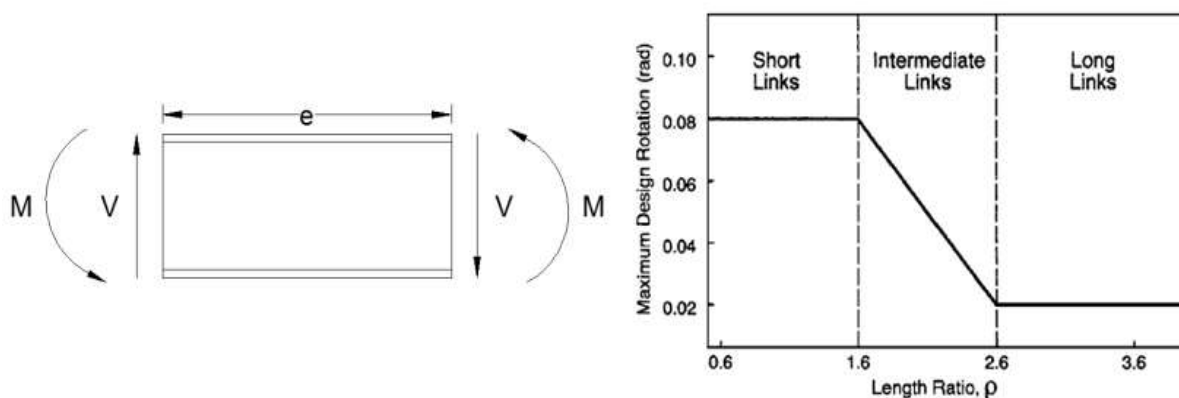


Figure 8. (Left) Static equilibrium in link element; (right) Maximum design link rotation [29]

Seismic links are crucial in the structural performance of EBFs. As presented in the introduction, links are classified into three according to their plastic mechanism, with the current study focusing on short links. **Roeder and Popov [31]** observed significant differences in the performance of seismic links as influenced by their lengths. While longer links allow more freedom to place openings, their experimental studies showed that short links have better strength and ductility when subjected to severe cyclic. Another study performed by **Malley and Popov [24]** also concluded that shear links exhibit higher energy dissipation than flexural links.

Short links have the ability to reach higher rotation capacities compared to longer links. For short links, the maximum plastic rotation is 0.08 rad while it is limited to 0.02 rad for long links due to buckling of the flange or lateral torsional buckling. While short links are designed to attain this rotation, recent tests performed by **della Corte et al [13]** showed other types of failure in the link before reaching this point. Links utilizing high strength materials exhibit web fracture as caused by varying welding processes and details of the stiffener.



Figure 9. Damage to specimens: (a) web buckling; (b) stiffener-to-flange weld fracture; (c) web fracture; (d) flange-to-end plate weld fracture [14]

As the link is a dissipative element, the connection between the link and the beam experiences maximum stresses. Proper design of the connection is therefore another crucial component to enable link plastification. There are two ways to design the connection: (1) providing it with

sufficient overstrength over the shear resistance of the link and (2) assuring the ductile behaviour of the connection.

Shear on the link web governs the response of short links and proper spacing of web stiffeners is important in achieving this. With insufficient stiffeners, plastic web buckling occurs and leads to strength degradation. Proper spacing of the stiffeners enables the link to attain the maximum shear strength, stable hysteretic response, and larger rotation capacity.

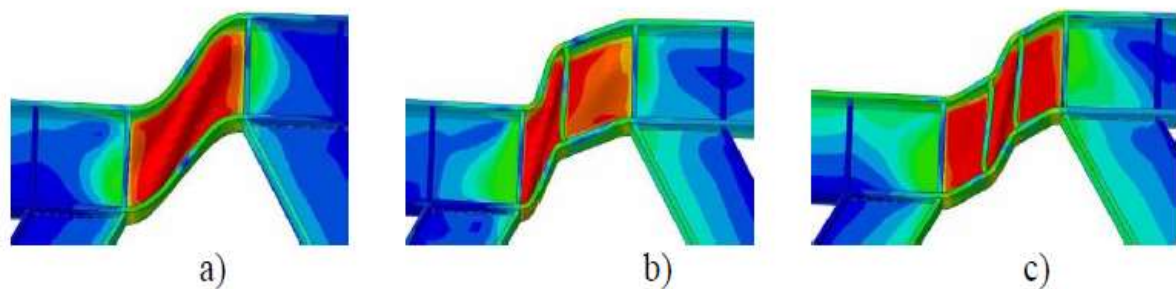


Figure 10. Deformation of the link as influenced by the intermediate web stiffener (a) no stiffener; (b) one stiffener, (c) three stiffeners [35]

Vataman et al [35] conducted a study on the influence of the presence and spacing on intermediate web stiffeners on the behaviour of the seismic link. They observed that the stiffeners divide the original shear panel into multiple panels, with each of them having separate web deformation. The elastic deformation is distributed for all the panels but upon plastification, it is concentrated in one of the panels with partial contribution from the others. Based on the experiments performed, it is recommended to limit link length to $0.8M_{pl}/V_{pl}$ to prevent excessive damage on the connection.



Figure 11. Increase in shear resistance in correlation with web stiffeners

Further improvement on EBFs have been to proposed to lessen the challenge of structural repair by designing the links to be replaceable

From **Mansour's [25]** EBF design philosophy, he identified some challenges with the design of EBF link as part of the same floor beam. It often results to oversized link elements since the floor beam is designed to yield in shear in the designated region of the link and resist the forces developed outside the link. Consequently, there are larger forces that must be satisfied for the design of other members (columns, bracings, foundations, connections), thereby increasing the total cost of construction. Through detachable EBF links, the designer has a control on the strength, stiffness and ductility of the link and still retain the same section of the beam. He also proposed the use of replaceable shear links for increased efficiency and economic benefits. He studied the appropriate details for replaceable shear links and came up with bolt end-plate link-to-beam connection, but with links smaller than the beam thereby enabling bolt rows outside the flanges of the link. This configuration, as in the case of extended end-plates, displayed high ductility and stable behaviour making it suitable for practical applications.

Clifton et al [6] summarized how a replaceable active link is developed in New Zealand in order to reduce the cost and time consumption of the repair of the damaged links. The removable link that has been used for structural repair after the Christchurch earthquake uses a bolted extended endplate for ease of removal. They have identified three main performance requirements of removable links, namely:

- They must be designed to achieve ≥ 0.08 radian plastic rotation in shear mode under the design earthquake or higher
- Inelastic demand must be limited to the link element
- Ease of removal and replacement

Other studies have been performed to investigate the onsite replaceability of links for increased efficiency and economic benefits. A replaceable link facilitates inspection and rapid replacement after a seismic event, therefore reducing the time of building repair. In 2003, **McDaniel et al [27]** conducted a study to assess whether replaceable links could be removed without difficulty upon yielding. The specimen links were brought to failure through cyclic loading. After the test, they were able to detach the links from the set-up without any difficulty by detensioning the flange and web splice bolts and subsequently removing the splice plates.

Stratan and Dubina [32] specifically conducted an investigation on EBFs with horizontal links that can be removed and replaced once damaged by an earthquake. Capacity design allows the plastification in predefined areas (dissipative zones).

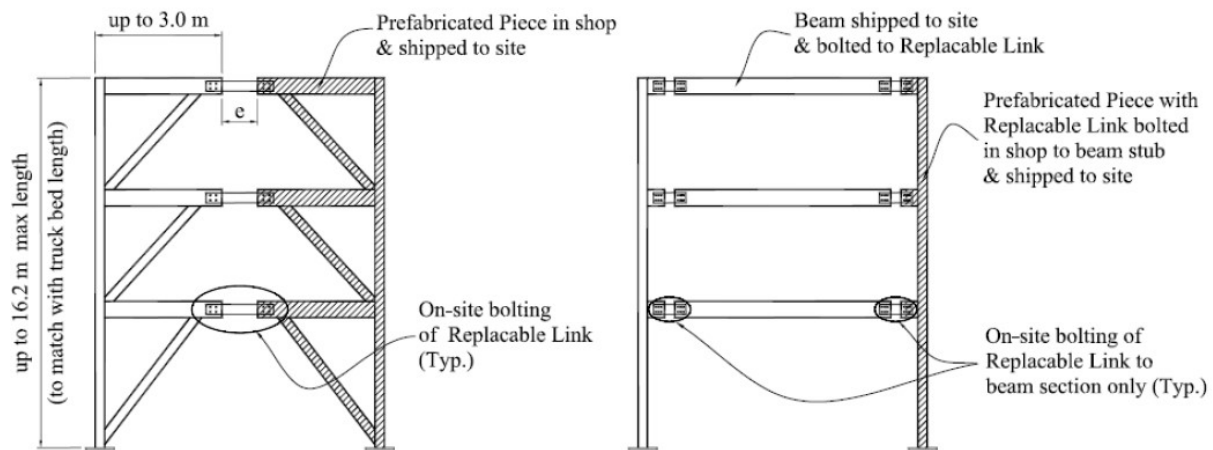


Figure 12. Replaceable link concept for EBFs (left); MRF (right) [32]

In the experiment, bolted flush-end plates were used. Bending in the end-plate, along with bolt thread stripping were observed. With the use of bolted connections, replacement of the affected dissipative elements becomes possible, therefore reducing the repair costs. The connection is made up of high-strength bolts and flush-end plate. With this type of connection, the link may be made of steel with lower grade and the elastic response of the elements connected to the link is assured.

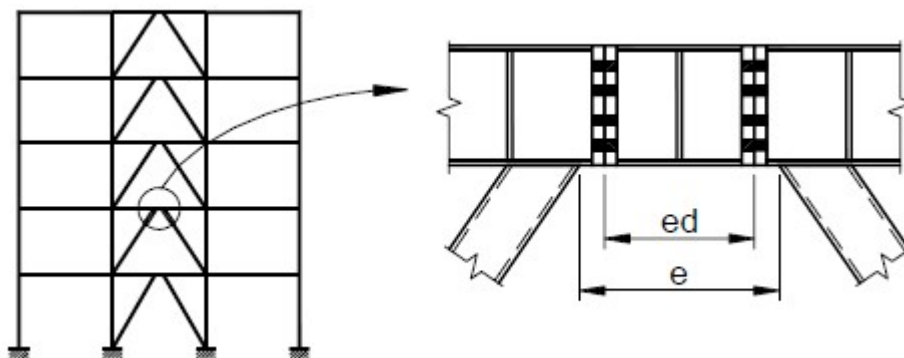


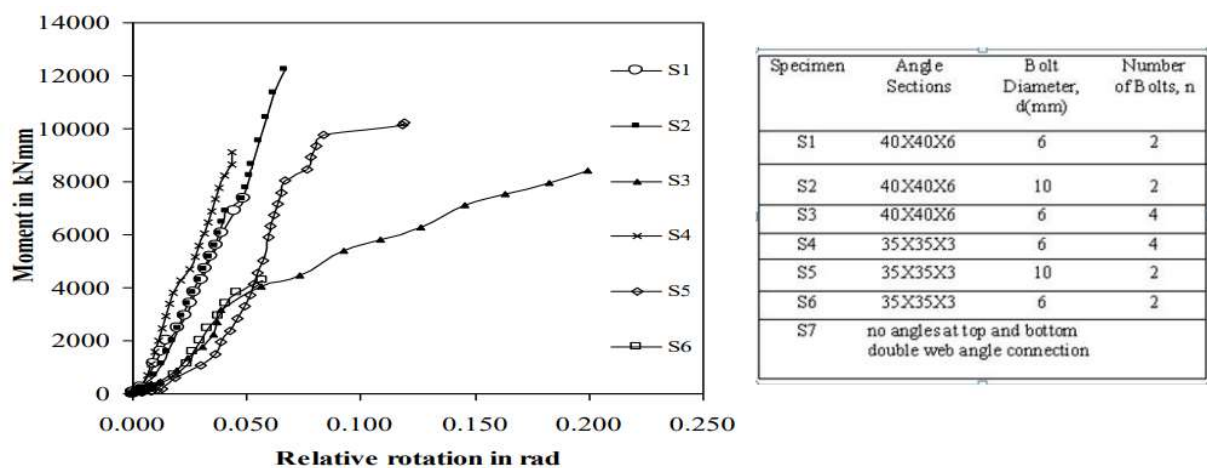
Figure 13. Bolted link [32]

The study concluded with a limit of 0.8 length ratio for a proper cyclic behavior. Succeeding studies by Ioan et al [19] focused on the re-centring capability of EBF with removable links. For a structure to exhibit a self-centering capability, the use of combined moment-resisting frame and EBF with detachable link is proposed. By using high-strength steel for some members, MRFs are made elastic and therefore, they can provide the force needed to re-center the structure once the links are removed.

For end-plate connected links, the replacement of the link requires the realignment of the frame to its plumb position prior to the reinstallation of the link between the beams. This requires a high degree of precision on the links. **Sumner and Murray [33]** aimed to resolve this challenge by fabricating the beams 5mm short and using finger shims to fill in the gap. In the experiment performed, no significant difference in the behavior of the connection was observed.

Design considerations for replaceable seismic links

Knowing that the use of bolted connections enables the replaceability of links, it is therefore necessary to understand their behavior. Bolted connections have been widely employed to provide the required ductility of steel structures. **Babu and Sreekumar [39]** performed a study on the ductility of bolted beam-column connections. As rigid connections are expensive and difficult to implement while pinned joints lack the resistance and stiffness to resist lateral loads, most of the joints use are in essence, semi-rigid. Their experiments show that as the diameter of the bolt and bolt rows are increased, the ultimate moment and ultimate rotation of the joint is also increased. In terms of energy dissipation on the other hand, increasing the number of bolt rows causes a significantly higher increase in the energy dissipated, compared to the effect of increasing the bolt diameter.



Specimen			Number of bolt	Energy dissipated (kNm.rad)
S1	6mm thick	d/t =1	2	177.4
S3			4	1019.8
S4	3mm thick	d/t =1	4	195.4
S6			2	132.4

Figure 14. Moment-rotation curves and energy dissipation of connections tested [39]

Analyzing bolted connections and their application in replaceable links, a more accurate design procedure requires us to understand the behavior of overstrength and axial forces, discussed in the subsequent works.

Shear overstrength refers to the maximum shear force that can develop in the link in proportion to its inelastic strength based on measured section and material properties. Since capacity design makes use of the maximum possible force that may develop within the link, the design requires an accurate value of these forces. Overestimating the design forces is uneconomical, but underestimating them may cause damage to non-dissipative members. Currently, Eurocode recommends the use of 1.5 as shear overstrength.

On the study performed by **della Corte et al [13]**, there are three basic parameters influencing shear overstrength on links: (i) axial forces, (ii) ratio of flange over web area and (iii) ratio of link length and cross section depth. It was also concluded that when web stiffeners are properly designed and the plastic rotation is less than or equal to 0.08 rad, the response of the link is stable and neither the buckling nor the web fracture affect the response.

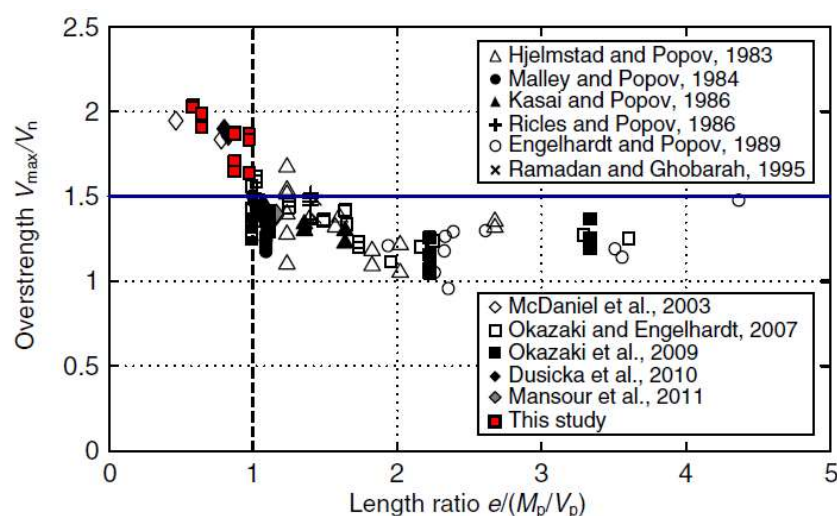


Figure 15. Overstrength factors of link test data [21]

The figure above shows the result of different studies conducted on the overstrength of links. As suggested by **Popov and Engelhardt [29]**, an overstrength factor of 1.5 can be considered conservative for links with a length ratio of more than 1.0, in accordance with Eurocode's provision. However, large values of overstrength are observed for shorter links. Studies performed by **McDaniel et al [27]** and **Dusicka et al [15]** observed the development of large shear overstrengths. In the experiment performed by **McDaniel et al [27]** on built-up steel shear links, the obtained overstrength factors are 1.55 times greater than what is prescribed in

the design code (AISC recommends 1.25 and the experimental result had 1.94). Similarly, **Dusicka et al [15]** arrived at 1.4 to 2.0 times higher. The study performed by **Ji et al [21]** arrived at even a slightly higher value as shown in red on the above graph.

The mentioned researchers agree that there are two probable causes of the significant increase in shear overstrength – (1) contribution of the shear in flanges and (2) the effect of cyclic hardening of the steel web when subjected to large inelastic strains. To further investigate on the influence of flanges on overstrength, **Ji et al [21]** made an elastic-perfectly plastic model in order to eliminate the effect of strain hardening on the web. Fig 14 (left) demonstrates that as the link rotation increases, there is also an increase in the flanges' shear force, reaching up to 17% of the plastic shear capacity considering 0.15 rad link rotation. This contribution of the flange further increases for shorter links as demonstrated by Fig 14 (right).

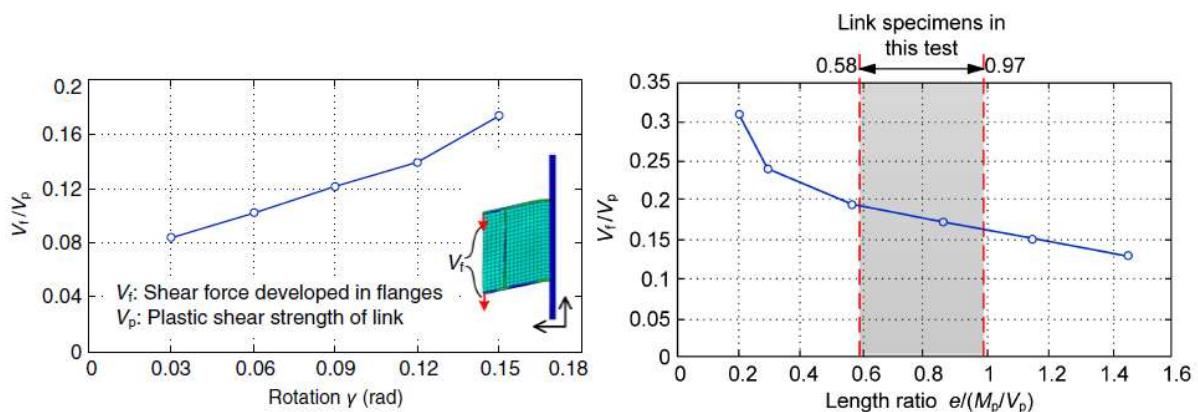


Figure 16. (Left) Shear in flanges; (right) Flange contribution on shear strength for different length ratios [21]

Apart from shear overstrength, axial force is another crucial consideration for the design of seismic links. More recent studies have been conducted highlighting its importance. The presence of axial force has a significant effect on the flexural capacity of joints and neglecting it at high levels can be unsafe. According to **da Silva et al [9]**, high level of axial force may develop for the following cases:

1. Regular frames with significant horizontal loads, in the case of a seismic event or extreme wind, especially for sway frames
2. Irregular frames subjected to gravity and horizontal loading
3. Portal frames with pitched roofs

The study aimed to address the limitation of the component method and the lack of available specific procedures for the analysis and design of joints under bending and axial force.

Numerical and experimental investigation on flush and extended-end plates were performed at the University of Coimbra. Different combinations of bending and axial forces were applied to the experimental set-ups and their response were observed.

The results show that the presence of tensile force in beam greatly reduces the bending resistance of the joint, while there is an increase in the moment resistance when compressive force less than 20% of the beam plastic resistance is applied. This highlights that there is a need to review the current Eurocode's limitation of 10% when a joint is subjected to axial force.

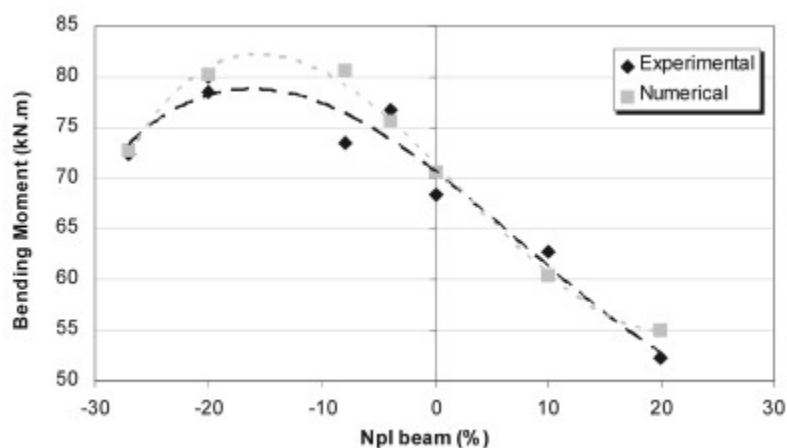


Figure 17. Interaction diagram for flush-end plates [9]

Jaspart and Cerfontaine [20] used the component method to obtain M-N interaction curves and initial stiffness of a joint. Additionally, several studies have been conducted in Liege to observe the behaviour of beam-to-column joints and beam splices when subjected to combined bending and axial force. Eurocode has established an axial force limit of 10% of the axial resistance of the connected beam, under which the rotational response of the joint is not significantly affected by the axial force. However, this value is fully arbitrary and is not satisfied by some joint configurations such as column bases and pitched-roof portal frames.

Da Silva and Coelho [8] also developed analytical expressions to determine the non-linear response of a beam-to-column joint when subjected to combined axial force and bending moment. However, these results are not supported and validated by experimental tests and therefore, **da Silva et al [9]** tested different end-plate connections (flush and extended) to simulate joint behaviour. The procedure tested nine FEP joints tested under pure bending as well as with combined bending and varying intensities of axial force.

The study concluded that for a compressive axial force of 20%, there is an increase in the bending resistance on the flush-end plate joints used. On the other hand, there is a reduction in

the bending resistance when the same joint is loaded in tension, showing asymmetry on the joint response.

Del Savio [12] proposed the use of correction factor to scale the bending moment-rotation curve originally generated without the influence of the axial force. Through the correction factor based on the axial force level, the bending moment is modified and the curve is shifted up or down accordingly. He further modified this idea by dividing the interaction factor into two parts: moment and rotation.

The current provision of Eurocode evaluates the rotational stiffness and moment capacity of joints when subjected to pure bending. Furthermore, the code allows designer to neglect the axial load during the analysis when it is less than 5% of the (link/beam) axial plastic resistance but no design guidelines if the axial force exceeds this value.

Considering all the relevant works presented above, the following observations are drawn:

- While the concept of EBF has been in existence for 40 years, the use of replaceable links has only been recently introduced. Replaceable links enable the reduction of time and financial resources required to repair structures after a seismic event.
- The research community agrees that the current design procedures provided by the Eurocode can be further improved with revised guidelines of shear overstrength and axial force.
- While many investigations have been performed showing that there is indeed a development of axial force in links, there needs to be an in-depth study to understand the phenomenon and the parameters that influence it.

CHAPTER III. ANALYTICAL BACKGROUND

3.1 Component method according to Eurocode 1993 Part 1-8

The component method presented in Eurocode 3 is a way to determine the behavior of a joint, bending in particular, as a result of the interaction between several components. Each of the component has its own strength and stiffness in tension, compression, or shear. The coexistence of several components within the joint is also considered as the stress interaction between them is likely to decrease the individual resistance of the component.

There are three steps involved in the characterization of components:

1. Identification of the active components of the joints
2. Determination of the stiffness and resistance of each component
3. Assembly of the single components to determine the prevailing stiffness and resistance of the joint as a whole

3.1.1 Joint classification

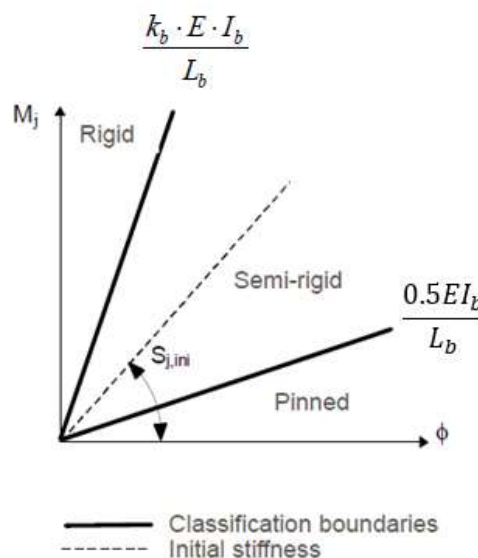


Figure 18. Classification of joints according to stiffness [36]

The Eurocode has three classifications of joints according to its initial stiffness. A joint is considered as nominally pinned when $S_{j,ini} \leq \frac{0.5EI_b}{L_b}$. They are capable of transmitting internal forces without developing significant moments, and are capable of accepting the rotation demand of the design load. On the other hand, it falls into the rigid category when $S_{j,ini} \geq$

$\frac{k_b \cdot E \cdot I_b}{L_b}$, where K_b is taken as 8 for frames where the bracing system reduces the horizontal displacement and 25 for other frames, provide that $K_b/K_c=1.0$. When $S_{j,ini}$ falls in between these two values and/or $K_b/K_c < 1.0$, the joint is considered as semi-rigid.

K_c – Average value of I_b/L_c for all the beams at the top of the storey

K_b – Average value of I_c/L_c for all the columns of the storey

I_b – Moment of inertia of the beam

I_c – Moment of inertia of the column

In terms of resistance, Eurocode also classifies joints into full and partial resistance.

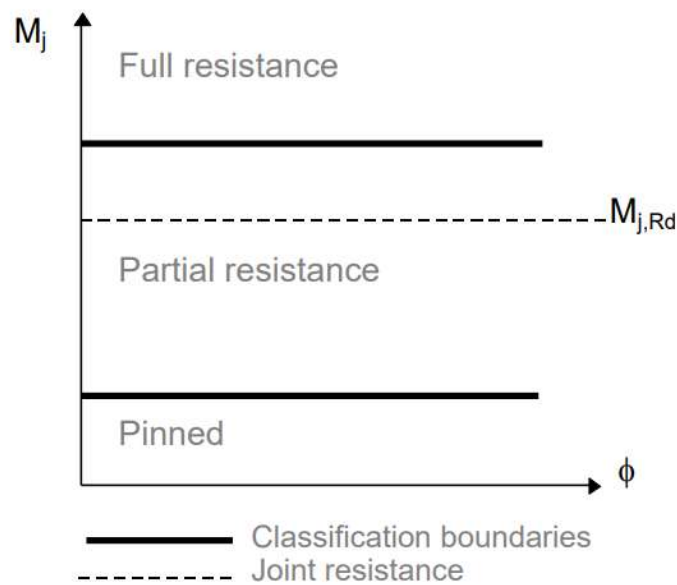


Figure 19. Classification of joints according to resistance [36]

A joint has **full resistance** if it meets either of the following criteria:

Joints at the top of column $M_{j,Rd} = M_{b,pl,Rd}$ or $M_{j,Rd} = M_{c,pl,Rd}$

Joints within column height $M_{j,Rd} = M_{b,pl,Rd}$ or $M_{j,Rd} = 2M_{c,pl,Rd}$

All other joints that don't meet the criteria for full resistance and nominally pinned has **partial resistance**.

3.1.2 Basis of component method

There are three relevant zones in the evaluation of a link-to-beam bolted joint namely tension, compression, and vertical shear. Each component is characterized by a resistance-displacement relation. Upon identification of the active components, they are then assembled to determine the overall behavior of the joint.

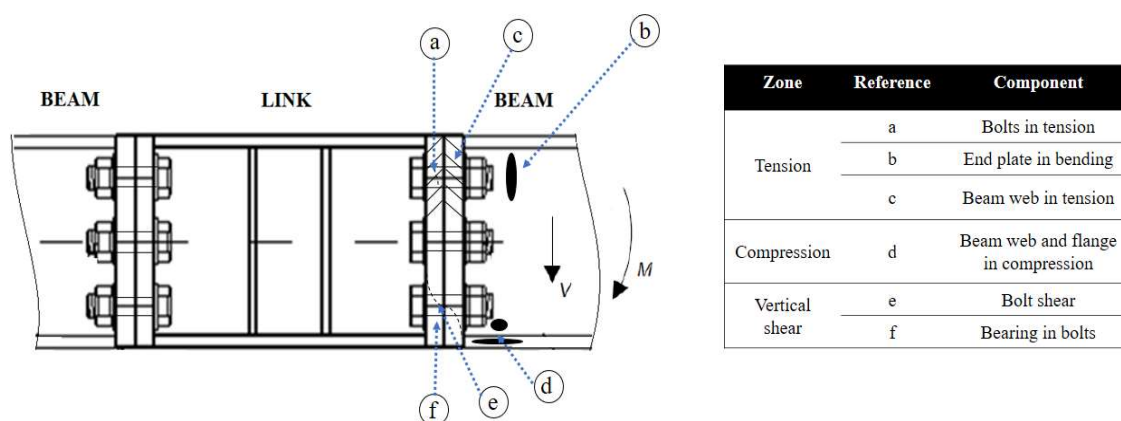
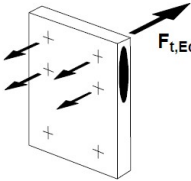
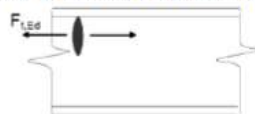



Figure 20. Active components in a link-beam joint

3.1.3 Characterization of the components

Eurocode has identified 20 components that may be present in a single joint but only a few of them are found in a link as shown in Figure 20. The table below discusses each component in further detail.

Table 1. Active components in a link-beam joint

Component	Link side	Beam side
 <p>End plate in bending</p> <p>The design resistance and failure mode of an end plate in bending, together with the associated bolts in tension, should be taken as similar to those of an equivalent T-stub flange (see 6.2.4) for both:</p> <ul style="list-style-type: none"> - each individual bolt row required to resist tension - each group of bolt rows required to resist tension 	✓	✓
<p>Beam web in tension</p> <p>EN 1993 1-8 6.2.6.8</p>  $F_{t,wb,Rd} = \frac{b_{eff,t,wb} t_{wb} f_{y,wb}}{\gamma_{M0}}$		

<p>$b_{\text{eff},t,\text{wb}}$ is the effective width of the beam web in tension; should be taken as equal to the effective length of the equivalent T-stub representing the end-plate in bending, obtained from 6.2.6.5 for an individual bolt row or a bolt group.</p>		✓
<p>Beam flange and web in compression</p>  $F_{c,fb,Rd} = \frac{M_{c,Rd}}{h - t_{fb}}$ <p>$M_{c,Rd}$ – is the design moment resistance of the beam cross-section, reduced if necessary to allow for shear, see EN 1993-1-1. h – depth of the connected beam t_{fb} – flange thickness</p>		✓

3.1.4 Assembly of the components

Upon identification of the components and their relevant characteristics, they are then analyzed as an assembly. In forming the assembly, the following conditions must be satisfied:

1. the internal forces in the components are in equilibrium with the external forces acting on the joint
2. no resistance of any component is exceeded (plasticity criteria)
3. no deformation capacity of any component is exceeded

3.1.5 Resistance of the joint

The bending resistance of the joint is given by

$$M_{j,Rd} = \sum z_i F_{t,Rd,i}$$

where $F_{t,Rd}$ is the tensile force on the bolt row and z_i is the corresponding lever arm

On the other hand, the shear resistance $V_{j,Rd}$ of the joint is the combined shear resistance of the bolts in compression and 28.5% of those in tension.

$$V_{j,Rd} = n_c F_{v,Rd} + \frac{0.4}{1.4} n_t F_{v,Rd}$$

For a single bolt, the shear resistance is given by:

$$F_{v,Rd} = \frac{\alpha_v f_{ub} A}{\gamma_{M2}}$$

For equilibrium, the sum of the tensile forces on the bolt rows has to be smaller than the compressive resistance of the beam flange and web $F_{cfb,Rd}$. With this condition, the contribution of the bolt rows in compression are not accounted in the bending resistance. However, if it is not satisfied, the tensile force is reduced starting from the bottom bolt rows until equilibrium is achieved.

The tensile resistance of each bolt row is taken as the minimum among all the active components.

3.1.6 Rotational stiffness of the joint

The initial rotational stiffness of the joint $S_{j,ini}$ is calculated by

$$S_{j,ini} = \frac{Ez^2}{\sum_i \frac{1}{k_i}}$$

where

E – Young's modulus of steel

k_i – stiffness k of component i

z – lever arm from the center of compression

Stiffness of bolt rows in tension are combined by considering a series assembly, given by:

$$k_{eff,r} = \frac{1}{\sum_i \frac{1}{k_{i,r}}}$$

Where $k_{i,r}$ is the stiffness of component i of bolt row r .

The following components can be combined for bolt rows in tension:

End plate in bending: $k_5 = \frac{0.9l_{eff}t_p^3}{m^3}$, where l_{eff} is the minimum effective length for the corresponding bolt row.

Bolts in tension: $k_{10} = \frac{1.6A_s}{L_b}$, where A_s is the nominal area of the bolt cross section and L_b is the tightening length.

Several bolt rows in tension can be combined by considering a parallel assembly to obtain a single stiffness coefficient k_{eq} .

$$k_{eq} = \frac{\sum k_r h_r}{z_{eq}}$$

Where k_r is the effective stiffness of bolt row r , h_r is its corresponding level arm and

$$z_{eq} = \frac{\sum k_i z_i^2}{\sum k_i z_i}$$

3.1.7 T-stub behavior of an end plate in bending

The end plate in bending is evaluated through its behavior as a T-stub. The T-stub model can be used for rigidly connected plates that are connected to another member by at least a bolt row. Under this model, one of the plates act as the flange of the T-stub while the connected member serves as the web.

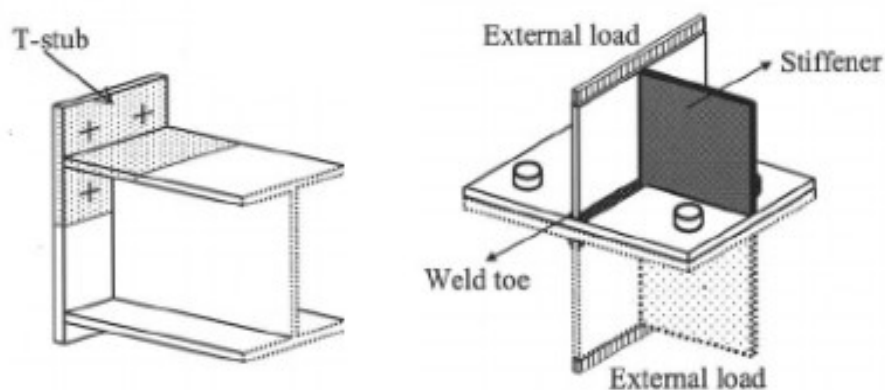


Figure 21. T-stub model for an end-plate connection [40]

The behavior of the bolt row is evaluated individually and as part of the group, the resistance of which is influenced by the effective length l_{eff} . This corresponds to the length of the yield lines that develop on each failure mode and is determined by the geometrical properties of the bolted connection. It is distinguished between two yield-line patterns: circular and non-circular.

Table 2. Effective lengths for a flush-end plate when bolt rows are considered individually

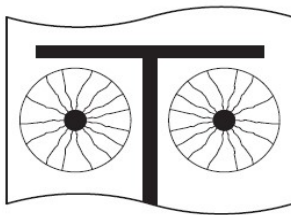
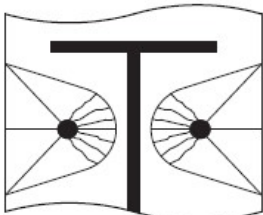
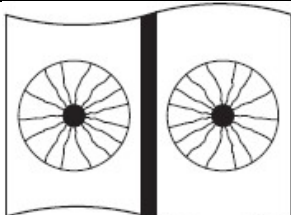
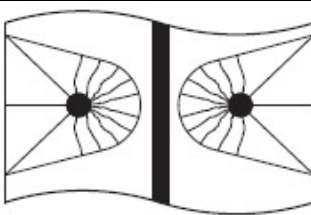
Bolt row location	Circular patterns	Non-circular patterns
First bolt row below tension flange of beam	 $\ell_{\text{eff}} = 2\pi m$	 $\ell_{\text{eff,nc}} = \alpha m$
Other inner bolt rows	 $\ell_{\text{eff}} = 2\pi m$	 $\ell_{\text{eff}} = 4m + 1.25e$

Table 3. Effective lengths when bolt rows are considered as part of a group

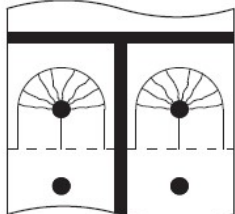
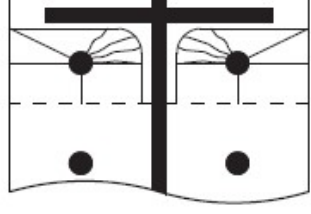
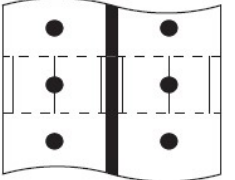
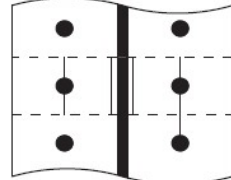
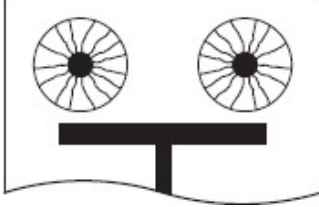
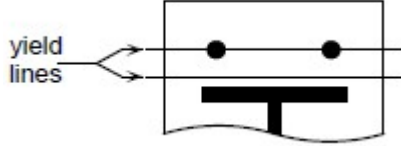
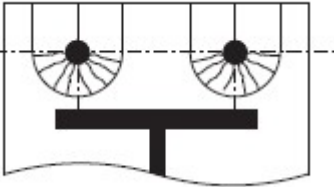

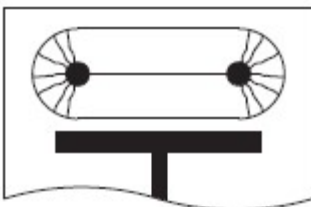
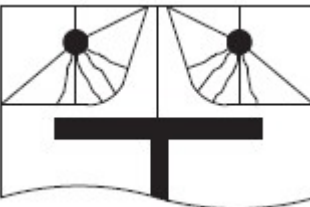
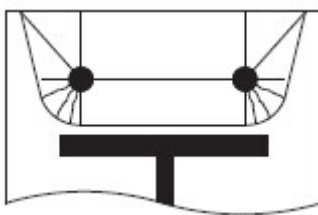
Bolt row location	Circular patterns	Non-circular patterns
First bolt row below tension flange of beam	 $\ell_{\text{eff,cp}} = \pi m + p$	 $\ell_{\text{eff,nc}} = \alpha m - (2m + 0.625e) + 0.5p$
Other inner bolt rows	 $\ell_{\text{eff,cp}} = 2p$	 $\ell_{\text{eff,nc}} = p$

Table 4. Effective lengths for bolt rows above the tension flange (EEP)

Circular patterns	Non-circular patterns
 <p data-bbox="204 566 427 600">Circular yielding</p> $\ell_{\text{eff,cp}} = 2\pi m_x$	 <p data-bbox="863 528 1086 562">Double curvature</p> $\ell_{\text{eff,nc}} = \frac{b_p}{2}$
 <p data-bbox="204 920 507 954">Individual end yielding</p> $\ell_{\text{eff,cp}} = \pi m_x + 2e_x$	 <p data-bbox="863 909 1166 943">Individual end yielding</p> $\ell_{\text{eff,nc}} = 4m_x + 1.25e_x$
 <p data-bbox="204 1301 507 1335">Circular group yielding</p> $\ell_{\text{eff,cp}} = \pi m_x + W$	 <p data-bbox="863 1301 1070 1335">Corner yielding</p> $\ell_{\text{eff,nc}} = 2m_x + 0.625e_x + e$
	 <p data-bbox="863 1715 1118 1749">Group end yielding</p> $\ell_{\text{eff,nc}} = 2m_x + 0.625e_x + \frac{W}{2}$

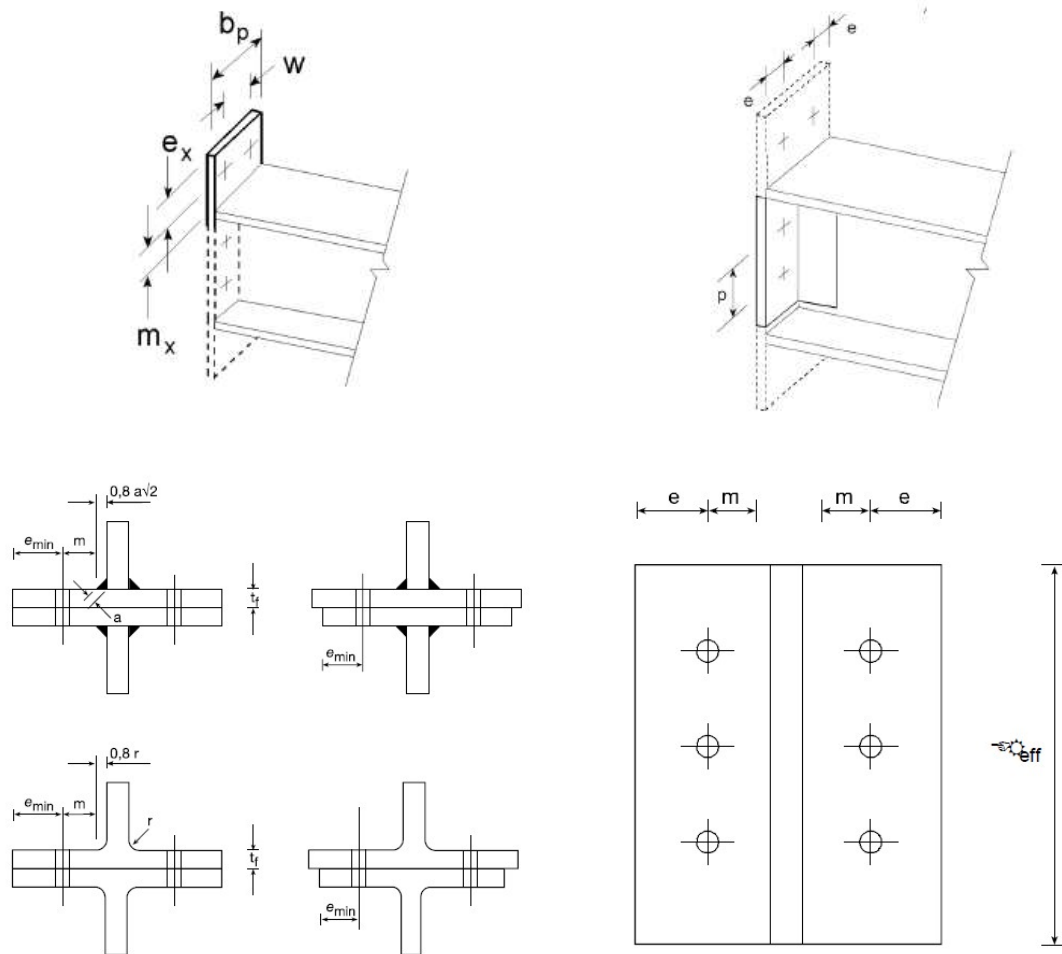


Figure 22. Geometrical parameters for the determination of effective length of the T-stub [3]

The T-stub has three possible modes of failure as shown in the Figure below.

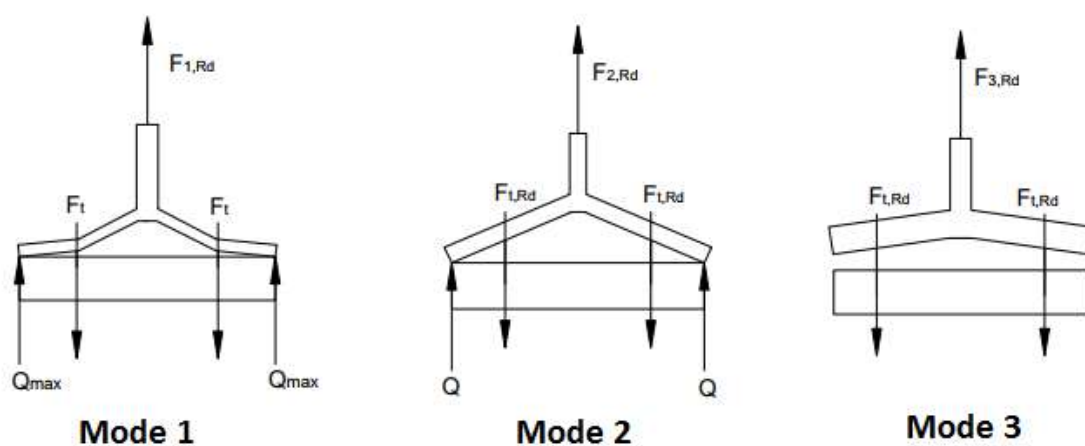


Figure 23. Modes of failure of a T-stub [40]

Mode 1 – Characterized by the complete yielding of the flange without the contribution of the bolts, and therefore, highly ductile. L_{eff} for Mode 1 corresponds to the minimum between the circular $l_{eff,cp}$ and non-circular $l_{eff,nc}$ patterns.

$$F_{T,1,Rd} = \frac{(8n - 2e_w) M_{pl,1,Rd}}{2mn - e_w(m + n)}$$

Mode 2 – Combined yielding of the flange and failure of the bolts. L_{eff} for Mode 2 corresponds to the non-circular patterns $l_{eff,nc}$.

$$F_{T,2,Rd} = \frac{2M_{pl,2,Rd} + n\Sigma F_{t,Rd}}{m + n}$$

Mode 3 – Brittle failure characterized by the failure of the bolts without yielding of the flange.

$$F_{T,3,Rd} = \Sigma F_{t,Rd}$$

where the tensile resistance is the minimum between the bearing resistance $F_{b,Rd}$ and tension resistance $F_{t,Rd}$

$$F_{b,Rd} = \frac{k_1 a_b f_u d t}{\gamma_{M2}}$$

$$F_{t,Rd} = \frac{k_2 f_{ub} A_s}{\gamma_{M2}}$$

3.2 Analytical methods to verify resistance of FEP connection for links

Three methods are used to design and check the link connections. Each link is designed to satisfy Method 1, and the same configuration is checked for Methods 2 and 3.

3.2.1 Method 1 – In terms of bending resistance, this method neglects the influence of axial force. For shear resistance, the contribution of the bolts in tension are reduced to 28% while those in compression have 100%.

The joint is designed to satisfy the following according to RC Part1-8:

$$M_{j,Ed} = 1.1 \cdot \gamma_{ov} \cdot 1.5 \cdot V_{pl,link} \cdot e_{link} \leq M_{j,Rd}$$

where $M_{j,Ed}$ is the design bending moment of the connection and $M_{j,Rd}$ is the bending resistance of the connection according to EN1993 Part 1-8

The shear resistance is then checked to be above the demand

$$V_{j,Ed} = 1.1 \cdot \gamma_{ov} \cdot 1.5 \cdot V_{pl,link} \leq V_{j,Rd} = n_c F_{v,Rd} + \frac{0.4}{1.4} n_t F_{v,Rd}$$

Where $V_{j,Ed}$ is the design shear force of the connection, $V_{j,Rd}$ is the connection shear capacity, n_c is the number of bolts in compression, n_t , is the number of bolts in tension and $F_{v,Rd}$ is the shear resistance of a single bolt.

The tensile force developed within the link is ignored and models designed for M+V will be made to observe the behavior of the connection under the M+V+N loading conditions.

3.2.2 Method 2 – *The calculation of the resistance considers the combined influence of bending and axial force. For the shear resistance, all bolts are assumed to be in tension).*

For this method, the M-N combined resistance is checked according to the EN 3 Part 1-8 for cases when the axial force in the connected beam N_{Ed} is larger than 5% of the design plastic resistance $N_{pl,Rd}$.

$$\frac{M_{j,Ed}}{M_{j,Rd}} + \frac{N_{j,Ed}}{N_{j,Rd}} \leq 1$$

Where $M_{j,Rd}$ is the design moment resistance of the joint, assuming no axial force and $N_{j,Rd}$ is the design tensile resistance of the joint, assuming no applied bending moment. $N_{j,Ed}$ in this case would be the tensile force in the link at 8% link rotation from analyses already performed, considering fully restrained BCs.

The shear capacity of the connection is then checked assuming that all bolts are in tension.

$$V_{j,Ed} = 1.1 \cdot \gamma_{ov} \cdot 1.5 \cdot V_{pl,link} \leq V_{j,Rd} = \frac{0.4}{1.4} \sum F_{v,Rd}$$

3.2.3 Method 3 – *This method makes use of M-N interaction curve, further explained in Chapter V.*

The third method of verification requires building the M-N interaction curve and checking the actual ($M_{j,Ed}$, $N_{j,Ed}$) position with respect to the curve. The shear capacity is then checked assuming that all the bolts are in tension as in Method 2.

3.3 Calculation of design forces on links

The design shear force V_{Ed} and bending moment M_{Ed} are based on the principle of capacity design, in which the connection has to remain elastic during the plastic deformation of the ductile link. Therefore, the design force must be at least equal to the maximum resistance of the link after yielding and is given by:

$$V_{Ed} = 1.1 \cdot \gamma_{ov} \cdot 1.5 \cdot V_{pl,link}$$

$$M_{Ed} = V_{Ed} \cdot \frac{e}{2}$$

where

γ_{ov} is taken as 1.25 to account for the variability of material strength

$V_{pl,link}$ is the plastic shear strength of the link and e is the geometrical length of the link.

$$V_{pl,link} = \frac{(d - t_f) \cdot t_w \cdot f_y}{\sqrt{3}}$$

$$M_{pl,link} = b_f t_f (d - t_f) f_y$$

$$e = \frac{1.6 M_{pl,link}}{V_{pl,link}}$$

The design tensile force N_{Ed} is given by

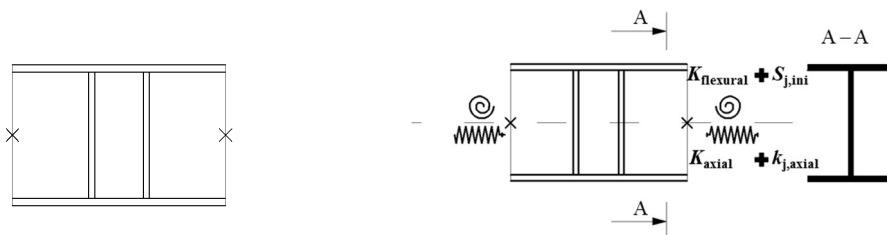
$$N_{Ed} = n_{fl} \cdot N_{pl,link,fl}$$

where

n_{fl} corresponds to the ratio of tensile forces in the link at 8% rotation from analyses already performed, considering two types of boundary conditions: fully restrained and deformable.

$N_{pl,link,fl}$ is the axial resistance of the link's flange given by

$$N_{pl,link,fl} = 2 f_y b t_f$$



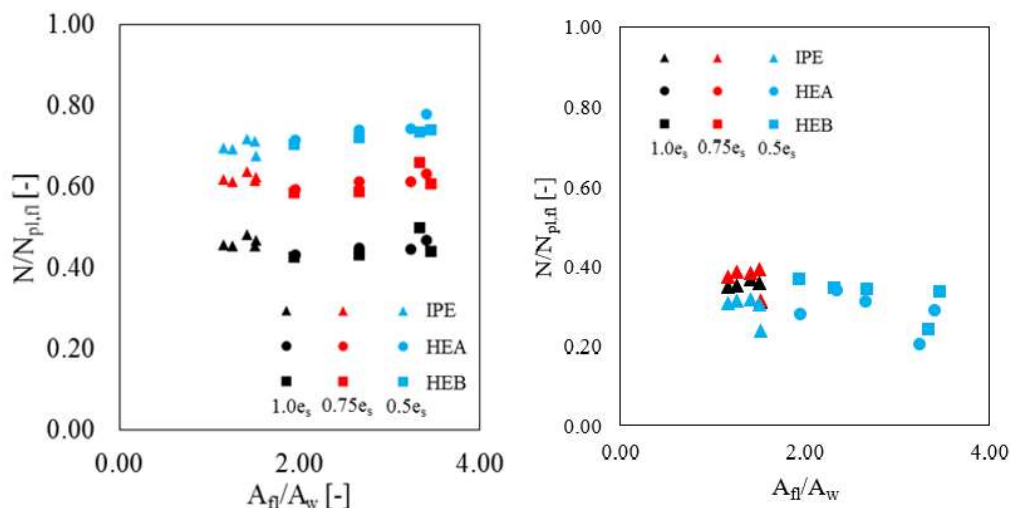


Figure 24. Axial force ratios for different profiles and link lengths considering fully rigid BC (left) and deformable BC (right)

Figure 19 shows the axial force in links for fully rigid and deformable boundary conditions, respectively. From the fully rigid condition, the plot shows that there are higher axial forces developed in shorter links ($e/e_s=0.5$) and it decreases for longer links ($e/e_s = 0.75$ and 1.0). Under the deformable conditions, it can be seen that there is a significant reduction of axial forces in general.

3.4 Evaluation of the axial and flexural stiffness of the frame

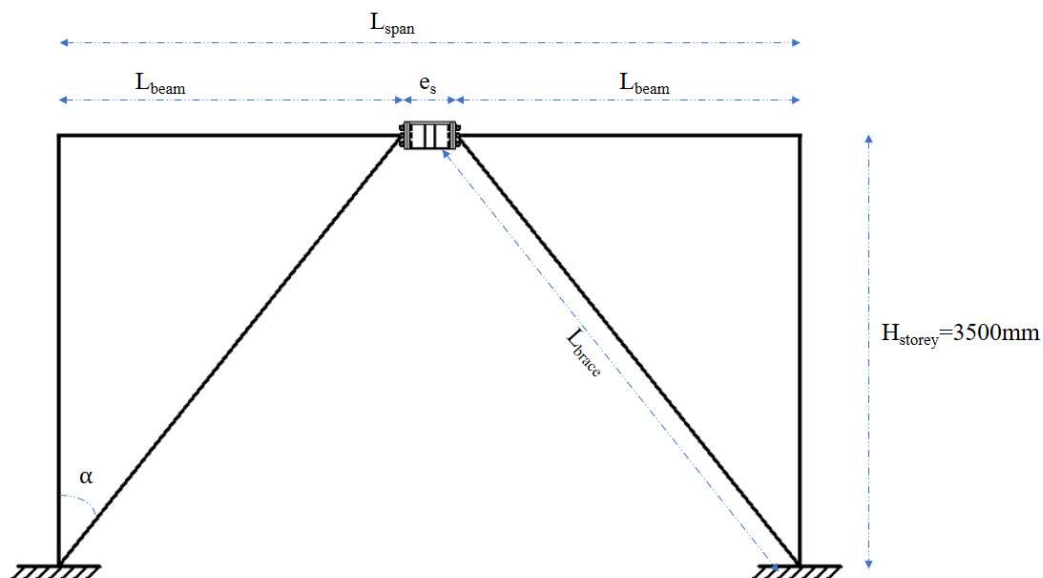


Figure 25. Configuration of the frame for the calculation of axial and rotational stiffness

Sample calculation of axial and flexural stiffness for IPE ($e/e_s=0.5$)

Link	e_s (mm)	Beam	L_{beam} (mm)	A_{beam} (mm ²)	$I_{y,beam}$ (mm ⁴)	Brace	L_{brace} (mm)	A_{brace} (mm ²)	$I_{y,brace}$ (mm ⁴)
IPE200	421	HEA200	3290	5380	3.69E+07	HEB200	4803	7810	5.70E+07
IPE300	626	HEA300	3187	11250	1.83E+08	HEB300	4733	14910	2.52E+08
IPE400	783	HEA400	4108	15900	4.51E+08	HEB300	5397	14910	2.52E+08
IPE500	869	HEA500	4065	19750	8.7E+08	HEB400	5364	19780	5.77E+08
IPE600	965	HEA600	4017	22650	1.41E+09	HEB400	5328	19780	5.77E+08

To account for the presence of the beams and braces connected to the links, deformable springs are imposed at the face of the connection. The deformable springs are defined with two properties: axial stiffness (K_{axial}) and rotational stiffness (K_{rot}).

Fig.25 shows the frame configuration used to design the members and calculate the stiffness. In accordance with this frame geometry, the profiles that satisfy the design requirements of the EBF are shown in the table, along with their corresponding properties.

Axial stiffness is calculated as follows:

$$K_{axial} = E \left(\frac{A_{beam}}{L_{beam}} + \frac{A_{brace}}{L_{brace}} \cdot \cos^2 \alpha \right)$$

where

$$\alpha = \tan^{-1} \frac{H_{storey}}{L_{beam}}$$

On the other hand, rotational stiffness is given by:

$$K_{rot} = 4E \left(\frac{I_{y,beam}}{L_{beam}} + \frac{I_{y,brace}}{L_{brace}} \right)$$

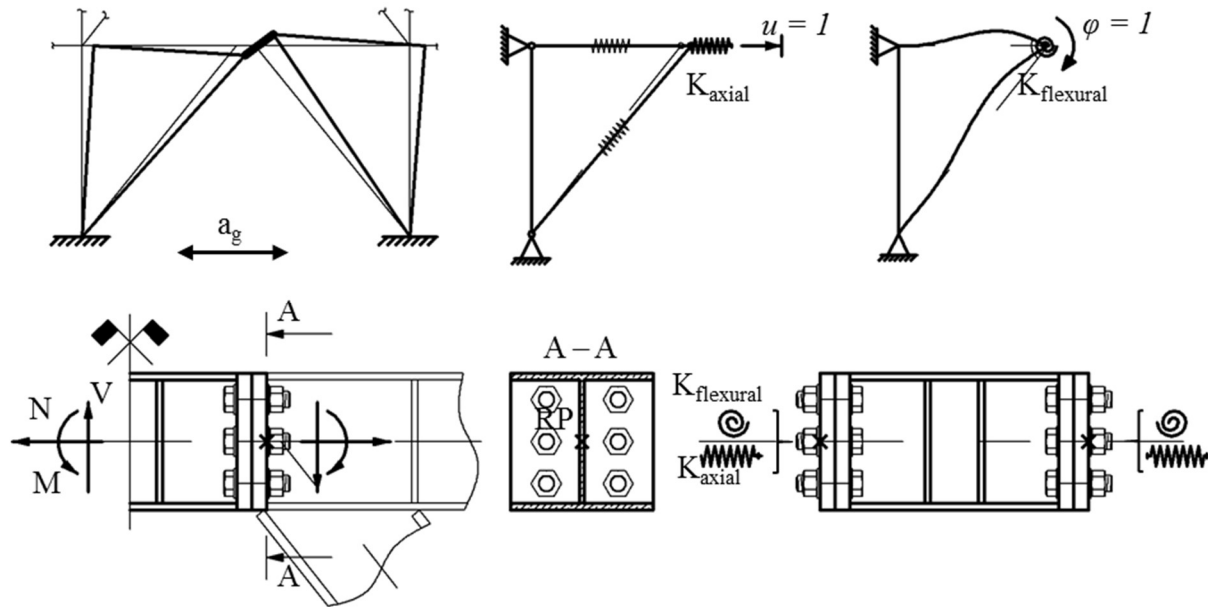


Figure 26. Modelling of deformable spring boundary condition [38]

CHAPTER IV – THE NUMERICAL MODEL ASSUMPTIONS AND VALIDATION

Twenty-five flush-end plate connections and 15 extended-end plates for short links are designed using the component method (Method 1) and verified according to Methods 2 and 3. This section discusses the modelling process and assumptions made for the numerical analysis of the designed links.

Geometry

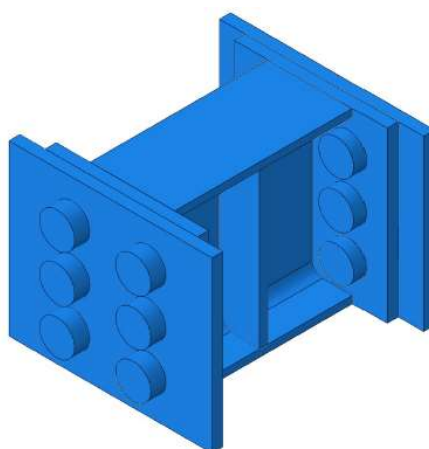


Figure 27. IPE200 ($e/e_s=0.5$) as modelled in Abaqus

All link assemblies are drawn using AutoCAD 2015 and subsequently imported to Abaqus 6.14. The numerical model is composed of the link profile, intermediate web stiffeners, end plates on the link side and beam sides, and bolts. As full penetration welds are used for link-to-plate and link-to-stiffener connections, they are not considered in the model and tie constraints are used for these surfaces. To simplify the analysis and further reduce the tie interactions that need to be defined, the link profile and intermediate web stiffeners are modelled as one part.

Units

Since Abaqus doesn't work with units, the following are used throughout the numerical modelling process to avoid inconsistencies.

	Length	Force	Stress	Young's Modulus	Density
<i>Unit</i>	mm	N	MPa	MPa	kg/mm ³

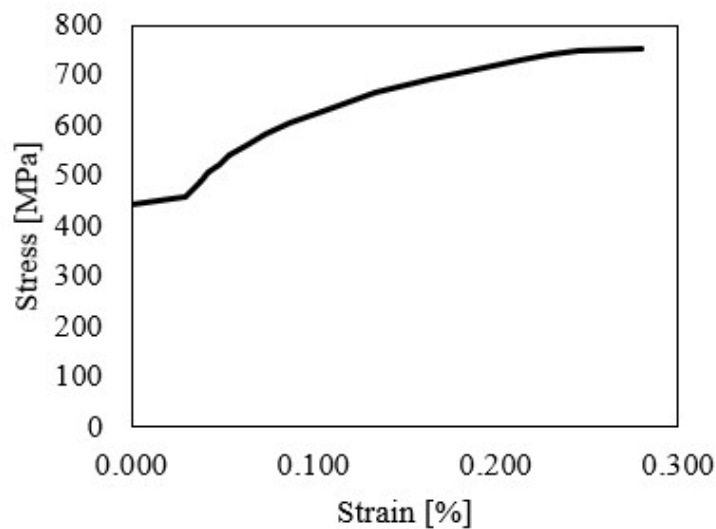
Table 5. Units used for numerical modelling in Abaqus

Material Property

Steel

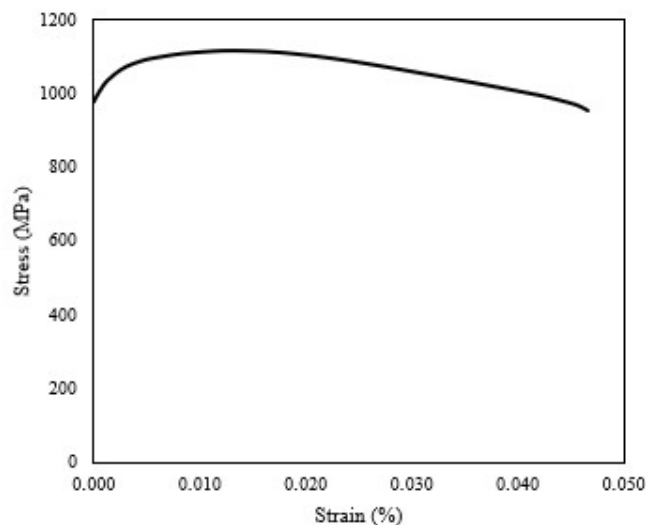
S355 steel is used for the link profiles, end plates, and intermediate web stiffeners. It has a density of $7.85 \times 10^{-6} \text{ kg/mm}^3$, Young's modulus of 210000 MPa and Poisson's ratio of 0.3. For the plastic properties of steel, combined nonlinear isotropic-kinematic hardening and half-cycle data type are selected. Since an overstrength factor of 1.25 is considered in the design and analytical checks, the properties introduced in Abaqus are also scaled up with this factor.

S355 Stress-strain curve $\gamma_{ov}=1.25$



Bolts

Stress-strain curve for M22 gr.12.9



Similarly, the density of the bolt is $7.85 \times 10^{-6} \text{ kg/mm}^3$. The nominal diameter is modelled but the actual diameter is reduced due to the threads. To account for this, the strength of the bolt materials is scaled with the ratio between the nominal area and net effective area of the shank (A_{nom}/A_s), as shown in the graph above. The threaded portion also causes a reduction in the bolt stiffness calculated as follows:

$$E_{bolt} = \frac{E}{\chi}$$

$$\chi = \frac{K_{b,nom}}{K_{b,act}}$$

$$\frac{1}{K_b} = \frac{f d_b}{A_b E} + \frac{L_s}{A_b E} + \frac{L_{tg}}{A_{be} E} + \frac{f d_b}{A_{be} E}$$

where E – nominal modulus of elasticity (210000 MPa)

$K_{b,nom}$ – stiffness of the bolt as modelled

$K_{b,act}$ – actual stiffness of the bolt

f – stiffness correlation factor (0.55)

d_b – nominal diameter of the bolt

A_b – nominal area of the bolt shank

A_{be} – effective area of the threads

L_s - shank length of the bolt

L_{tg} - length of the threaded portion included in the bolt's grip

Step

Dynamic, implicit procedure is chosen for the step setting with a quasi-static load application. The model is loaded in two steps. Under the clamping step, the pretension force on the bolts are applied incrementally until the maximum bolt force specified is reached. In the loading step, the entire link assembly is loaded until the specified displacements are attained.

Interaction

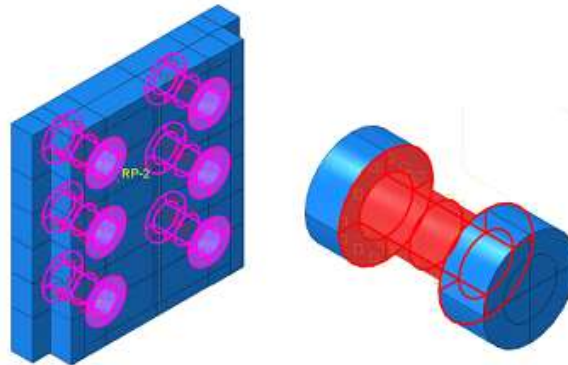


Figure 28. Interaction surfaces between bolts and end-plates

All the surfaces in contact between separate parts are defined to accurately correspond to their interaction behavior. For the tangential behavior of the interaction between bolts and end-plate, and between two adjacent end plates, Coulomb friction model is used. With the penalty friction formulation, a friction coefficient of 0.4 is specified. This option permits some relative motion between the surfaces in contact, but with a limited sliding magnitude depending on μ . For the normal behavior, hard contact is used for the pressure-overclosure relationship. This option minimizes the penetration of the slave surface into the master surface and prevents the transfer of tensile stress across the interface.

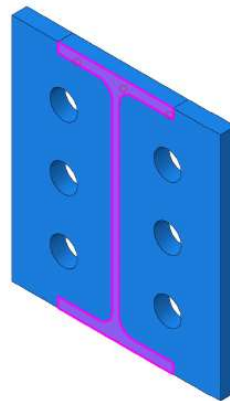
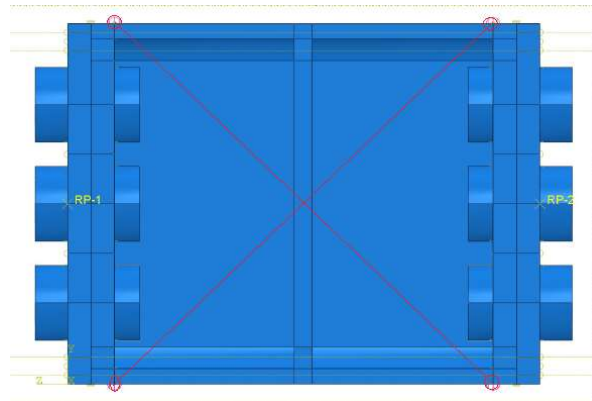


Figure 29. Tie constraint on the profile-plate interface

The surfaces in contact between the link profile and the end plates on the link side are modelled as ties as shown above, such that there is no relative motion between these surfaces.



To calculate the rotation of the link (γ_{link}), the displacements of the link's vertices are required. Two diagonal springs with stiffness of 1.0 are introduced to connect two vertices.

γ_{link} is then obtained through the following formula:

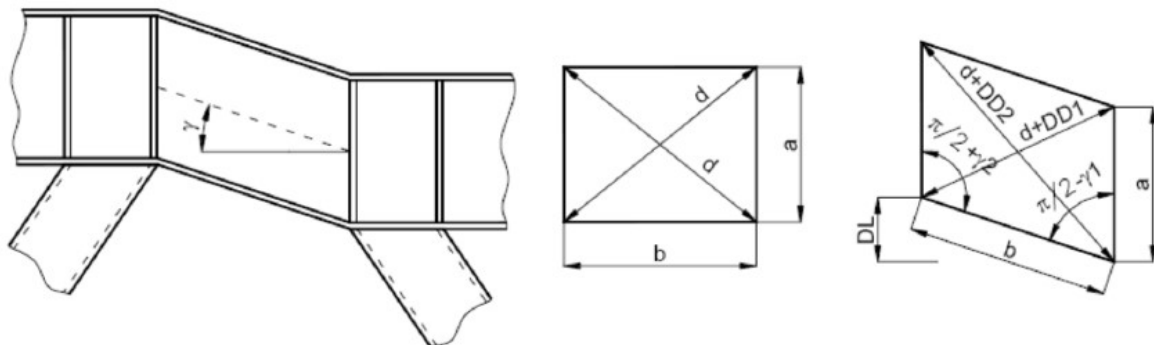


Figure 30. Geometry of obtaining the link rotation [5]

$$\gamma_{link} = \frac{\sqrt{a^2 + b^2} \cdot (DD2 - DD1)}{2ab}$$

Loads

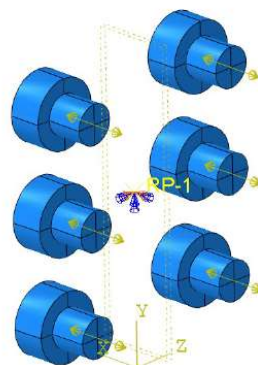


Figure 31. Pretension force on bolts

Pretension force is applied on each bolt through the Bolt Force option. It is calculated through:

$$P = 0.7A_s f_u$$

where P – pretension force on bolt

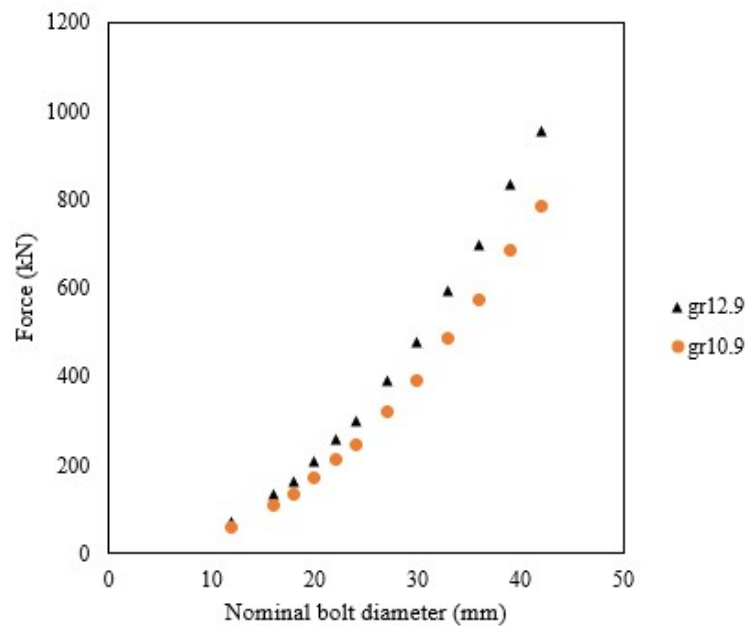
A_s – net area of the bolt cross-section

f_u – ultimate strength of the bolt (1000 MPa for gr10.9 and 1220 MPa for gr12.9)

Table 6. Pretension force for bolts

Bolt size	Pretension force for gr10.9 (kN)	Pretension force for gr12.9 (kN)
M12	59.01	71.99
M16	109.90	134.08
M18	134.40	163.97
M20	171.50	209.23
M22	212.10	258.76
M24	247.10	301.46
M27	321.30	391.99
M30	392.70	479.09
M33	485.80	592.68
M36	571.90	697.72
M39	683.20	833.50
M42	784.00	956.48

Pretension force on bolts



Boundary conditions

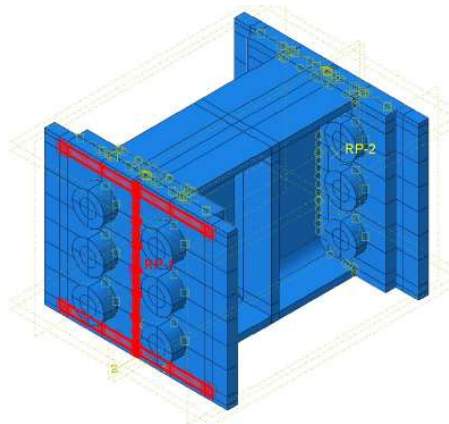


Figure 32. Rigid body constraint corresponding to HEA200 beam (IPE200 0.5 e_s link)

For FEP, a rigid body constraint with the cross-section of the beam is defined on the beam side of the end-plates. As a simplification, the curvature of the beam is neglected and the thickness of the web is considered constant.

Link	Beam	Link	Beam	Link	Beam
IPE200	HEA200	HEA200	HEB200	HEB200	HEM200
IPE300	HEA300	HEA300	HEB300	HEB300	HEM300
IPE400	HEA400	HEA400	HEB400	HEB400	HEM400
IPE500	HEA500	HEA500	HEB500	HEB500	HEM500
IPE600	HEA600	HEA600	HEB600	HEB600	HEM600

For EEP, there are two ways in which the corresponding beam is defined. First, a beam that spans the whole depth of the plate is chosen. However, this is not always applicable since for other cases, the flange of the beam will coincide with the bolts. For such cases, beam depths similar to those used for FEPs are used and rib stiffeners are added for the remaining depth, as shown in the figure below.

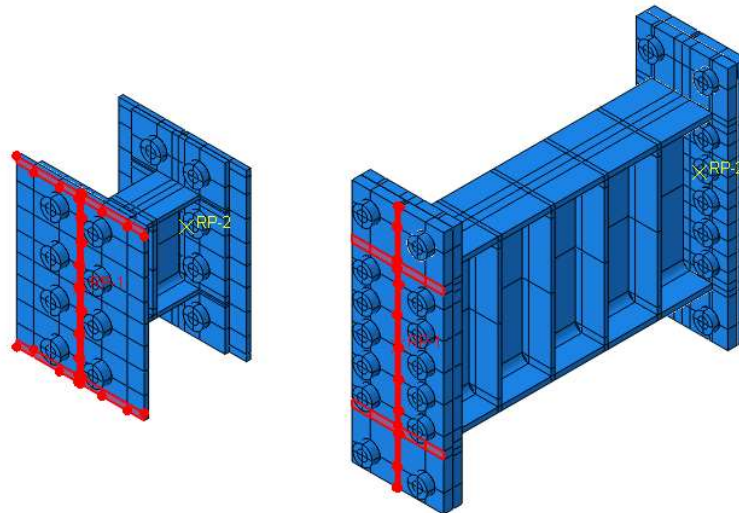


Figure 33. (Left) IPE200R05 link with a full-depth beam corresponding to HEA400; (Right) IPE500R1 link with HEA500 beam and rib stiffener on the remaining depth

The thickness of the rib stiffener is determined according to the American Institute of Steel Construction. According to this provision, the thickness of the stiffeners shall be greater than or equal to the beam web thickness when the beam and end-plate stiffeners have the same material strengths. In case of different material strengths, the thickness of the stiffener shall not be less than the ratio of between the yield stresses of the beam-to-stiffener, multiplied by the web thickness of the beam.

Two boundary conditions are considered: fully rigid and deformable. For the fully-rigid boundary condition, all degrees of freedom except for vertical displacement are blocked. To simulate the presence of the frame for the deformable boundary condition, rotational and axial stiffness are introduced as springs on the region corresponding to the beam. This has been previously calculated in a frame design with beams and bracings corresponding to each link. For axial deformation, the degree of freedom along the axis of the link is released while for flexural deformation, in-plane rotation is allowed. For the loading step, the assembly is allowed to have a displacement corresponding to a link rotation of 10%.

Element type

All numerical models are meshed using 3D solid elements. The finite element is of type C3D8R (8-node brick linear element with one integration point in the middle of the element). To prevent shear locking on thin elements (web, flange, end plates, stiffeners), four elements per thickness are applied. To verify the mesh, the mesh verification option of Abaqus is employed and the meshed model is accepted when the error is less than 5%.

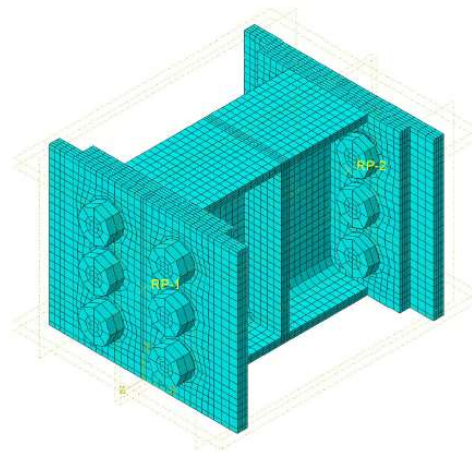
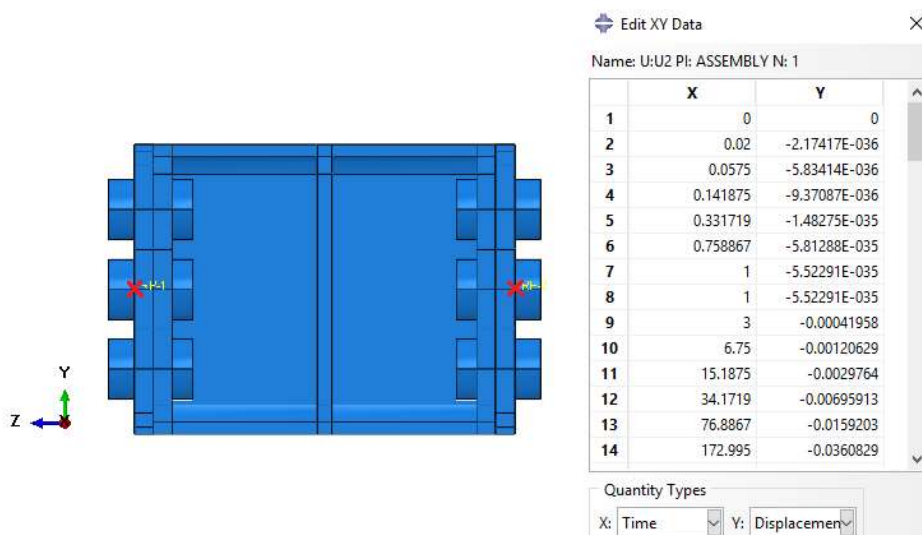


Figure 34. Meshed model of IPE200 0.5es

Output

The outputs from Abaqus, extracted as explained below, provide the data for shear and axial forces, as well as for link and total assembly rotations.

The displacement along y-axis (U2) of the reference point is used to calculate for the total rotation of the link-connection assembly $\gamma_{total} = \frac{U2}{L_{assembly}/2}$, where $L_{assembly}$ is the total length of the link and end plates on both sides.



The deformations of the two diagonal springs for the link rotation's calculation are the E11 components obtained from ODB Field Output – Element Nodal. The rotation of the is calculated using equation[] previously shown. Shear and axial forces are obtained from the cross-section of the link as force components 3 and 1, respectively.

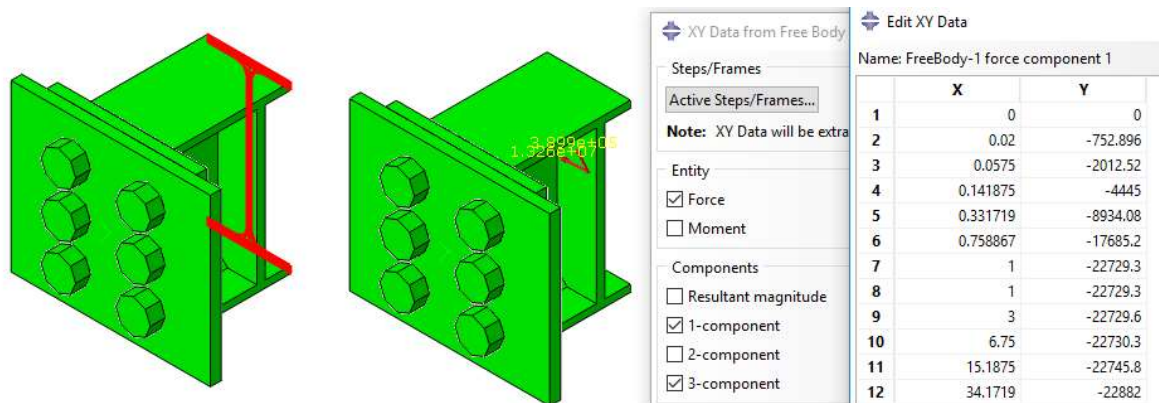
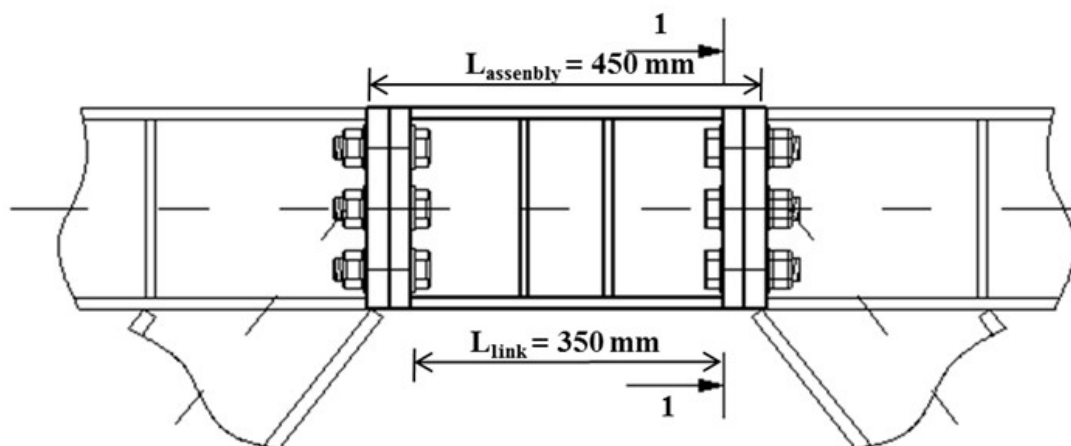


Figure 35. Free body cut of the link's cross-section to obtain shear and axial forces

Calibration of the links

To validate the modelling assumptions, links with geometry shown below are modelled in Abaqus 6.14 using the actual mechanical properties tested as part of the DUAREM research project and with the modelling assumptions presented above.

L4 corresponds to the link-connection assemblies located on the 1st and 2nd floor while L3 corresponds to those on the 3rd floor. L4 is subjected to two different displacement time histories namely S1 and S2, while L3 is subjected to S3.



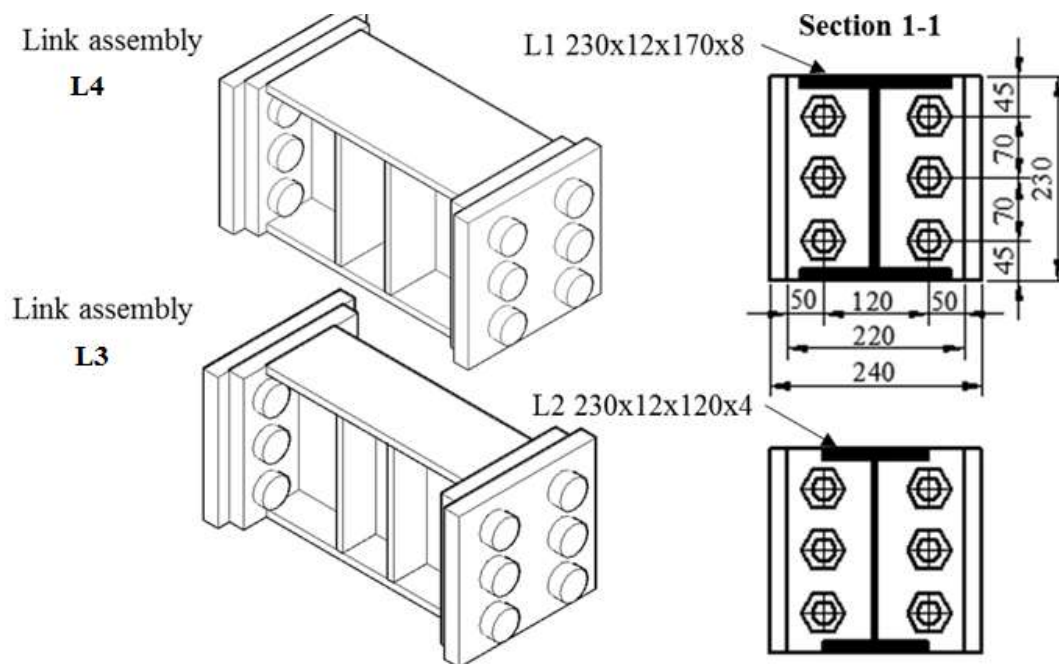


Figure 36. Geometry of links from calibration [38]

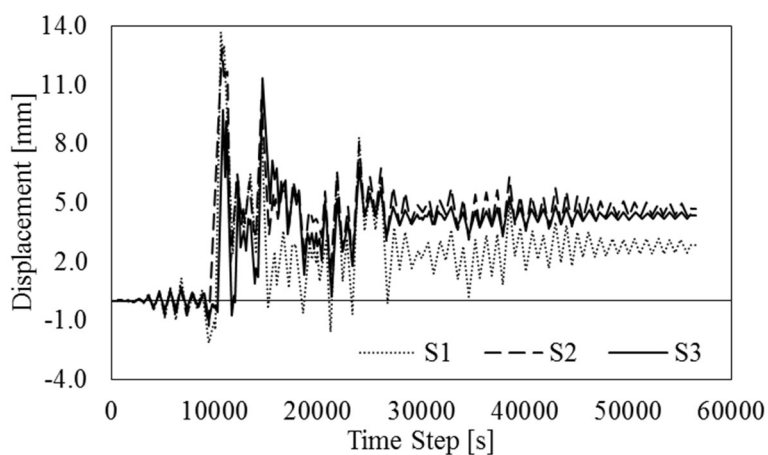


Figure 37. Displacement time histories applied to the links [38]

The cyclic responses of the assemblies are plotted below for both numerical and experimental tests. This confirms that the numerical modelled is an accurate representation of the actual link and the modelling assumptions made are justified.

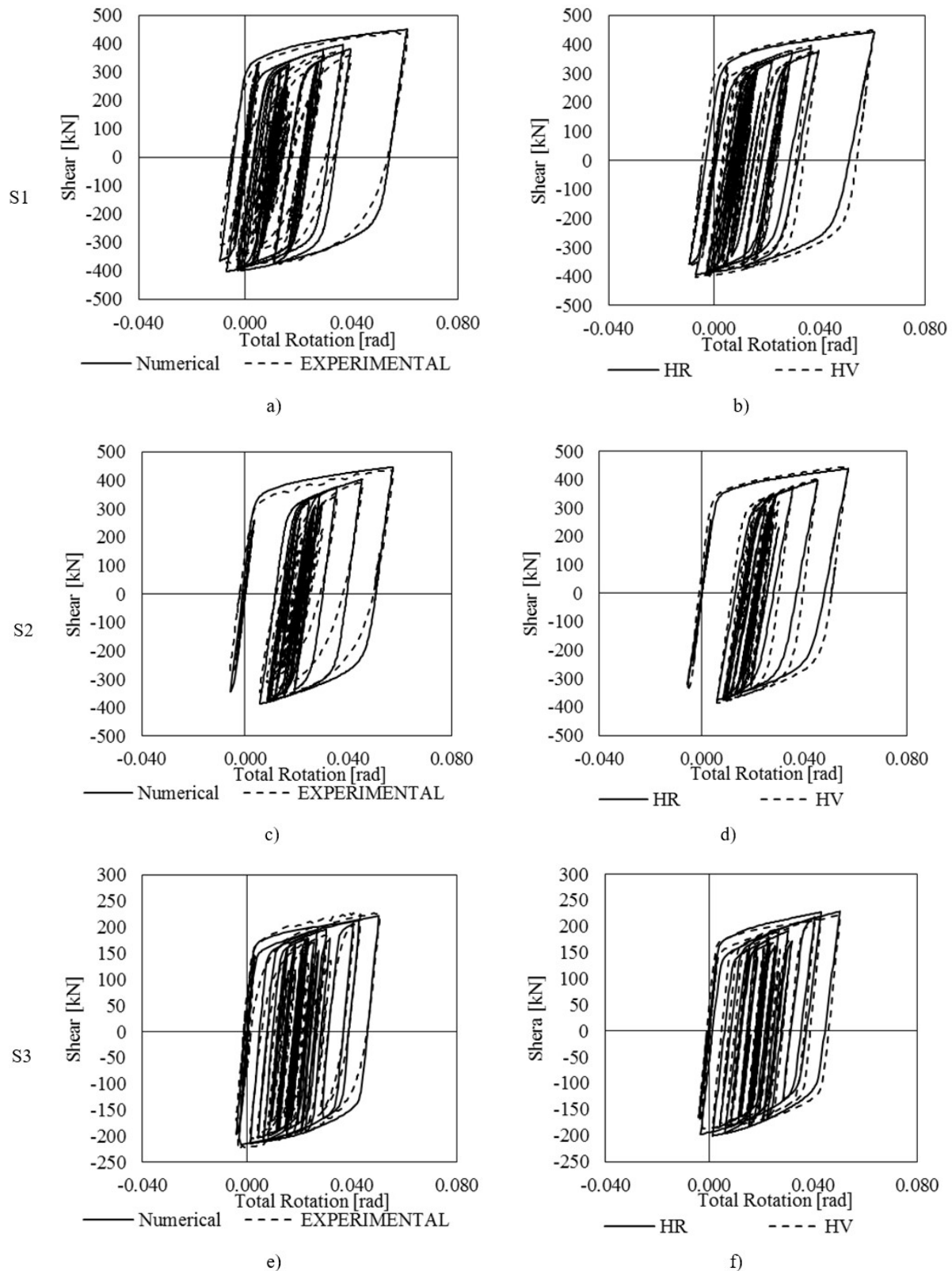


Figure 38. Cyclic response of the 3 link assemblies. Experimental and numerical comparison and the HR and HV numerical models comparison [38]

CHAPTER V. PARAMETRIC STUDY

This chapter discusses the parameters investigated within the study, the numerical analyses performed, results of the study and the conclusions derived from them.

To investigate the development of axial force in seismic links, numerical analyses have been performed using Abaqus 6.14. Two types of connections are modelled: flush-end plate and extended-end plate. Each profile type has five depths: 200, 300, 400, 500, and 600. All IPE profiles are used for three link lengths considered, namely $0.5e_s$, $0.75e_s$, and e_s while HEA and HEB profiles are only used for the shortest links with flush-end plate connections. In addition, all models are analyzed with two boundary conditions: the first neglecting the deformation of the frame by imposing fully rigid restraints at the face of the connection, hereafter referred to as fully rigid BC or FR BC, and the second one considering the frame's deformability by imposing springs with axial and rotational stiffness (deformable BC or Def BC). Lastly, all IPE profiles with FEP connections are also analyzed by considering S235 steel grade for the link and retaining S355 for the end plates. The results are used to investigate on the effect of material property on the axial forces.

Table 7. Models used for parametric analysis of seismic links

Link length	Flush-end plate			Extended-end plate
	IPE	HEA	HEB	IPE
$0.5e_s$	✓	✓	✓	✓
$0.75e_s$	✓			✓
e_s	✓			✓
Number of models	40			
Number of analyses performed	110			

Apart from the models created in this study and the calibrated links discussed in Chapter IV, the analysis also makes use of the data on shear overstrength and axial forces considering just the links. These models have been previously included in the study performed by **Zimbru et al [38]**.

Intermediate web stiffeners are not considered during the analytical verification but for the numerical analysis, they need to be included in the model. Seismic links are designed with intermediate web stiffeners to guarantee ductility and prevent buckling or fracture of the web

prior to the plastification of the link. EN 1998-1 6.8.2(10) provides the following guidelines in designing intermediate web stiffeners for short links:

- for a link rotation of 0.08 rad, the maximum interval of the stiffeners should not exceed $(30t_w - d/5)$
- intermediate web stiffeners should be full depth. For links that are less than 600 mm in depth d , stiffeners are required on only one side of the link web. For links that are 600mm in depth or greater, the stiffeners should be placed on both sides of the web
- the thickness of one-sided stiffeners should not be less than t_w or 10 mm, whichever is larger
- the width of the stiffener should not be less than $b/2 - t_w$

5.1 Investigation on the Flush-end plate connections

5.1.1 Analytical analysis

From the three methods of previously discussed in Chapter III, each link is designed to satisfy Method 1 and the same configuration is checked for Methods 2 and 3.

Method 1 – All assemblies with IPE and HEA profiles satisfy the first method of verification. On the other hand, no sufficient FEP connection could be designed for HEB profiles due to high flexural requirement and limitation on bolt configuration. Therefore, they are accepted with minimum exceedance from the limit (18% for M and 28% for V). Despite exceeding the limits for some methods of link verification, analyses are carried on considering that there may exist geometrical differences between the nominal values used in modelling and the actual configuration of once the links are fabricated. Additionally, comparing the results provides an insight on how each method considers the forces and possible overestimation.

The table below shows the ratio M_{Ed}/M_{jRd} for the link configurations.

Table 8. Design ratios for FEP

Link	$e/e_s=1.0$		$e/e_s=0.75$		$e/e_s=0.5$	
	$\frac{M_{Ed}}{M_{jRd}}$	$\frac{V_{Ed}}{V_{jRd}}$	$\frac{M_{Ed}}{M_{jRd}}$	$\frac{V_{Ed}}{V_{jRd}}$	$\frac{M_{Ed}}{M_{jRd}}$	$\frac{V_{Ed}}{V_{jRd}}$
IPE200	0.92	0.65	0.78	0.65	0.88	0.45
IPE300	0.95	0.85	0.92	0.32	0.96	0.46
IPE400	0.99	0.76	0.89	0.91	0.59	0.91
IPE500	0.95	0.80	0.75	0.80	0.67	0.81
IPE600	0.98	0.85	0.89	0.87	0.62	0.87
HEA200					0.97	0.59
HEA300					0.93	0.97
HEA400					0.97	0.78

HEA500					0.98	0.91
HEA600					0.97	0.74
HEB200					1.10	1.22
HEB300					0.99	1.28
HEB400					1.11	0.84
HEB500					1.09	0.96
HEB600					1.18	0.90

Method 2 – Since most of the connections are designed close to their bending limit and they are all subjected to significant axial forces, all design ratios for Method 2 are not satisfied.

Table 9. Design force to resistance ratio according to Method 2 (FEP)

Link	e/e_s=1.0		e/e_s=0.75		e/e_s=0.5	
	$\frac{M_{Ed}}{M_{jRd}} + \frac{N_{Ed}}{N_{jRd}}$	$\frac{V_{Ed}}{V_{jRd}}$	$\frac{M_{Ed}}{M_{jRd}} + \frac{N_{Ed}}{N_{jRd}}$	$\frac{V_{Ed}}{V_{jRd}}$	$\frac{M_{Ed}}{M_{jRd}} + \frac{N_{Ed}}{N_{jRd}}$	$\frac{V_{Ed}}{V_{jRd}}$
IPE200	1.30	1.49	1.41	1.49	1.54	1.49
IPE300	1.22	1.06	1.36	1.06	1.74	1.54
IPE400	1.47	1.51	1.60	1.87	1.39	1.87
IPE500	1.41	1.60	1.41	1.60	1.42	2.25
IPE600	1.46	1.57	1.53	2.16	1.36	2.16
HEA200					2.22	1.40
HEA300					1.76	1.21
HEA400					2.22	1.76
HEA500					2.32	1.82
HEA600					2.10	2.07
HEB200					1.92	1.25
HEB300					2.13	1.33
HEB400					2.26	1.91
HEB500					2.21	1.94
HEB600					2.15	1.99

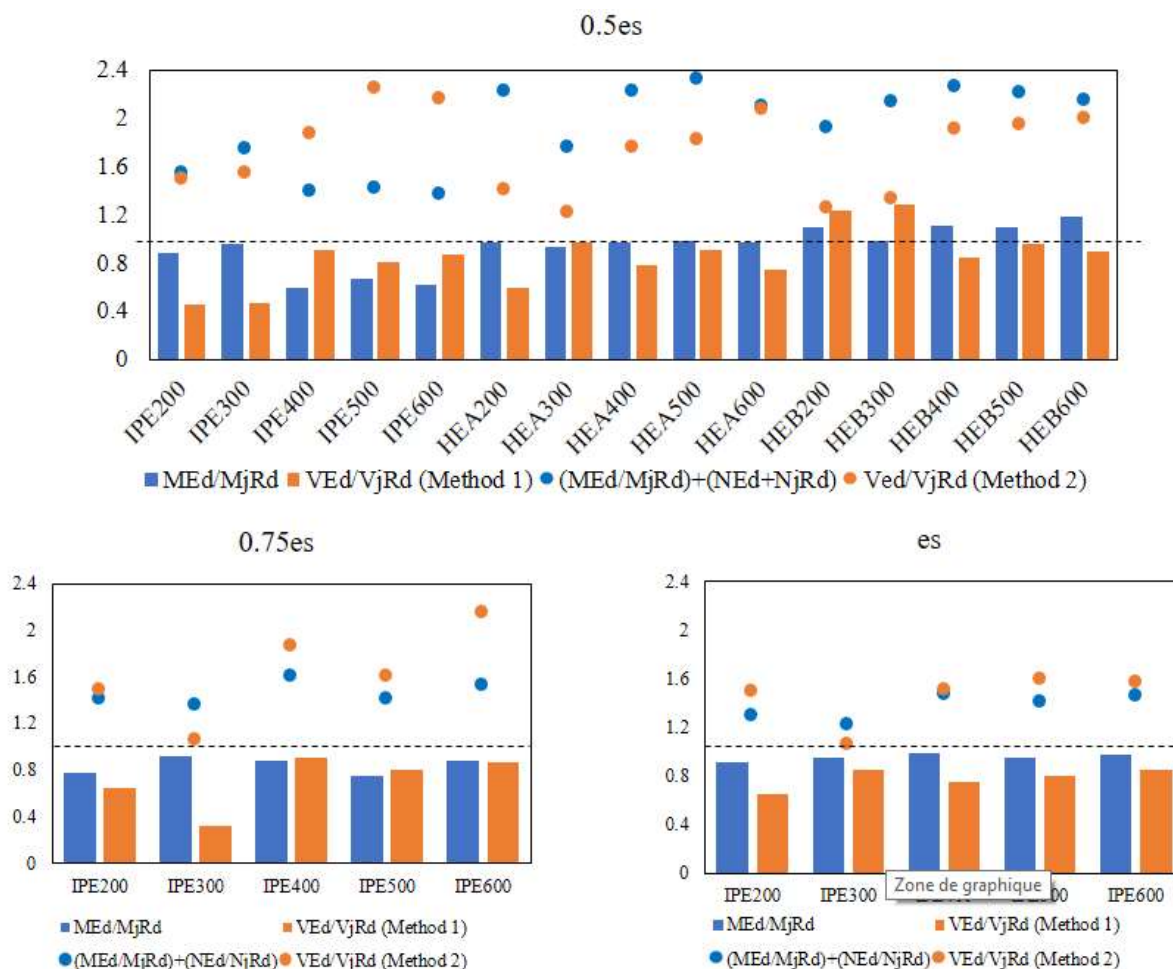
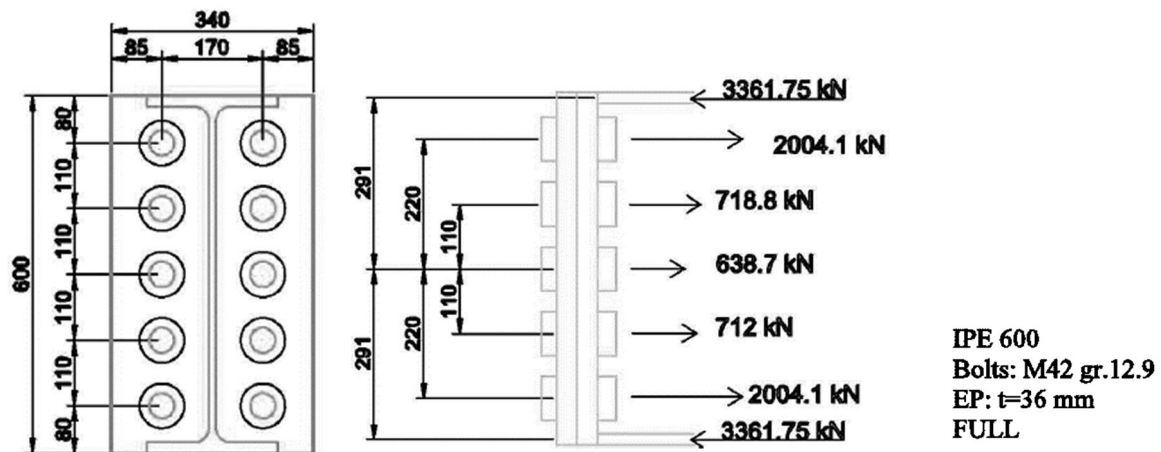


Figure 39. Design ratios for FEP assemblies

Method 3 - For this method, the M-N interaction curve for each link configuration is built. To demonstrate the process, IPE600 with $e/e_s=1.0$ is used. The assembly is divided along its axis of symmetry and the lever arms are referenced from this axis. Axial forces considered include the top and bottom flanges of the beam in compression and the bolt rows in tension. To obtain the points of the curve, the neutral axis is considered in different locations and the corresponding axial forces and bending moments are calculated. The succeeding values presented are based on γ_{M2} of 1.0.



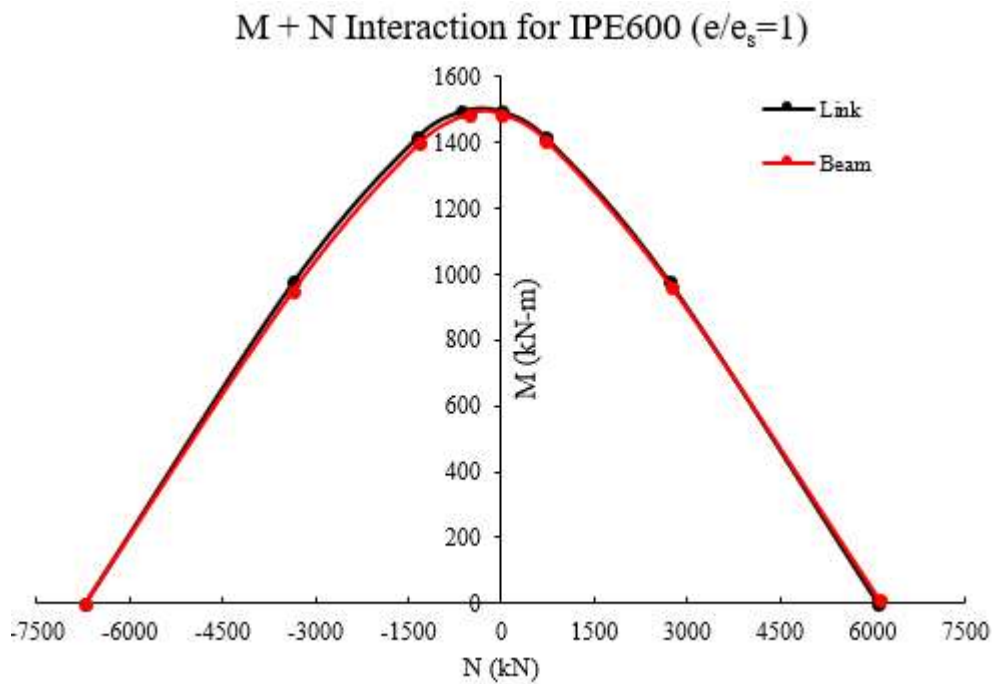
	F_{beam} (kN)	Z_{beam} (mm)	F_{link} (kN)	Z_{link} (mm)
$F_{c,fb,Rd}$	3361.75	282.5	3361.75	290.5
F1	2031.7	220	2004.1	220
F2	810.4	110	718.8	110
F3	519.5	0	638.7	0
F4	717	-110	712	-110
F5	2031.7	-220	2004.1	-220

- a – NA at the top edge (top and bottom flanges in compression)
- b – NA between top flange and BR1 (bottom flange in compression)
- c – NA between BR1 and BR2 (bottom flange in compression and BR1 in tension)
- d – NA between BR2 and BR3 (bottom flange in compression, BR1 BR2 in tension)
- e – NA between BR3 and BR4 (bottom flange in compression, BR1 BR2 BR3 in tension)
- f – NA between BR4 and BR5 (bottom flange in compression, BR1 BR2 BR3 BR4 in tension)
- g – NA between BR5 and bottom flange (bottom flange in compression, all bolt rows in tension)
- h – NA at the bottom edge (all bolt rows in tension)

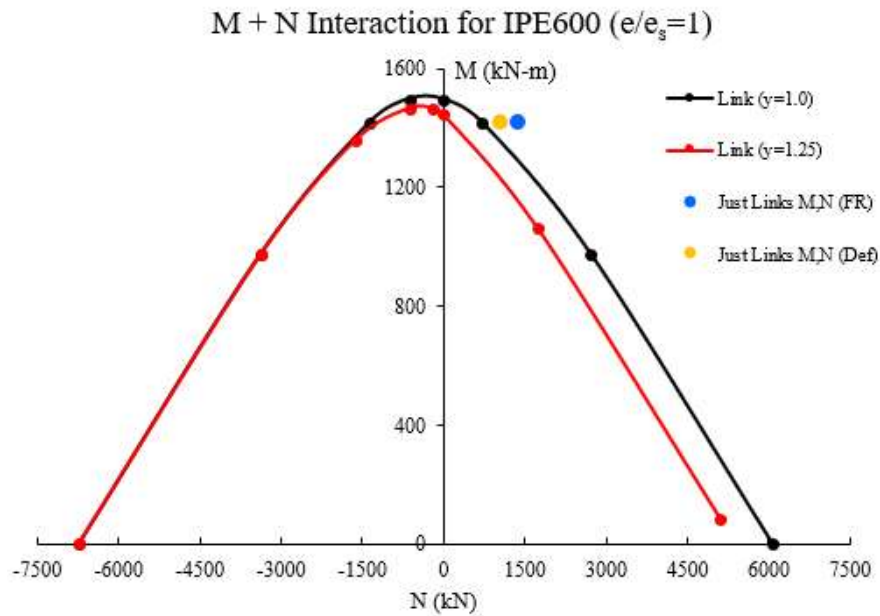
The first point of the curve represents the maximum negative axial force on the joint associated to zero bending moment, which occurs when NA is at the top edge. This corresponds to both beam flanges in compression (-6723.49 kN, 0 kNm). At point B, only the bottom flange is in compression so the axial force is -3361.75 kN and the corresponding bending moment is obtained by multiplying it with its lever arm, 290.5mm, resulting to 976.59 kNm. At point C, the first bolt row is now in tension so the axial force is (-3361.75 + 2004.1 = -1357.65 kN) and the bending moment is (3361.75 * 290.5 + 2004.1 * 220 = 1417.49 kNm). The remaining points are obtained by considering the resistance of the succeeding bolt rows. For bolt rows in

compression in which the resultant force is negative, the minimum positive resistance is used.
The same process is done on the beam side and the results are plotted below.

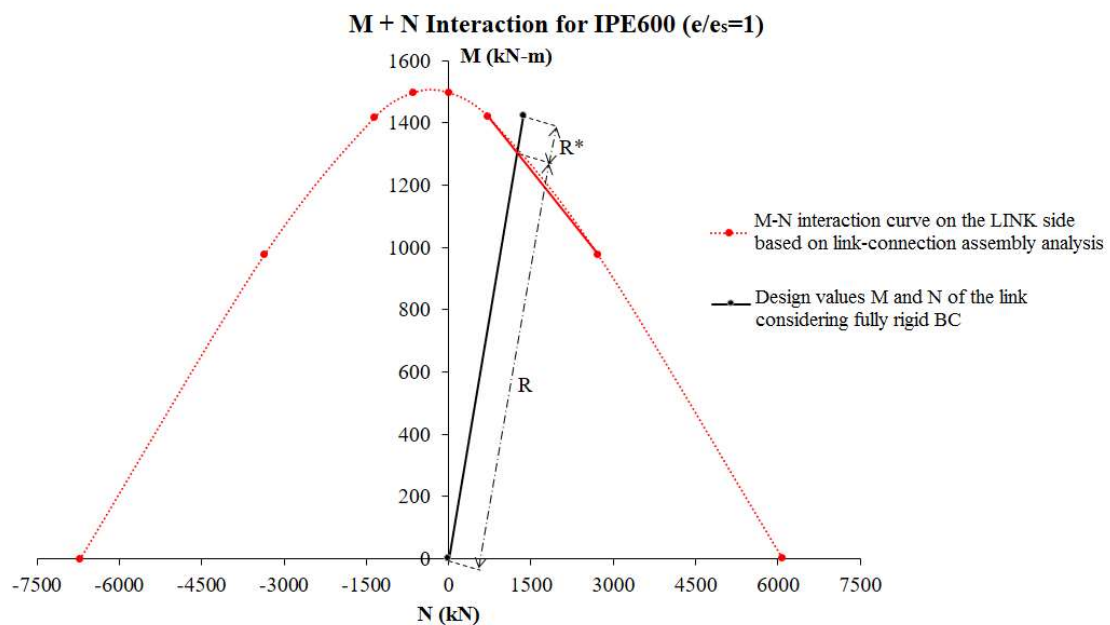
Link	a	B	c	d	e	f	g	h
<i>N (kN)</i>	-6723.49	-3361.75	-1357.65	-638.85	-0.15	711.85	2715.95	6077.70
<i>M (kNm)</i>	0.00	976.59	1417.49	1496.56	1496.56	1418.24	977.34	0.75
Beam	a	B	c	d	e	f	g	h
<i>N(kN)</i>	-6723.49	-3361.75	-1330.05	-519.65	-0.15	716.85	2748.55	6110.30
<i>M (kNm)</i>	0.00	949.69	1396.67	1485.81	1485.81	1406.94	959.97	10.27



To observe the effect of γ_{M2} , the curve below shows that using γ_{M2} of 1.0 instead of 1.25 only causes a gradual shift of the MN curve. This can be attributed to the governing mode of failure of the bolt rows. At Mode 2, failure is characterized by the combined yielding of the flange and failure of the bolts, with only the latter influenced by γ_{M2} .

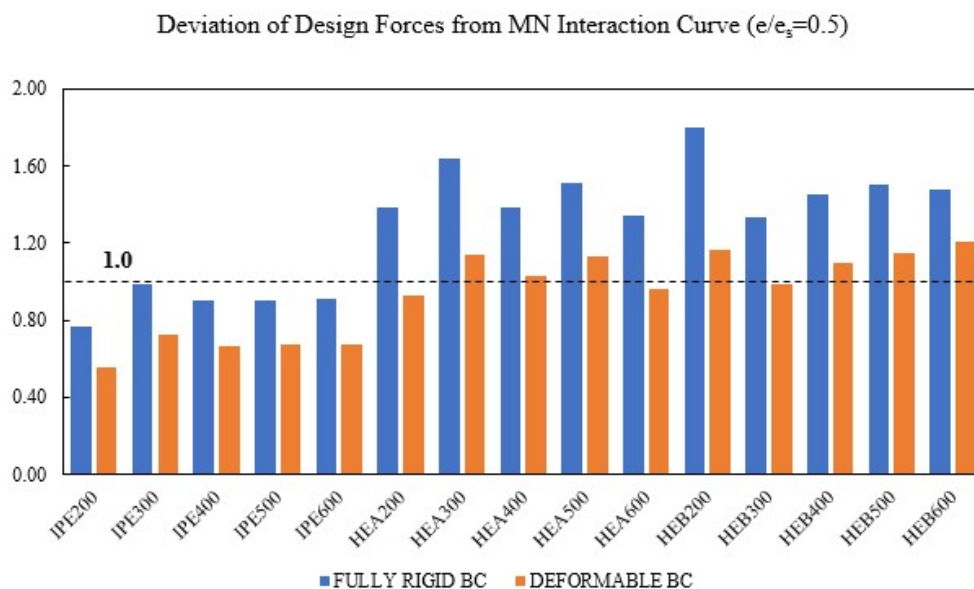
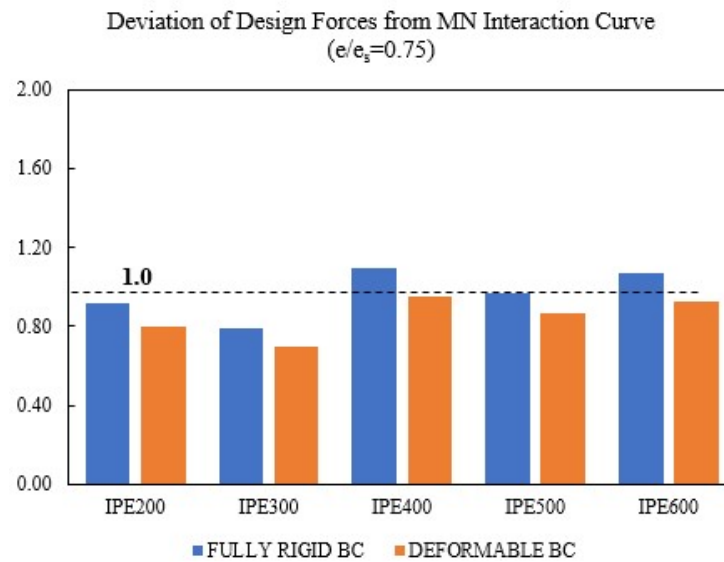
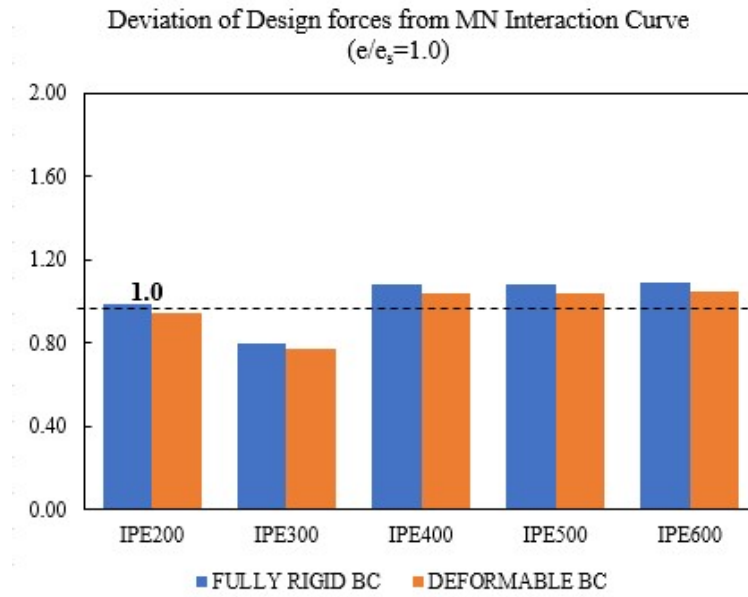


The next step is to determine the deviation of the design forces N_{Ed} and M_{Ed} from the interaction curve. To do this, two intersecting lines are considered: (1) the line where the design forces will intersect with the curve upon its projection from the origin (2) the line formed by the two relevant points in the M-N interaction curve. The intersection points of these two lines are calculated based from the equations of the line.



The same method is performed for the other joints and the results are shown below.

$e/e_s = 1.0$					
LINK	FULLY RIGID BC			DEFORMABLE BC	
	M_{Ed}/M_{jRd}	N_{Ed}/N_{jRd}	$(R+R^*)/R$	N_{Ed}/N_{jRd}	$(R+R^*)/R$
IPE200	0.92	0.38	0.99	0.32	0.94
IPE300	0.95	0.27	0.80	0.20	0.77
IPE400	0.99	0.47	1.08	0.35	1.04
IPE500	0.95	0.46	1.08	0.35	1.04
IPE600	0.98	0.47	1.09	0.36	1.05
$e/e_s = 0.75$					
LINK	FULLY RIGID BC			DEFORMABLE BC	
	M_{Ed}/M_{jRd}	N_{Ed}/N_{jRd}	$(R+R^*)/R$	N_{Ed}/N_{jRd}	$(R+R^*)/R$
IPE200	0.78	0.63	0.92	0.2859	0.80
IPE300	0.83	0.45	0.79	0.2398	0.70
IPE400	0.89	0.71	1.10	0.4168	0.95
IPE500	0.75	0.66	0.97	0.4172	0.87
IPE600	0.90	0.63	1.07	0.3889	0.93
$e/e_s = 0.5$					
LINK	FULLY RIGID BC			DEFORMABLE BC	
	M_{Ed}/M_{jRd}	N_{Ed}/N_{jRd}	$(R+R^*)/R$	N_{Ed}/N_{jRd}	$(R+R^*)/R$
IPE200	0.88	0.66	0.76	0.19	0.56
IPE300	0.96	0.78	0.98	0.27	0.72
IPE400	0.59	0.80	0.90	0.33	0.67
IPE500	0.67	0.75	0.90	0.34	0.68
IPE600	0.62	0.75	0.91	0.33	0.68
HEA200	0.97	1.25	1.39	0.39	0.92
HEA300	0.93	0.83	1.64	0.34	1.14
HEA400	0.97	1.25	1.39	0.50	1.03
HEA500	0.98	1.33	1.51	0.62	1.13
HEA600	0.97	1.13	1.34	0.41	0.96
HEB200	0.99	0.92	1.80	0.35	1.17
HEB300	0.92	1.21	1.33	0.58	0.99
HEB400	0.99	1.27	1.45	0.61	1.10
HEB500	0.98	1.23	1.50	0.61	1.15
HEB600	0.98	1.17	1.48	0.61	1.21



For longer links ($e/e_s=1.0$), the deviation of the design forces at fully rigid BCs are limited to 1.09 when the M_{Ed}/M_{jRd} ratios are as close to 1.0 as possible. Higher axial forces develop on shorter links so links with $e/e_s=0.5$ have the highest deviation, reaching 1.8 for M_{Ed}/M_{jRd} of 0.99. All IPE links with $e/e_s=0.5$ have design forces within the M-N curve while HEA and HEB profiles have ratios significantly higher than 1.0.

Comparing the results from the fully rigid boundary conditions with the deformable springs, there is a significant reduction in the axial force and consequently, in the deviation of the design forces from the M-N curve. The average decrease is 6% for $e/e_s=1.0$, 12% for $e/e_s=0.75$ and 27% for $e/e_s=0.5$.

5.1.2 Numerical analysis

Shear overstrength

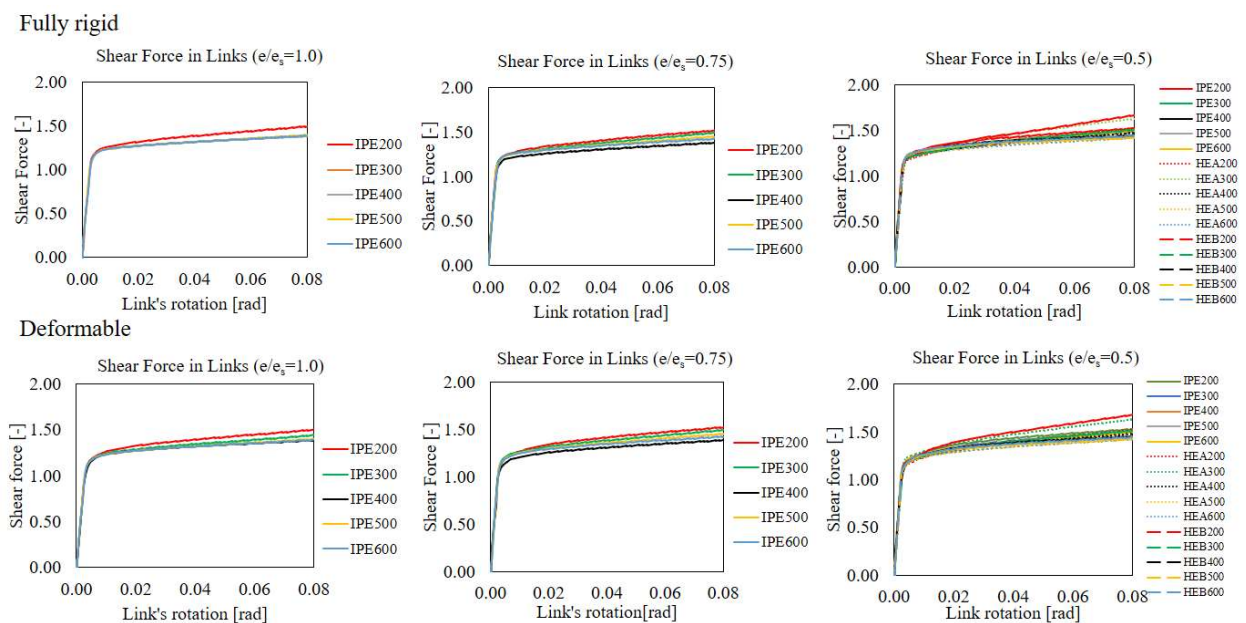


Figure 40. Shear response of FEP assemblies modelled

From the graphs shown above, it can be seen that different seismic links have identical response in the elastic region. When intermediate web stiffeners are added, the shear force at which the seismic link yields increases since buckling of the web is prevented. Since all web stiffeners are designed as prescribed by the Eurocode with a maximum tolerance of 6 mm, the links reach their full plastic capacity.

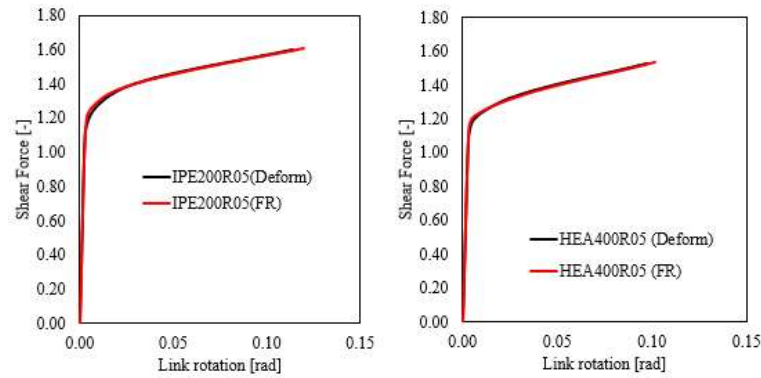


Figure 41. Shear response considering different boundary conditions

The shear response of link is independent from boundary conditions. Comparing the results for full restraints and deformable springs for the same assembly, all links have similar response as shown in Fig.41.

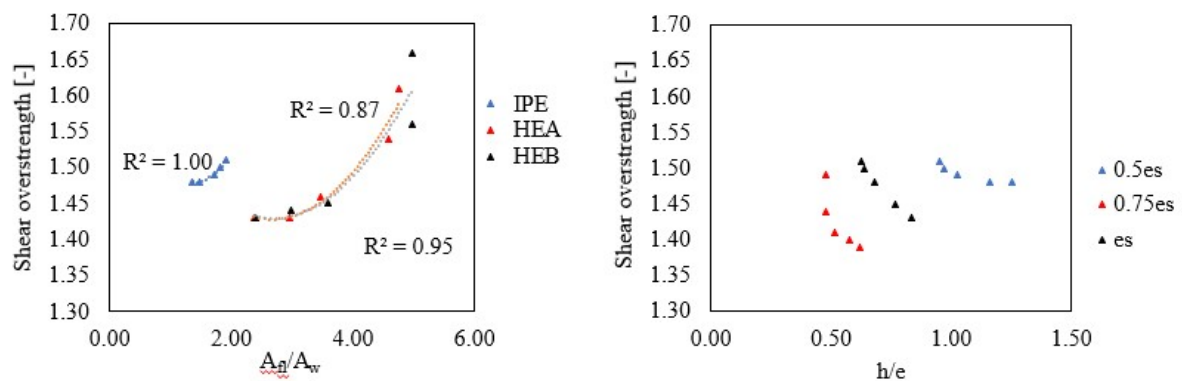


Figure 42. (Left) Shear overstrength of 0.5e_s links at 8% link rotation vs. A_{fl}/A_w ; (Right) Shear overstrength at 8% link rotation vs. depth-link length ratio

Fig.42 shows the relationship of shear overstrength with flange-web ratio and depth-link length ratio. For short links (0.5e_s), more compact sections such as HEA and HEB profiles tend to develop higher shear overstrength. However, there are only slight differences in terms of average value (1.492 for HEA, 1.494 for HEA, and 1.508 for HEB). The graph shows that IPE profiles have precise values of shear overstrength while for HEA and HEB, they are scattered on a wider range. Additionally, it also shows that shear overstrength decreases as profile depth increases. On the other hand, the figure on the right shows that shear overstrength decreases for longer links. The average of 0.5e_s is 1.5, 1.46 for 0.75e_s and 1.42 for e_s, bringing an overall average of 1.48. For all the cases analyzed, the maximum shear overstrength is 1.66.

Axial force

For all analyses performed, most assemblies remain in compression beyond 8% link rotation. In general, the following factors have been observed to affect the development of axial force within the links:

- Boundary conditions (full restraints vs. deformable springs)
- Link length
- Strength of the connection
- Stiffness of the connection

Comparison of the response of the assembly (link + connection) for fully rigid and deformable boundary conditions

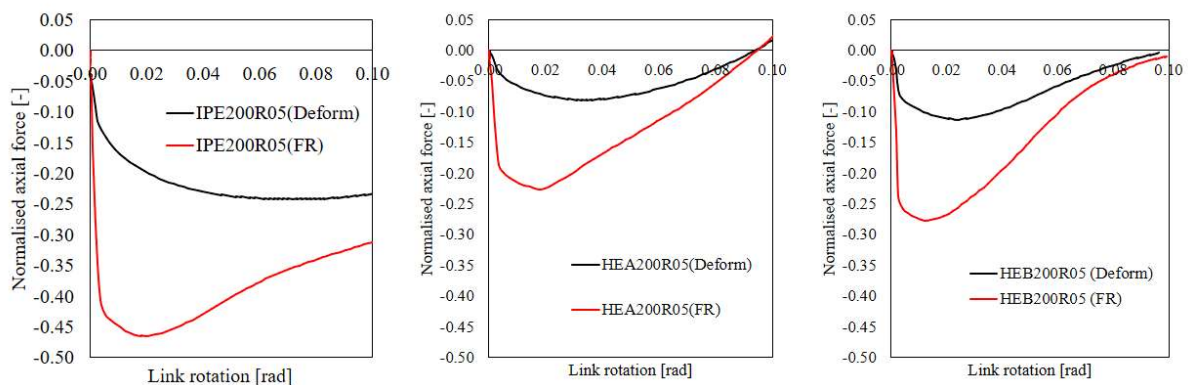


Figure 43. Difference in the development of axial force considering different boundary conditions

All assemblies showed significant increase in the compressive arch when fully rigid boundary conditions are imposed instead of deformable springs. The link rotation at which the maximum compression is reached is higher for deformable BCs. The axial force-link rotation curve is also more gradual, compared to steeper curves in rigid BC. The graphs below show the detailed comparison of compressive forces for all links.

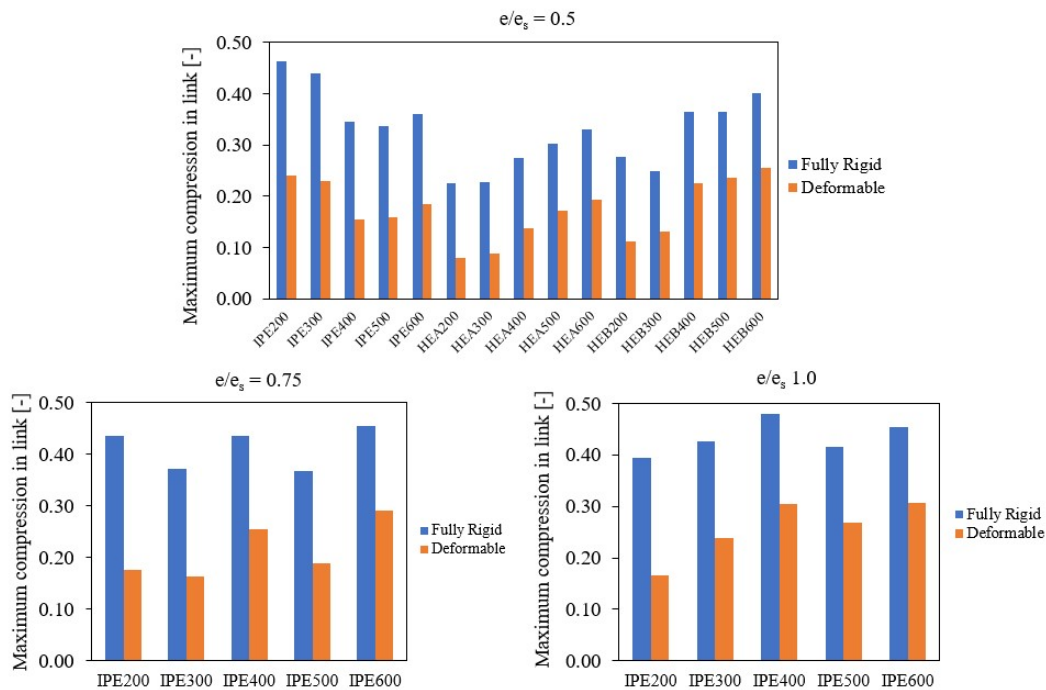


Figure 44. Difference in compressive force from fully rigid to deformable BC

There is an average decrease of 47% in compressive force when the same model is analyzed using fully rigid restraints and deformable springs. This decrease is more significant for shorter links, with an average of 49% for both $0.5e_s$ and $0.75e_s$, and 41% for e_s . This signifies that considering the deformability of the frame to which the link is connected greatly influences the behavior of the compressive arch, and therefore, the axial demand on links. Referring to Method 3 of link verification, the M-N curves generated are not perfectly symmetrical along the moment axis (y-axis), but are slightly translated to the left. This means that for the same magnitude of axial force, one in tension and the other in compression, the corresponding bending resistance under the presence of a tensile force is significantly lower than the bending resistance for a compressive force. In effect, compression in links does not have the same detrimental effect on the bending resistance compared with tension. Since all of the FEP assemblies remained in compression, these differences in compressive arches and tensile forces will be discussed further in EEP links as they mostly reached tension.

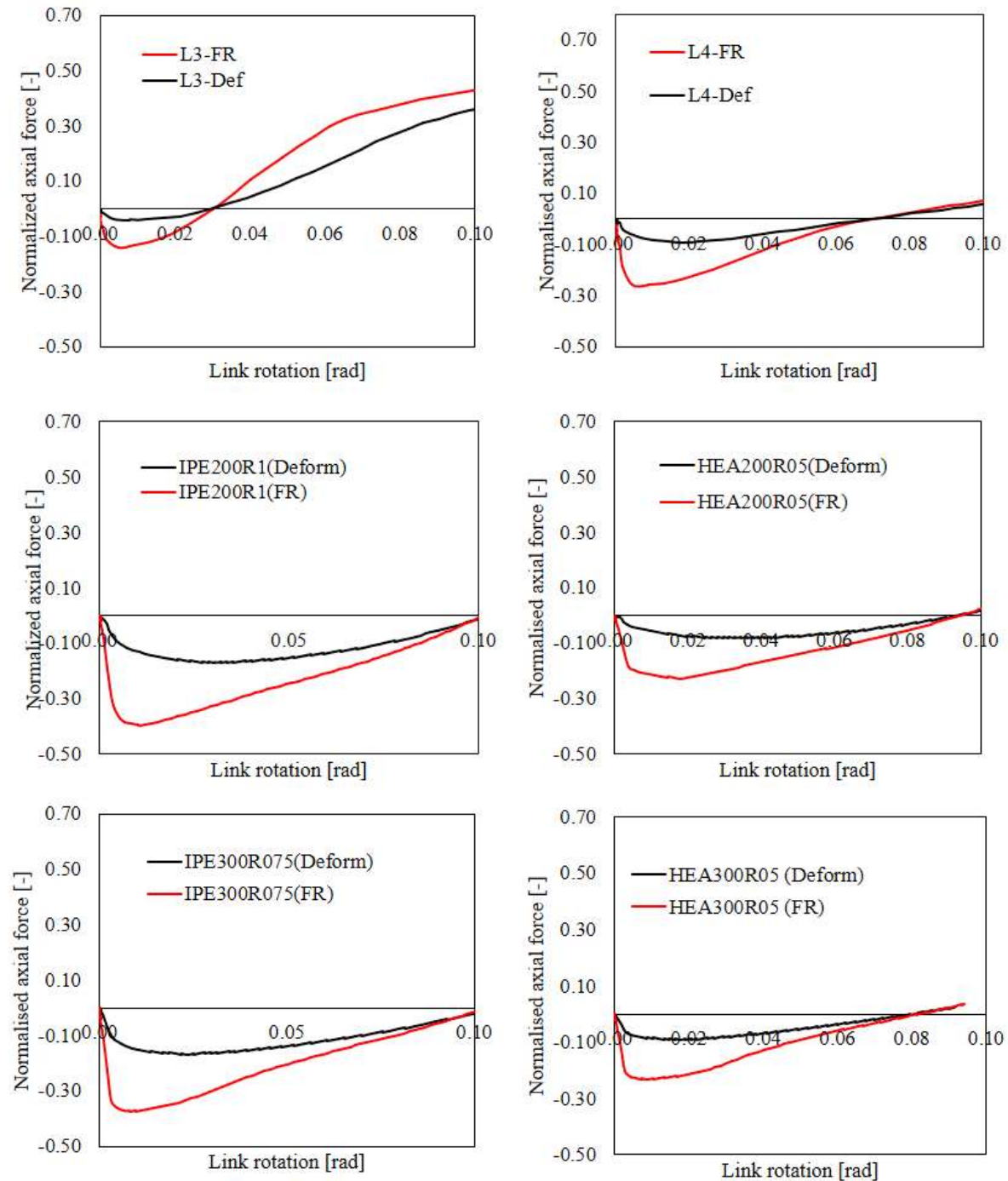


Figure 45. Comparison of axial force considering FR and deformable springs for links that reached tension

Lastly, models that reached tension in between 8-10% link rotation are shown in Fig.45. Considering the same assembly, the difference in boundary conditions only causes a change in the area of the compressive arch due to increase in compression. However, the link rotation at which tension is reached remains the same.

Comparison of axial force developed in links alone and in assemblies

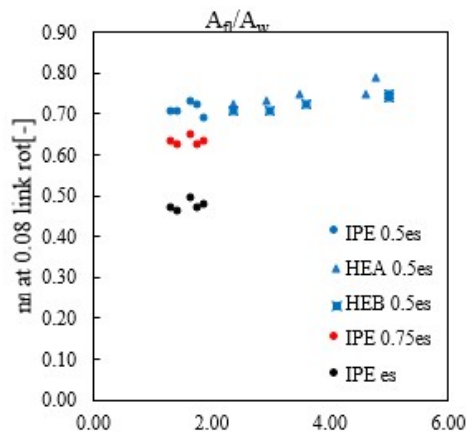


Figure 47. Axial force (tension) considering links only

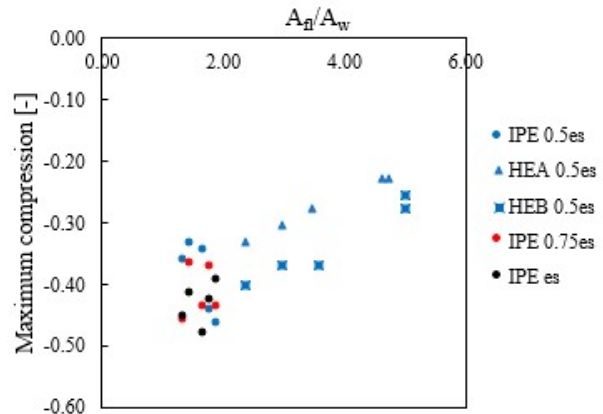


Figure 46. Axial force (compression) considering link + connection

Considering the models with only the links, the magnitude of the axial forces develop are higher compared to the assembly. It is noted that these are pure tensile forces and therefore, tension at 0.08 rad is also the maximum axial force ($N_{\max} = N_{0.08}$). On the other hand, the link-connection assemblies develop very high compressive forces. In most cases, they remain in compression beyond 0.08 rad, with the maximum compression occurring at a lower link rotation. For this case, N_{\max} does not correspond to $N_{0.08}$ but to the maximum compressive force.

Considering the links alone, it can be noticed that there is no significant difference among the axial forces in IPE and HE profiles under the same link ratio. The axial force therefore depends on the link length and it is observed to be highest for shortest links. This trend, however, is not easily seen when considering the axial forces within the assembly. Since the connection is now included in the analysis along with the link, the characteristics of the connection also affect the level of axial force.

Effect of stiffness and strength of connection on the axial force

To investigate further on the factors affecting the axial force in assemblies, IPE200 (0.75e_s) is used and other models are created by modifying its strength and stiffness.

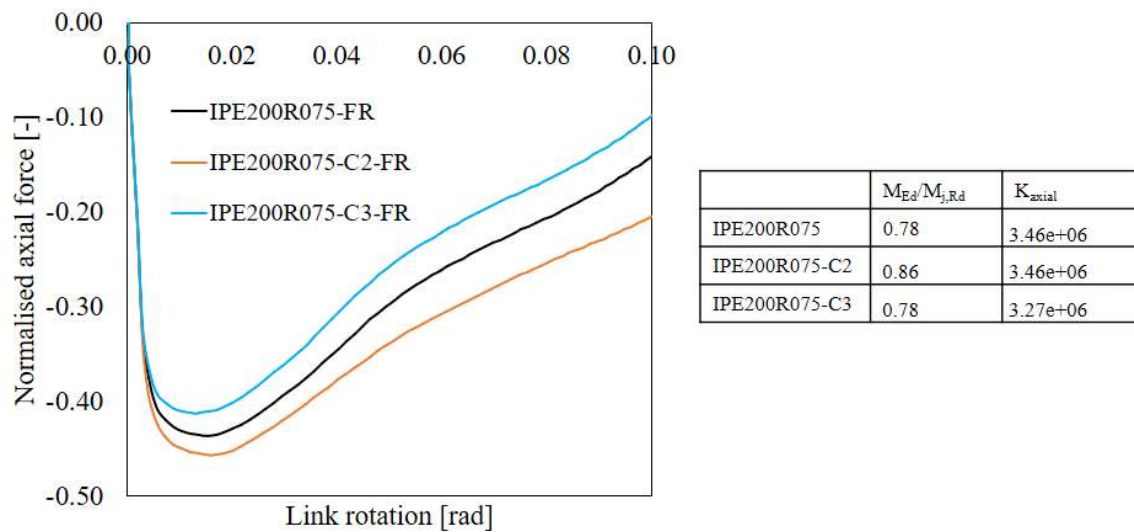


Figure 48. Comparison of different models for IPE200R075

The initial model of IPE200 has properties as shown in the table. IPE200R075-C2 is created by changing the grade of bolts used, thereby modifying the strength of the connection while keeping the axial stiffness constant. On the other hand, IPE200R075-C3, with the same strength but with different stiffness, is created by adjusting the position of the bolts while keeping all material properties constant.

Running the modified models and plotting the results, IPE200R075-C2 shows that considering the same stiffness, a weaker connection develops a larger compressive arch. Using IPE200R075-C3 to consider the same strength but different stiffness, the graph shows that a stiffer connection induces larger compressive arch as well. Comparing IPE200R075-C2 and IPE200R075-C3, the latter has smaller compressive arch since it is stronger and less stiff. It is also observed that all three responses have the same behavior and are almost simply scaled throughout the inelastic region.

The models above show that stiffness and strength both affect the behavior of the compressive arch. However, the models are designed such that both factors are causing the same effect (C3 is stronger and less stiff – smaller compressive arch with lower peak of compression; C2 is weaker and stiffer – larger compressive arch with higher peak of compression). Another model is designed to observe the effect when stiffness and strength are causing opposite effects.

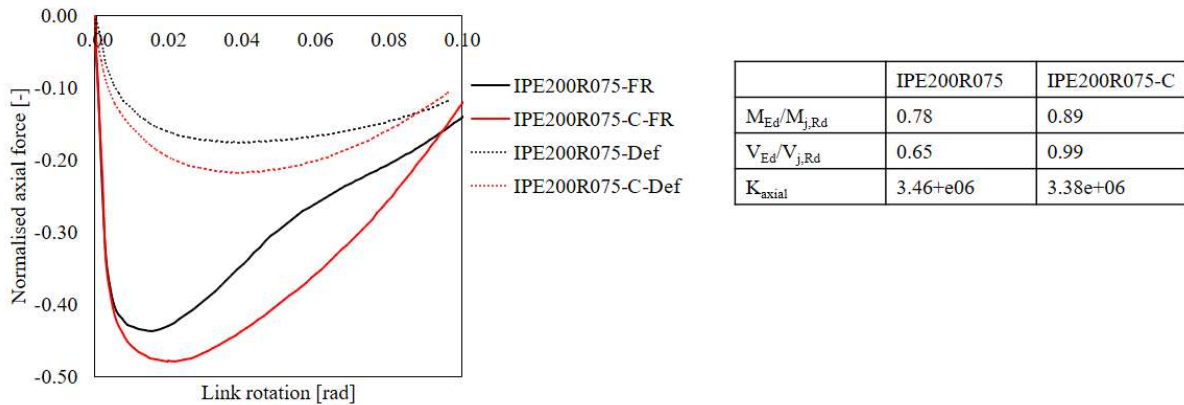


Figure 49. Effect of varying both stiffness and strength (IPE200R075)

Considering the same control model of IPE200 ($0.75e_s$), IPE200R075-C is designed to be weaker but less stiff. From the previous results, lower strength is expected to cause larger compressive arch while lower stiffness has been observed to cause a reduction. There is an increase in the compressive arch but the behavior of the curve changed. It becomes steeper and is expected to reach tension at an earlier link rotation compared to the control model. This is observed for both fully rigid and deformable BC.

Analysis of assemblies with shorter links (links from calibration L3 and L4)

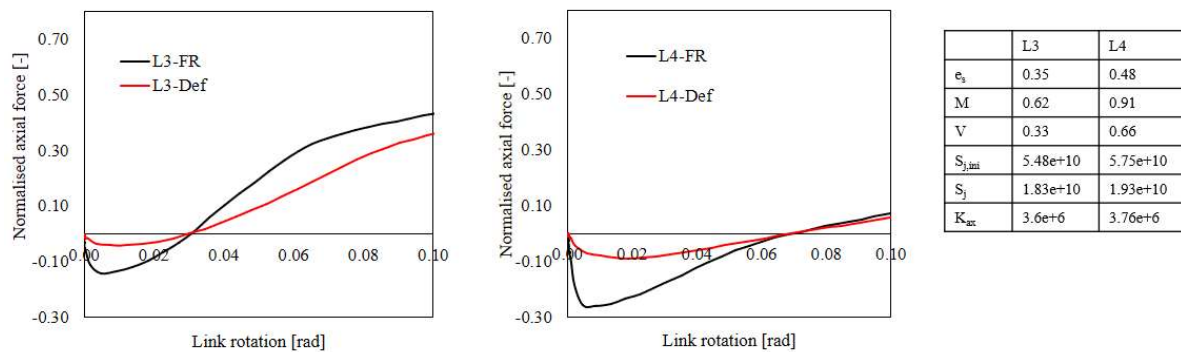


Figure 50. Development of axial force in L3 and L4

Links from calibration, L3 and L4, with lower length ratios are also analyzed for comparison. For L3, the assembly reaches tension at 0.03 rad and the maximum axial force is therefore the tension at 0.08 rad. On the other hand, L4 has a large compressive arch and is also subjected to small level of tensile force. Increase in flange's width brings an increase in $M_{pl,link}$ and $N_{pl,link,f}$. Since the configuration of the connection is not changed, the design ratios are also higher. For both links, changing the boundary condition has significant effect on the compressive arches

and level of axial force. In both cases, the tensile force at 0.08 rad considering deformable BC is 26% lower than what is developed with fully rigid BC.

Influence of material strength

Both of the calibrated links have significant tension at 0.08 rad – in contrast with the FEP links modelled that are subjected to pure compression at the same link rotation. Considering that the length ratio of the calibration link L4 is comparable to $0.5e_s$ links and its geometry to HEA200, a separate analysis is performed on the said link to understand its behavior. L4 is initially designed using S235 on the link web and S355 for the end plates and stiffeners, while the other models have S355 for both. Implementing both material configurations to L4, the results are plotted below.

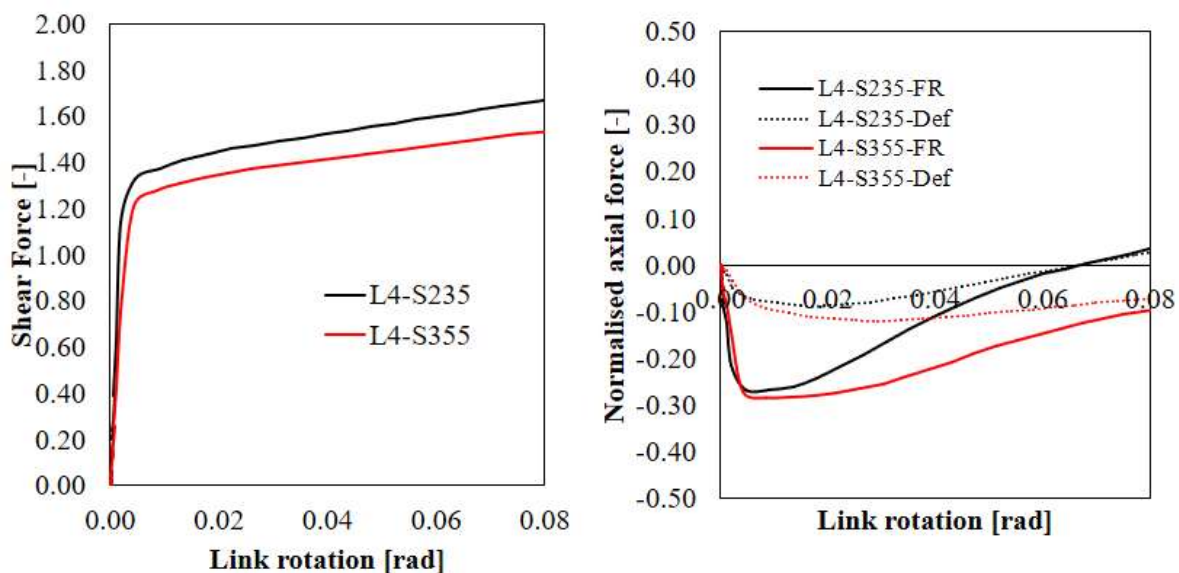


Figure 51. Shear and axial response of L4 considering two types of steel grade of link

The analysis of L4 using S355 for both the link and end plate yielded the same results observed for the FEP assemblies modelled in this study - it is subjected to pure compression within the scope of analysis, with a compressive arch wider than the one developed considering S235. In terms of shear overstrength, modifying the material property induced a shift of 8%, with a value of 1.67 for S235 and 1.53 for S355. The same method is performed for HEA200R05 and the comparison of its response using different link material properties are plotted below.

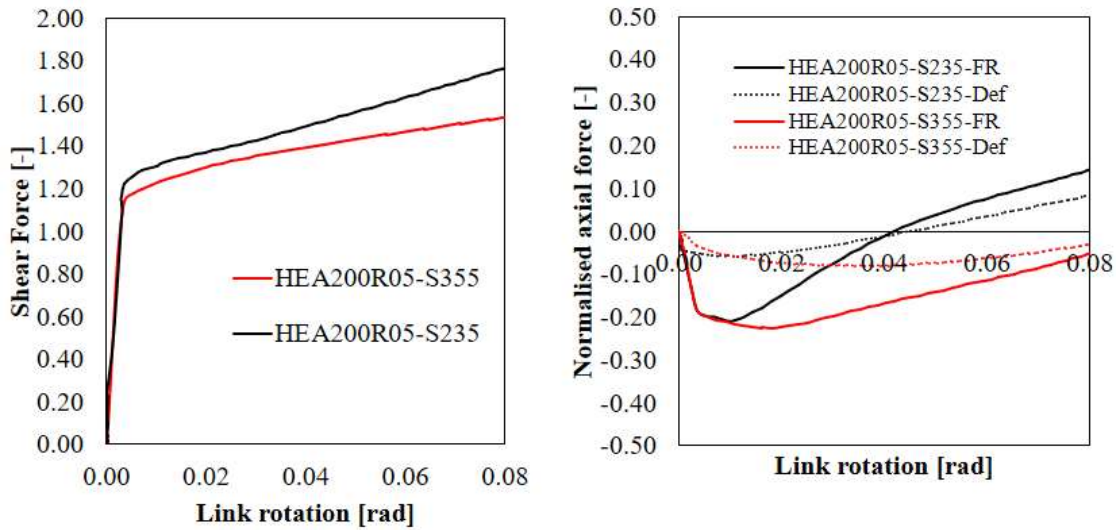


Figure 52. Shear and axial response of HEA200R05 considering two types of steel grade of links

Assemblies with similar lengths but varying beam depths

The succeeding graphs show the development of axial force in assemblies superimposed with other models belonging to the same length ratio. From the analysis of links alone, it has been observed that the axial force is independent of the link depth and this remains true for assemblies. No correlation between the depth axial force has been observed. In understanding the development of axial force, it is important to note that the strength and stiffness of the links are varying simultaneously.

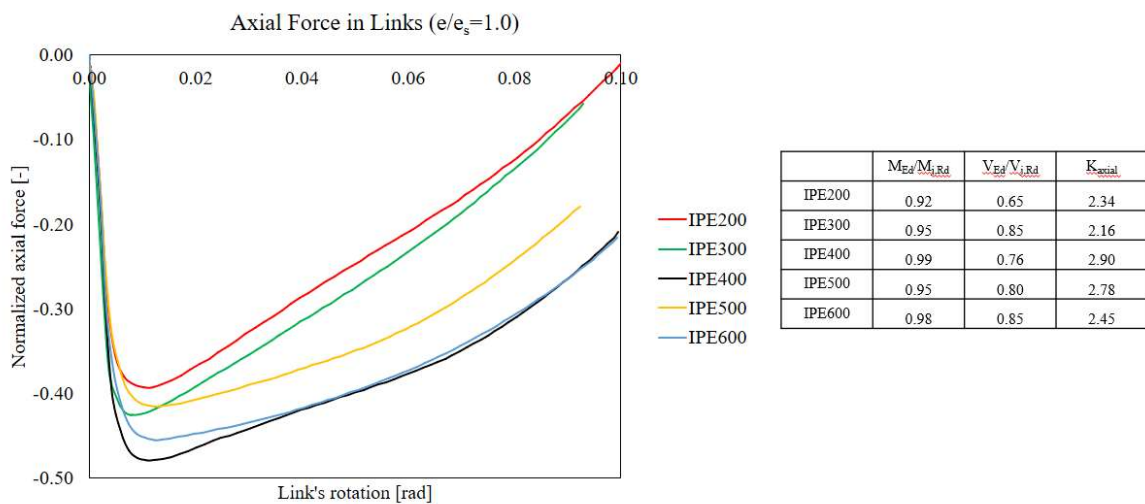


Figure 53. Comparison of axial force on different link depths ($e/e_s=1.0$)

For $e/e_s=1.0$, the highest compression is generated by IPE400, which is also designed very close to its bending resistance. It is then followed by IPE600 with low strength and high stiffness that both causes an increase in axial force. IPE200, on the other hand, is the strongest

connection and also the least stiff, thereby generating the minimum axial force among the five models.

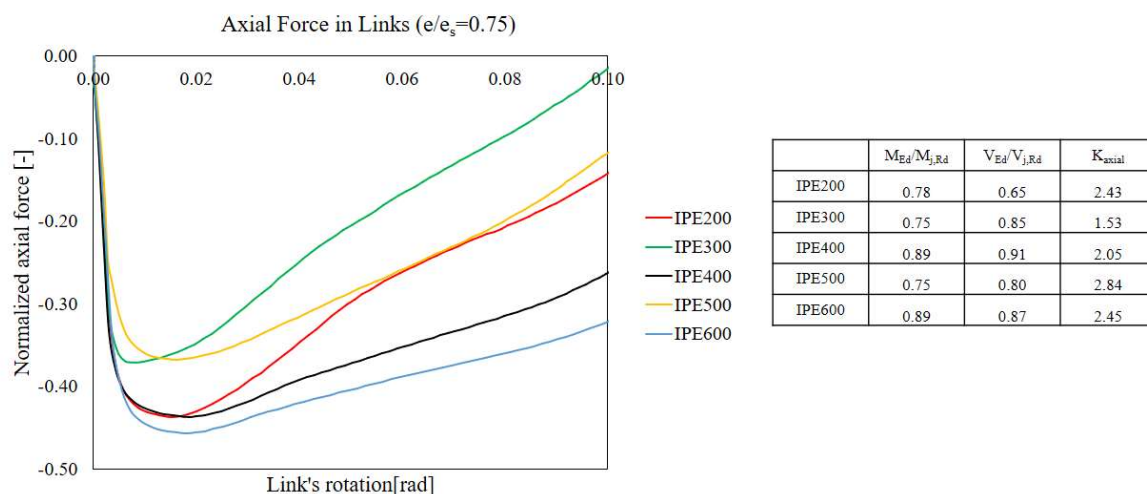


Figure 54. Comparison of axial force on different link depths ($0.75e_s$)

For $0.75e_s$, IPE400 and IPE600 are the weakest connections. However, IPE600 has higher stiffness and as a result, higher compression is developed. IPE300 and IPE500 are the strongest connections and have the minimum compressive forces.

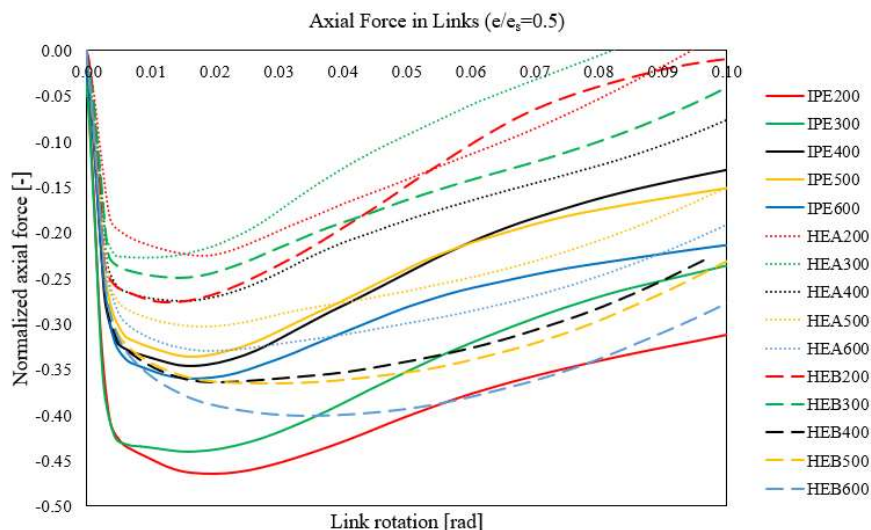
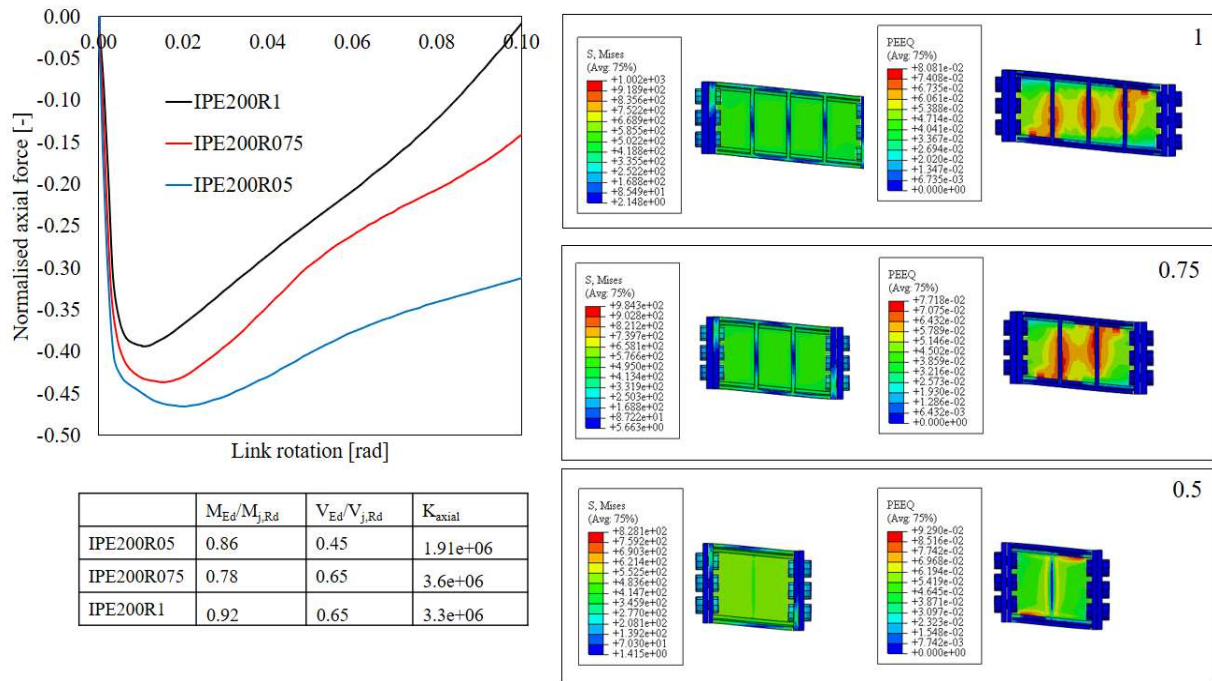


Figure 55. Comparison of axial force on different link depths ($0.5e_s$)

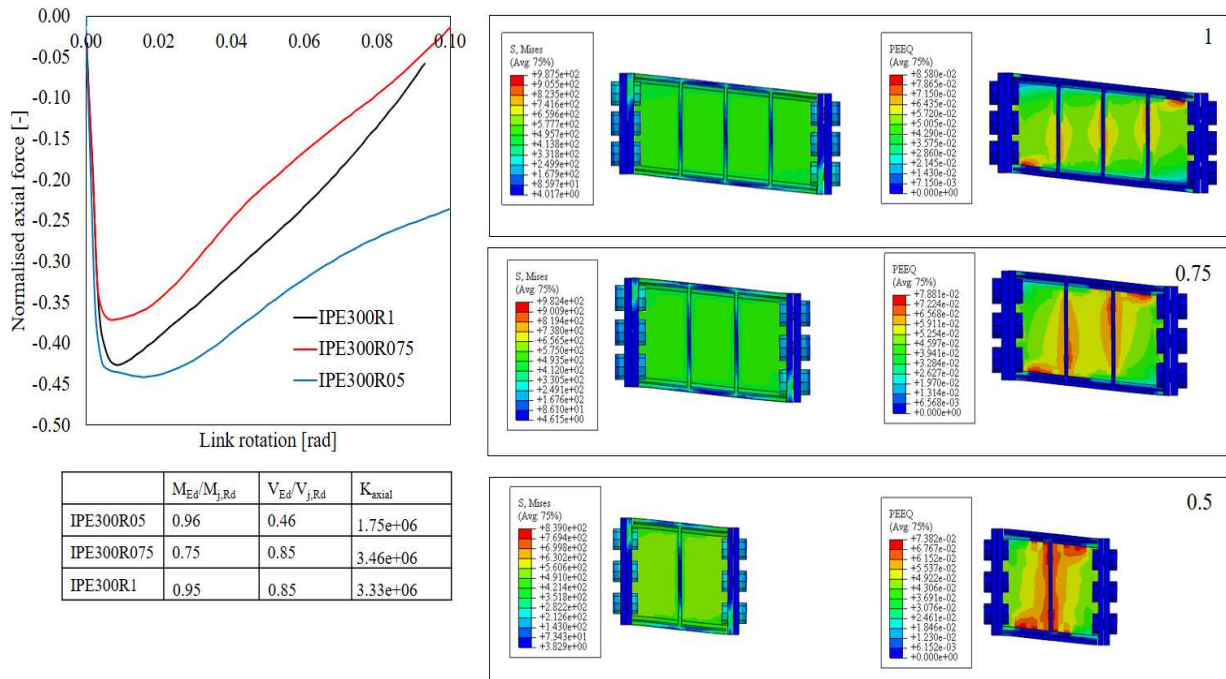
The same trend is observed for $0.5e_s$ considering the same profiles types. From the graphs above, IPEs generally have the highest compression while HEA profiles have the minimum. However, there needs to be further investigation on the difference among IPE, HEA and HEB and how the profile type affects the axial force as no correlation can be established by observing only the trends from one length ratio.

Assemblies with constant beam depths but varying link lengths

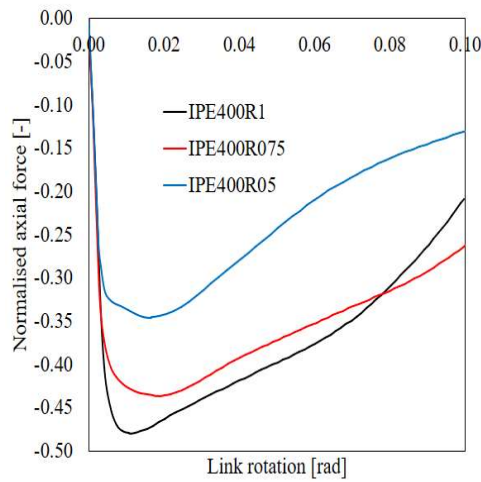
IPE200



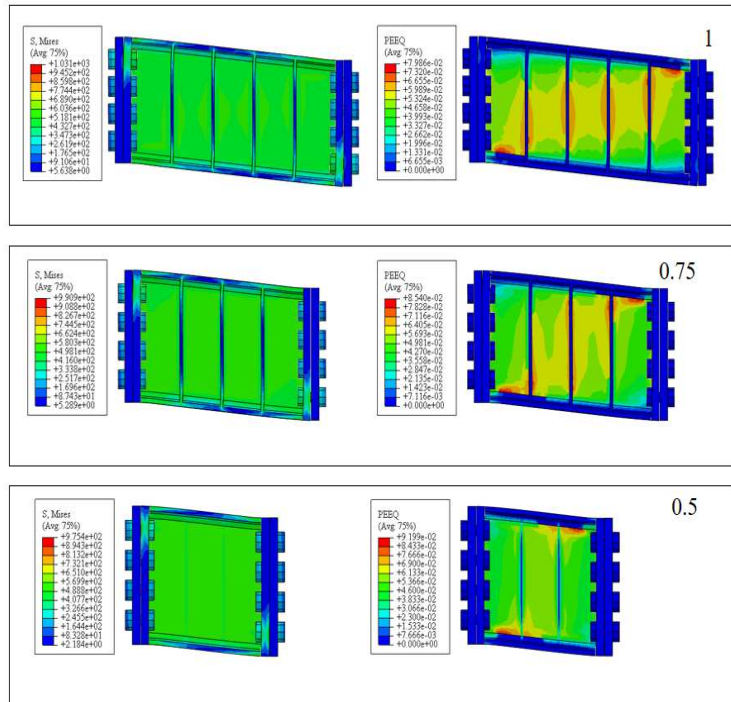
IPE300



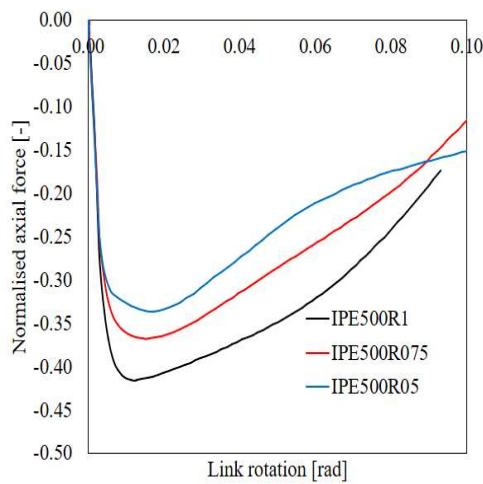
IPE400



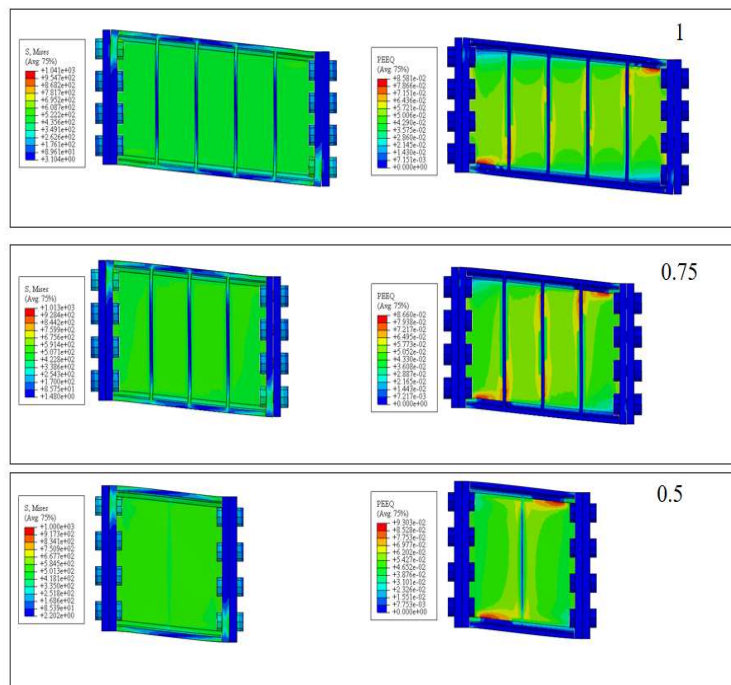
	$M_{Ed}/M_{j,Rd}$	$V_{Ed}/V_{j,Rd}$	K_{axial}
IPE400R05	0.59	0.91	$5.58e+06$
IPE400R075	0.89	0.91	$5.58e+06$
IPE400R1	0.99	0.76	$6.60e+06$



IPE500



	$M_{Ed}/M_{j,Rd}$	$V_{Ed}/V_{j,Rd}$	K_{axial}
IPE500R05	0.67	0.81	$6.76e+06$
IPE500R075	0.75	0.80	$7.96e+06$
IPE500R1	0.95	0.80	$7.76e+06$



IPE600

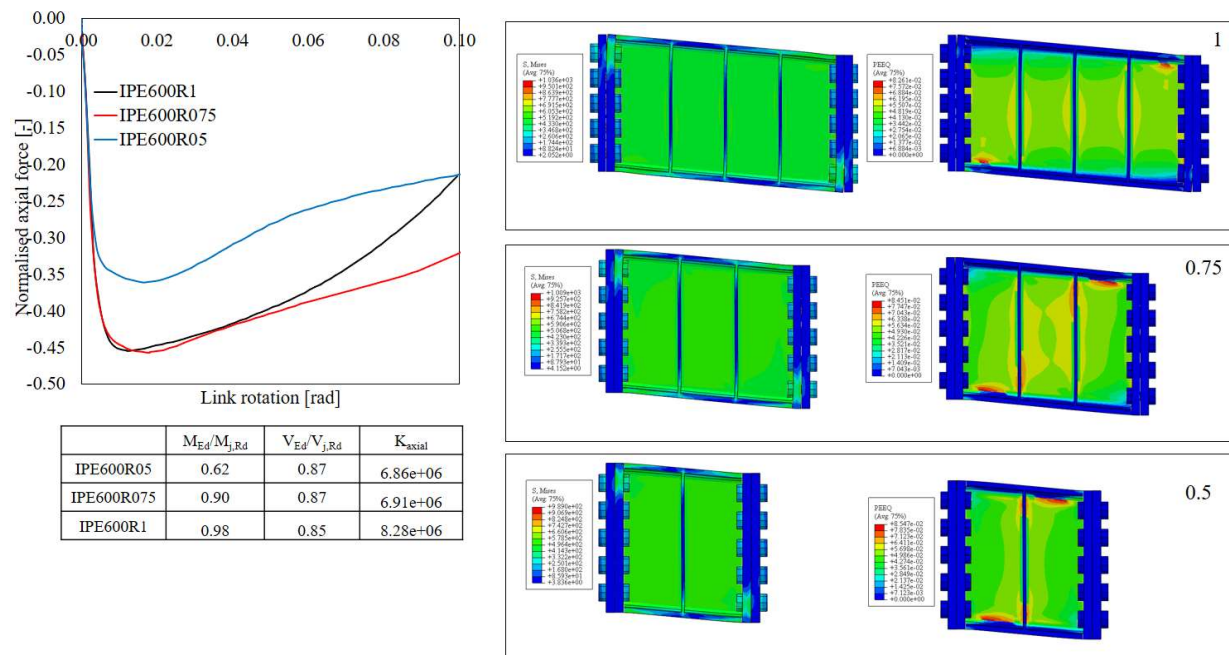
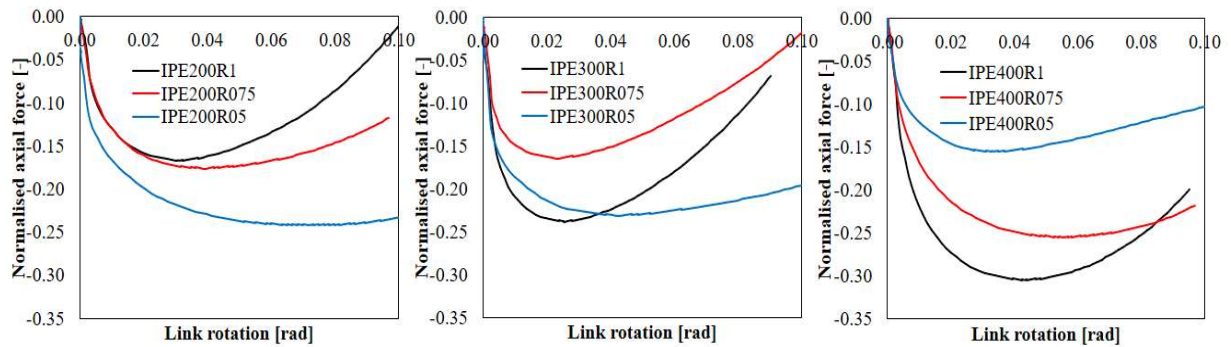


Figure 56. Comparison of axial force on the same link depth but varying link lengths

From the analysis of links alone, it has been observed that the shorter the link is, the higher axial force is developed. However, this is not easily observed in the analysis of assemblies due to the contribution of the stiffness and strength of the connection. While it is expected that long links (e_s) will develop lower compression, these sections are designed close to the limit with an average bending moment ratio of 0.98, while $0.75e_s$ has 0.83, and $0.5e_s$ has an average M design of 0.74. Alongside with this, the stiffness is also varying. For IPE200, maximum compression develops in the shortest link even if it's strength is 6.5% higher than the minimum strength among the three. For IPE300, the shortest link is at the same time the weakest, and therefore it has the highest compressive force. For IPE400, IPE500, and IPE600, the shortest links have the lowest compressive force. For these links, it is important to note that the strengths of these connections are 30-40% more than the others.

These results show that link length, stiffness, and strength of the connection have simultaneous effect on the axial force. There needs to be further investigation on the exact effect of each factor. For instance, if the strength differences between the link is small, the trend is to be governed by the link length. On the other hand, huge differences in strength may outweigh the effect of the link length and the strength will predominantly affect the axial force.

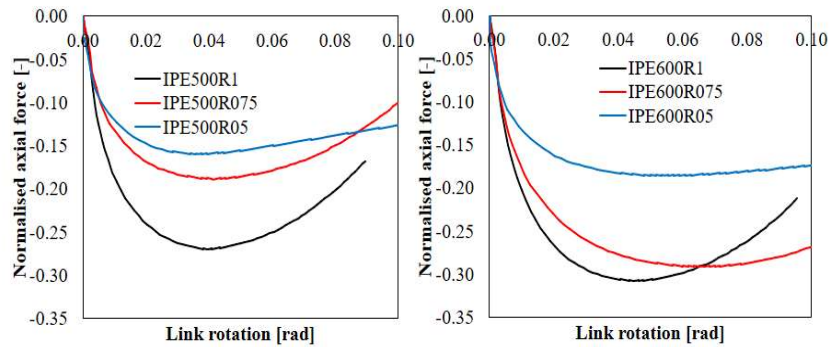
Considering deformable boundary conditions



	$M_{Ed}/M_{j,Rd}$	$V_{Ed}/V_{j,Rd}$	K_{axial}
IPE200R05	0.86	0.45	1.91e+06
IPE200R075	0.78	0.65	3.6e+06
IPE200R1	0.92	0.65	3.3e+06

	$M_{Ed}/M_{j,Rd}$	$V_{Ed}/V_{j,Rd}$	K_{axial}
IPE300R05	0.96	0.46	1.75e+06
IPE300R075	0.75	0.85	3.46e+06
IPE300R1	0.95	0.85	3.33e+06

	$M_{Ed}/M_{j,Rd}$	$V_{Ed}/V_{j,Rd}$	K_{axial}
IPE400R05	0.59	0.91	5.58e+06
IPE400R075	0.89	0.91	5.58e+06
IPE400R1	0.99	0.76	6.60e+06

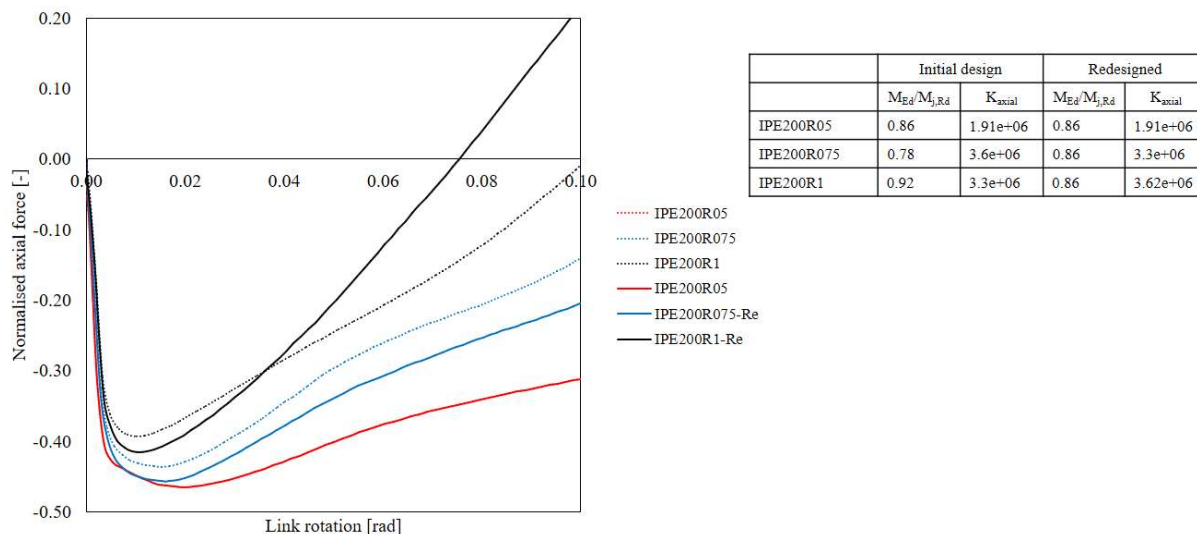


	$M_{Ed}/M_{j,Rd}$	$V_{Ed}/V_{j,Rd}$	K_{axial}
IPE500R05	0.67	0.81	6.76e+06
IPE500R075	0.75	0.80	7.96e+06
IPE500R1	0.95	0.80	7.76e+06

	$M_{Ed}/M_{j,Rd}$	$V_{Ed}/V_{j,Rd}$	K_{axial}
IPE600R05	0.62	0.87	6.86e+06
IPE600R075	0.90	0.87	6.91e+06
IPE600R1	0.98	0.85	8.28e+06

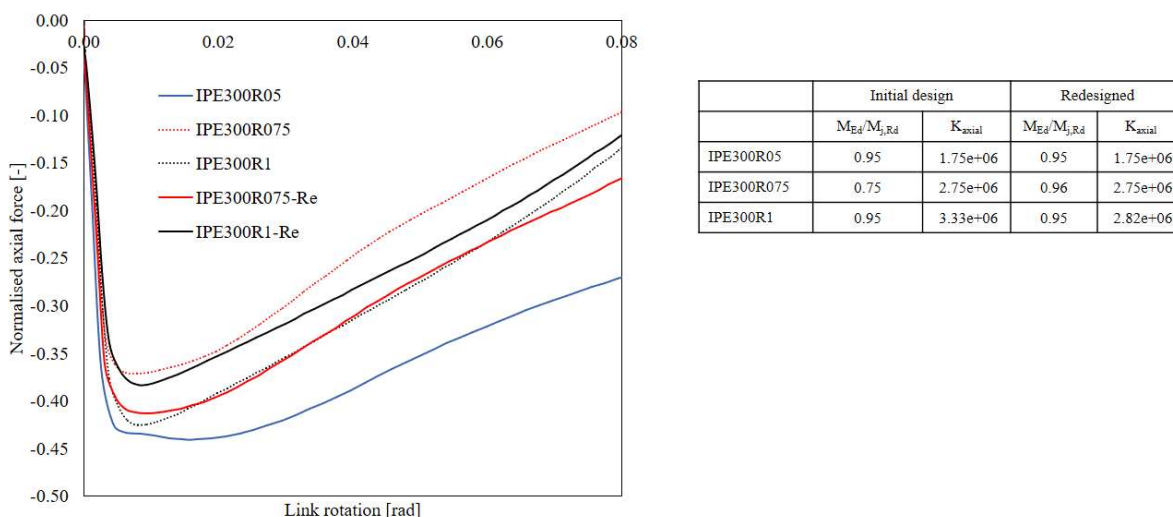
To observe the trend that occurs within assemblies, it is necessary to isolate the link length and control strength and stiffness. IPE200 and IPE300 are used as they are less limiting in terms of strength compared to deeper profiles.

IPE200



Despite the differences among the strengths of the three IPE200 links, the result of the initial design shows that the $0.5e_s$ has the maximum axial force while e_s has the minimum. IPE200R075 and IPE200R1 are then redesigned to have a moment ratio of 0.86 and the results are superimposed. There are changes with the development of axial force, but the trend observed remains the same – shorter links develop high axial forces.

IPE300



For IPE300 links, $0.5e_s$ still has the maximum axial force but $0.75e_s$ has the minimum, noting the 21% difference between their strengths. IPE300R075 is redesigned to have lower bending resistance, while the stiffness of IPE300R1 is modified to be closer to the other values.

IPE300R05 is kept unchanged even with a significantly lower stiffness since increasing it to be as stiff as the other two will only further increase the compression, and therefore has no detrimental effect on the trend of interest. The new set of assemblies, now with more precise values of strength and stiffness, exhibit the same length-dependence as previously shown – IPE300R05 has the maximum axial force, followed by IPE300R075, and IPE300R1 has the minimum.

M-N Curves of FEP Assemblies

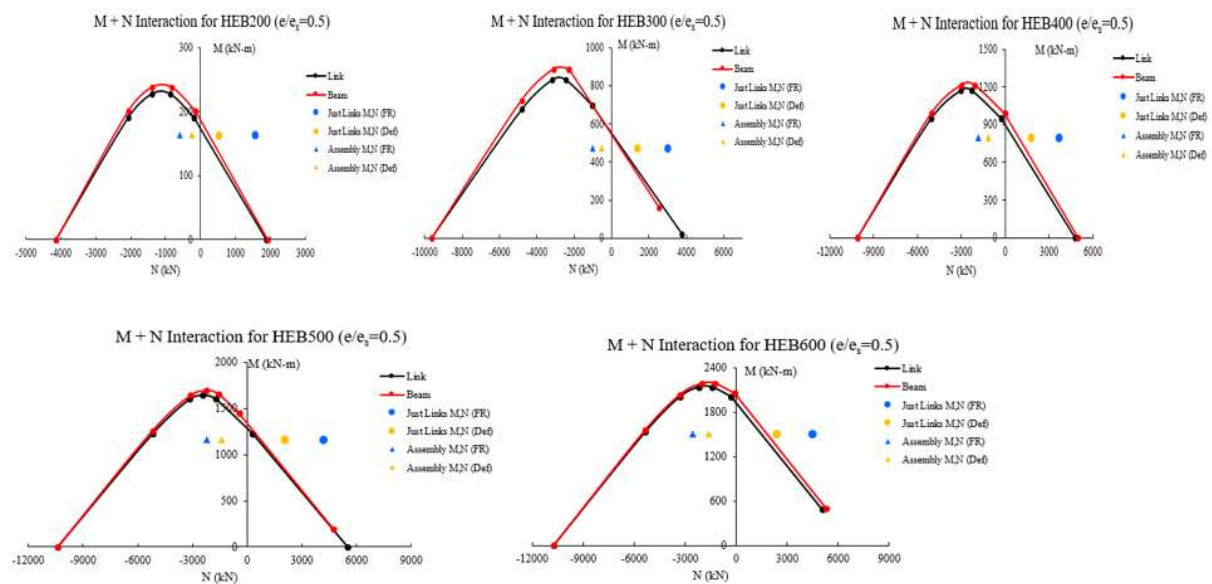


Figure 57. *M-N interaction curves with design forces from links alone and assembly*

When analytical analyses were performed, the design moment and axial force from just the links were plotted with the M-N interaction curve of the assemblies. It was observed that the design forces for IPE links are within the curves or have minimum deviation while for HEA and HEB profiles, these design forces are significantly beyond the interaction curves. From the graphs above, the maximum compressive force obtained from the numerical analysis of assemblies are also plotted in the curve. All the forces are now within the interaction curve but on the opposite side since they are in compression.

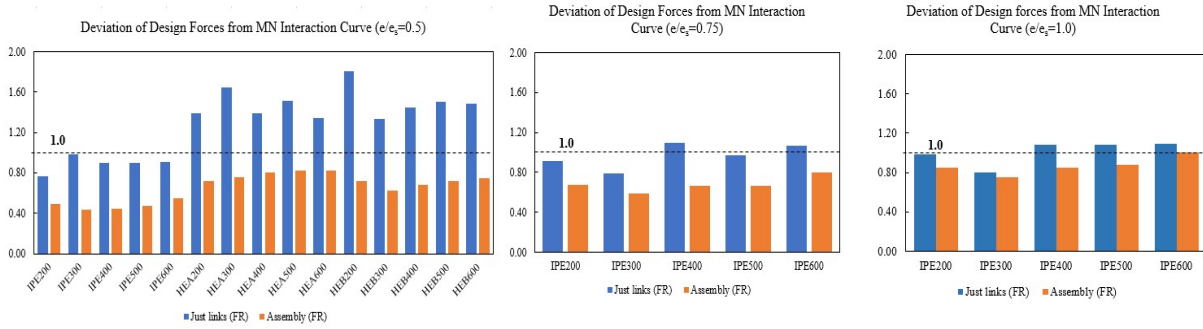


Figure 58. Comparison of the axial force based on the analysis of JUST LINKS and ASSEMBLY (Fully rigid)

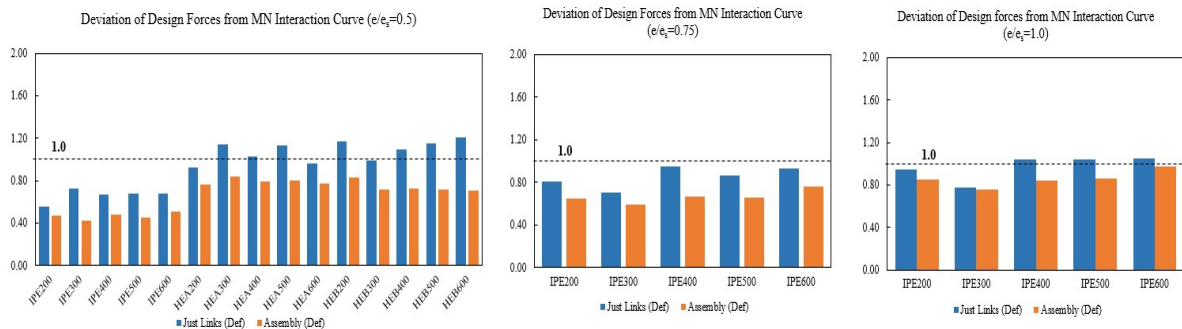


Figure 59. Comparison of the axial force based on the analysis of JUST LINKS and ASSEMBLY (Deformable)

Fig.58 and Fig.59 show the decrease in magnitude of axial force for the links alone and for the assembly. For both fully rigid and deformable boundary conditions, there is a significant reduction in the magnitude of axial force developed in the link.

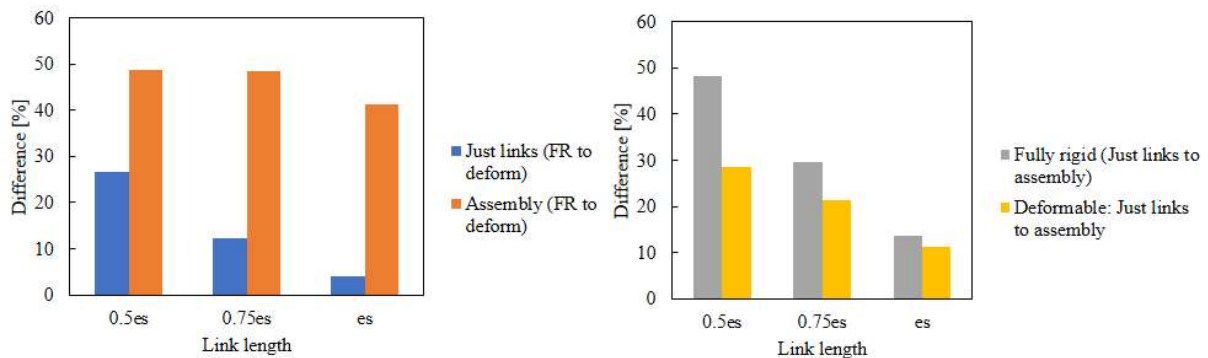


Figure 60. Average decrease in axial force for different cases

The graph above shows the average decrease in axial force for four different cases (i) just links with varying boundary conditions, (ii) assembly with varying boundary conditions, (iii) fully rigid BC from just links to assembly, and (iv) deformable BC from just links to assembly. For all cases, shortest links experience the highest difference in axial forces while this effect is lowest for longest links.

To summarize the results of the completed analysis, the table shows the influence of different parameters on the development of axial force on links.

Table 10. Effect of studied parameters on axial force

Compressive force/Compressive arch for FEP assemblies		
Parameter	Higher values	Lower values
Frame deformability (boundary conditions)	Fully rigid	Deformable springs
Stiffness of connection	Stiff connection	Less stiff connection
Strength of connection	Weak connection	Strong connection
Link length	Short link	Long link

For the succeeding analysis, the same analytical and numerical investigations are performed on extended-end plate connections (EEP).

5.2 Investigation on the Extended end-plate connections

5.2.1 Analytical analysis

Method 1

Table 11. Design ratios for EEP according to Method 1

Link	e/e_s=1.0		e/e_s=0.75		e/e_s=0.5	
	$\frac{M_{Ed}}{M_{jRd}}$	$\frac{V_{Ed}}{V_{jRd}}$	$\frac{M_{Ed}}{M_{jRd}}$	$\frac{V_{Ed}}{V_{jRd}}$	$\frac{M_{Ed}}{M_{jRd}}$	$\frac{V_{Ed}}{V_{jRd}}$
IPE200	0.82	0.56	0.91	0.81	0.82	0.56
IPE300	0.99	0.85	0.96	0.85	0.81	0.85
IPE400	0.87	0.85	0.89	0.85	0.59	0.85
IPE500	0.93	0.94	0.90	0.94	0.80	0.94
IPE600	0.93	0.88	0.69	0.88	0.47	0.88

All EEP assemblies are designed to satisfy Method 1 with the design ratios shown in Table 5. The assemblies are then checked according to Method 2 and both results are superimposed in the graphs below.

Method 2

Table 12. Design force to resistance ratio according to Method 2 (EEP)

Link	e/e_s=1.0		e/e_s=0.75		e/e_s=0.5	
	$\frac{M_{Ed} + N_{Ed}}{M_{jRd} + N_{jRd}}$	$\frac{V_{Ed}}{V_{jRd}}$	$\frac{M_{Ed} + N_{Ed}}{M_{jRd} + N_{jRd}}$	$\frac{V_{Ed}}{V_{jRd}}$	$\frac{M_{Ed} + N_{Ed}}{M_{jRd} + N_{jRd}}$	$\frac{V_{Ed}}{V_{jRd}}$
IPE200	1.21	1.17	1.71	1.69	2.07	1.17
IPE300	1.50	1.72	1.78	1.72	1.94	1.72

IPE400	1.24	1.52	1.53	1.52	1.32	1.52
IPE500	1.27	1.57	1.48	1.57	1.74	1.57
IPE600	1.44	1.88	1.38	1.88	1.29	1.88

Since most of the assemblies are designed close to its bending resistance and they all develop significant axial forces, the limits in terms of shear and combined bending-axial force are not satisfied. Meanwhile, the assemblies are retained as such as designing them to satisfy Method 2 will make them highly conservative. The behavior of the assemblies is further verified through numerical investigation in Abaqus.

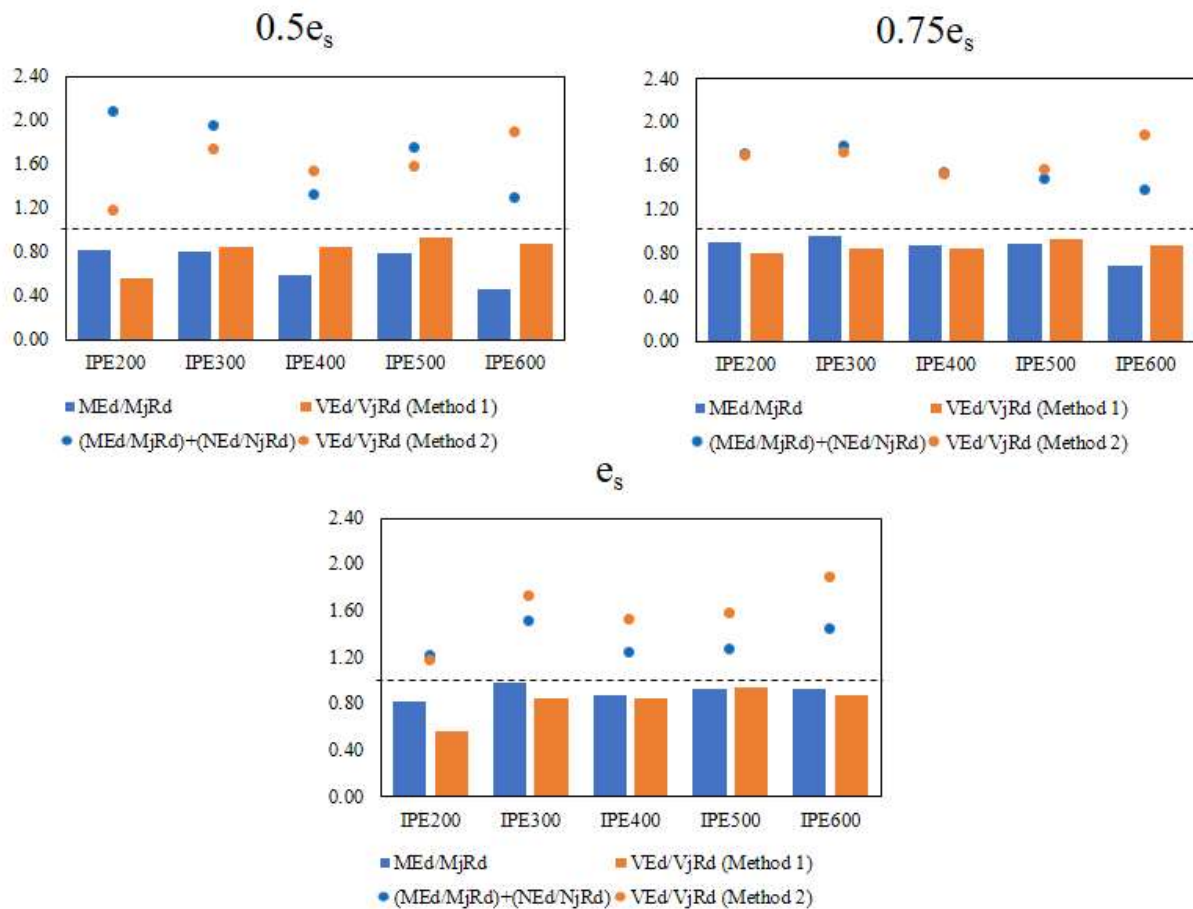
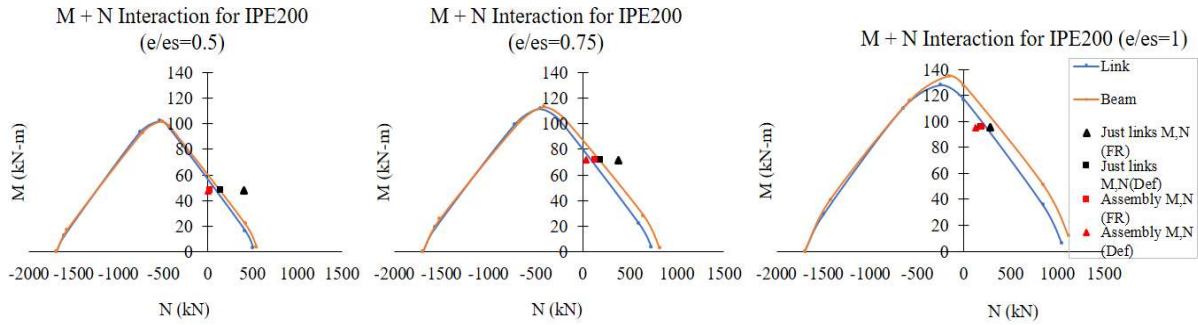


Figure 61. Design ratios for EEP assemblies according to Method 1 and Method 2

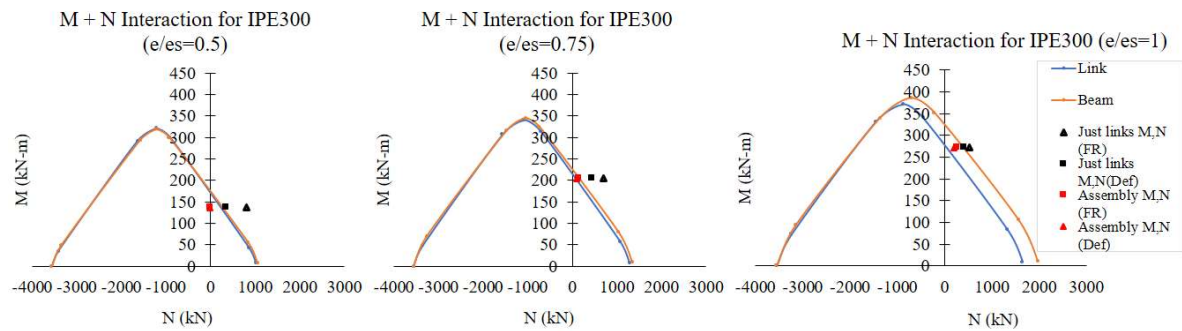
Method 3 (M-N Curves)

For EEP assemblies, all values plotted with the M-N interaction curves are the axial forces at 0.08 rad of link rotation. For most cases, these are tensile forces except for IPE200R05, IPE300R05, and IPE200R075 that stay within the compression zone but with low magnitude.

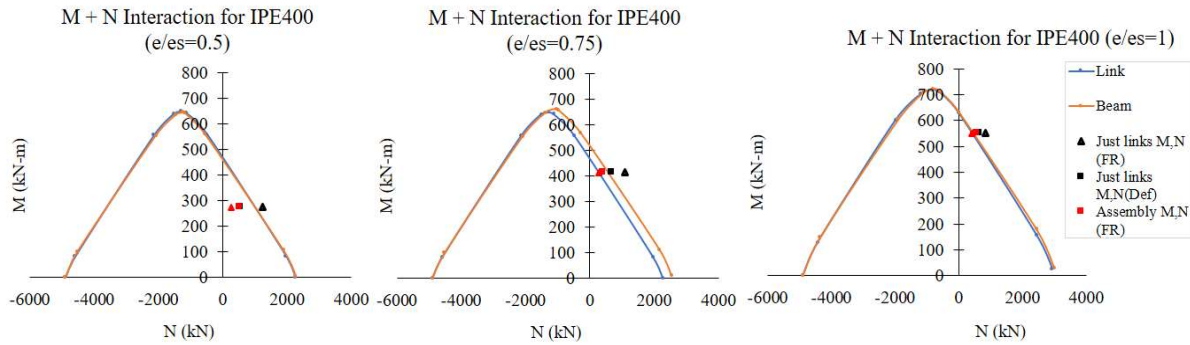
IPE200



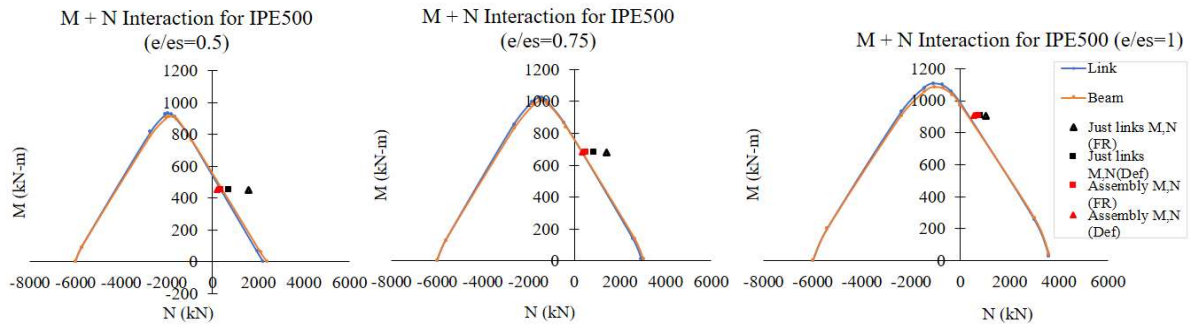
IPE300



IPE400



IPE500



IPE600

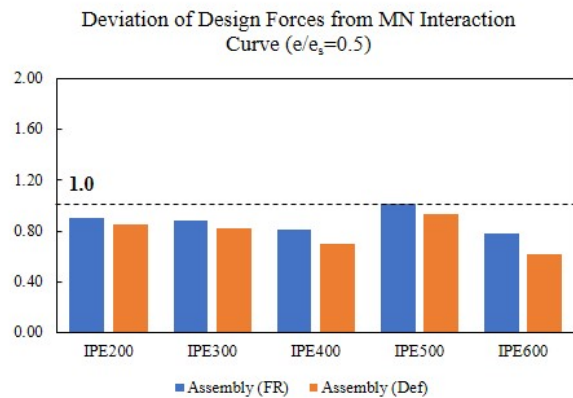
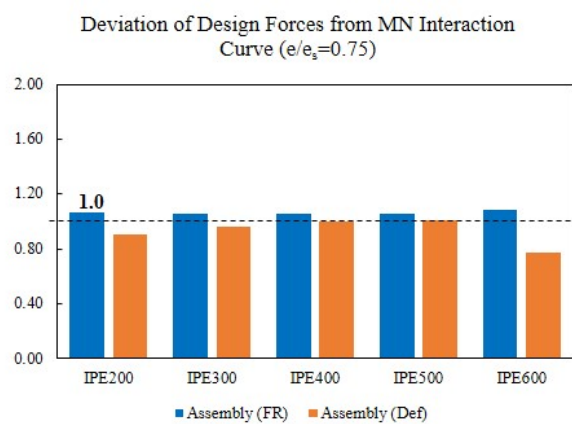
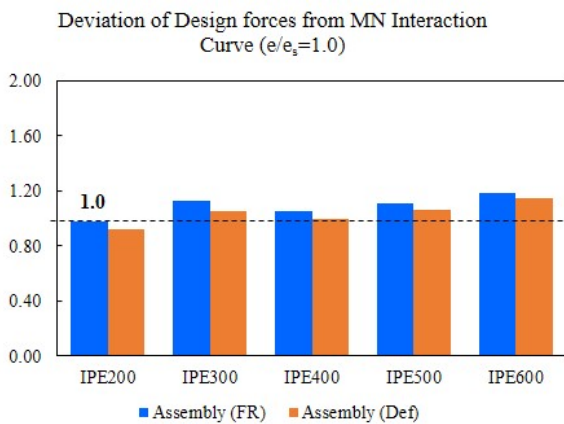
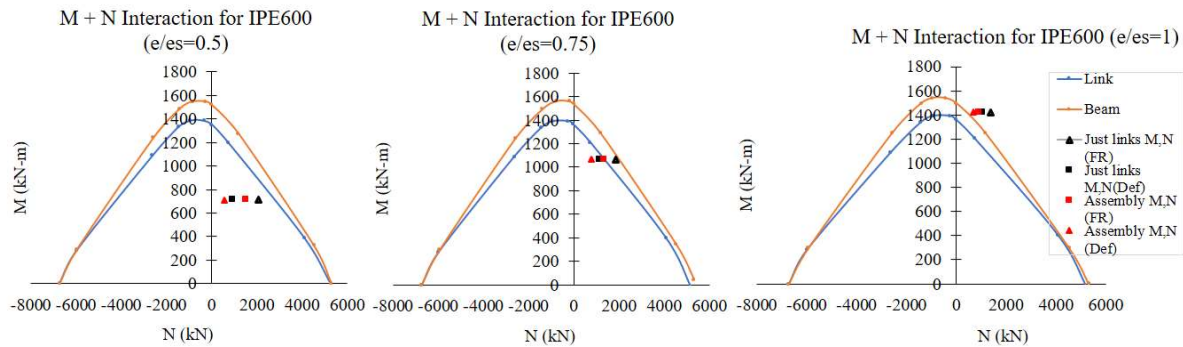


Figure 62. Deviation of design forces from M-N curves of EEP assemblies

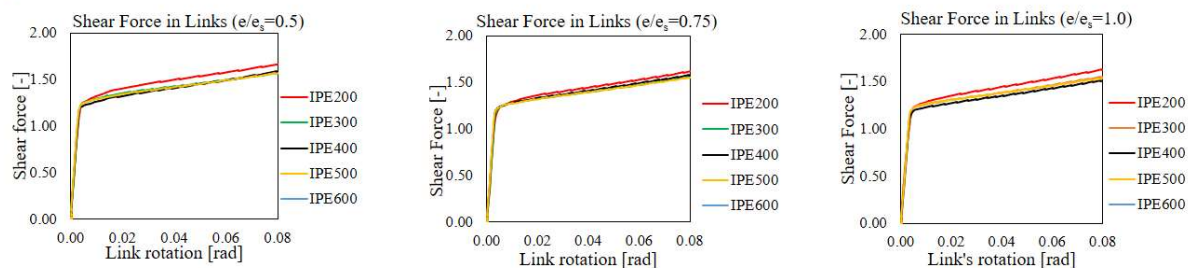
The graphs above demonstrate the deviation of the design forces from the M-N interaction curve of the link. The axial forces induced by fully rigid BC remain higher compared to those considering deformable springs, with an average difference of 10%. For $0.5e_s$ links, the design forces for all assemblies are within the M-N curves. On the other hand, they are generally exceeded for $0.75e_s$ and e_s links, especially when fully rigid BC is considered. Recalling the results from FEP assemblies, the design forces for IPE profiles remain within the M-N curves. This can be attributed to the fact that while the axial forces are higher in magnitude for FEP

assemblies, they are all in compression. In the case of EEP assemblies, the axial forces are of smaller magnitude but are now in tension. This further highlights that tensile forces in link induce more significant reduction in the bending resistance.

5.2.2 Numerical analysis

Shear overstrength

Fully rigid



Deformable

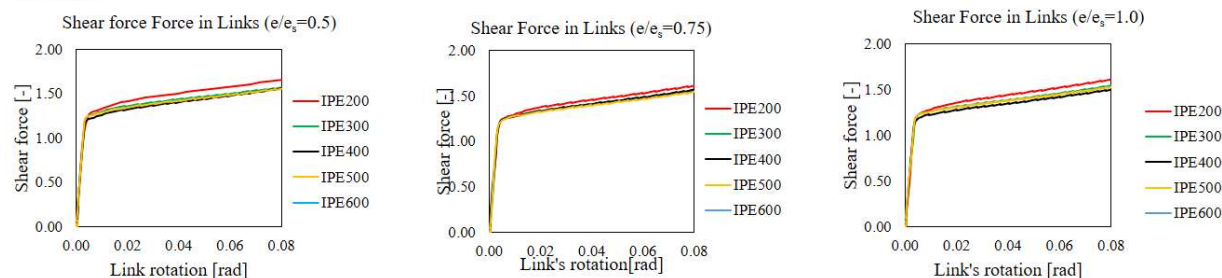


Figure 63. Shear response of EEP assemblies modelled

The observations based from FEPs are still valid for EEPs – the seismic links have identical response in the elastic regions and there are small differences among the shear overstrength at 0.08 rad of link rotation.

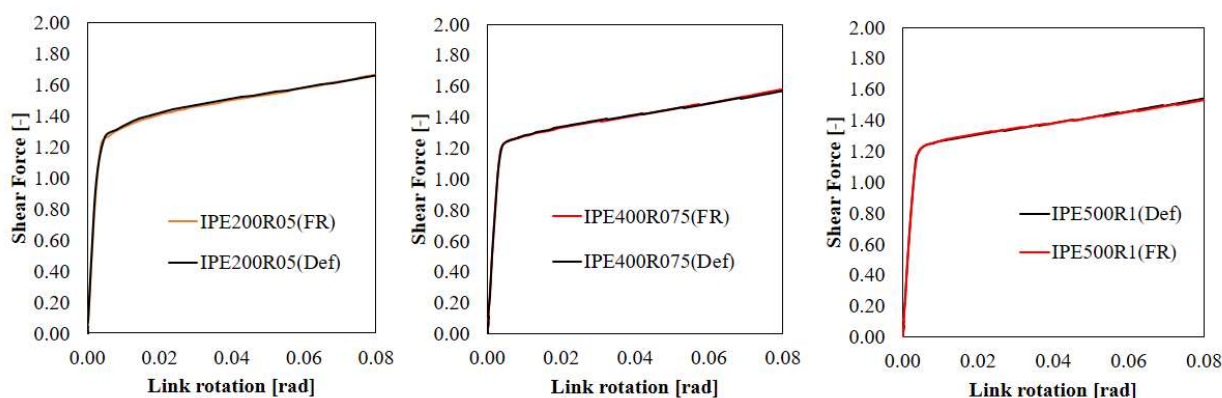


Figure 64. Shear response of an assembly considering deformable and fully rigid boundary conditions

The shear response of the link for EEPs is also independent from boundary conditions as shown by the graphs. The response for fully rigid and deformable boundary conditions for the same link configuration remains constant.

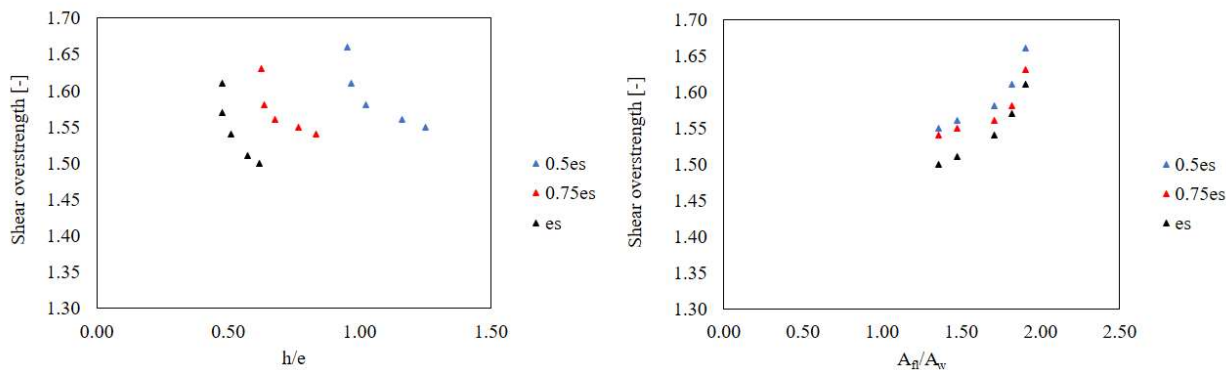


Figure 65. Shear overstrength at 0.08 rad link rotation as function of h/e (left) and of A_{fl}/A_w (right)

Plotting the shear overstrength at 0.08 rad link rotation with respect to the ratio of profile depth h to link length e , the graph shows that there is a decrease in shear overstrength as profile depth increases. Moreover, the graph with respect to the ratio of the link's flange area to its web area (A_{fl}/A_w) demonstrates that shear overstrength decreases for longer links. The average of $0.5e_s$ is 1.60, 1.58 for $0.75e_s$, and 1.56 for e_s , bringing an overall average of 1.58. For all cases analyzed, the maximum shear overstrength is 1.66.

Axial force

The next section discusses the development of the axial forces within the EEP assemblies.

Comparison of axial force development considering fully rigid and deformable boundary conditions

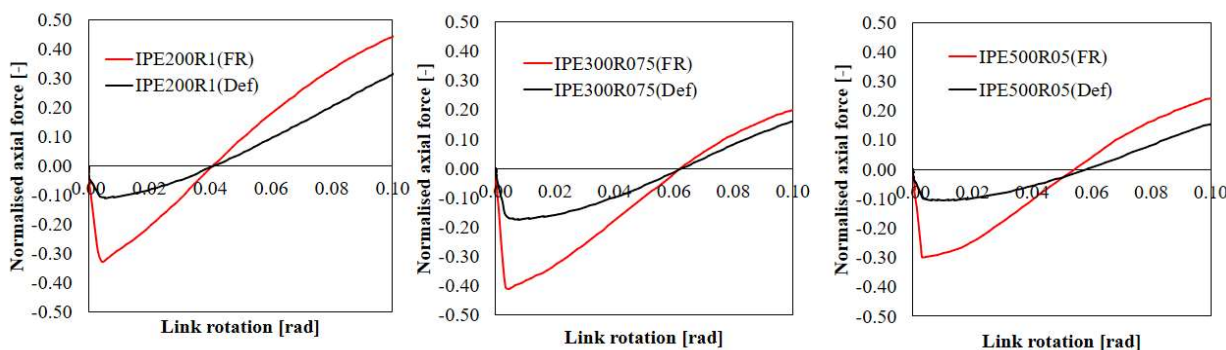
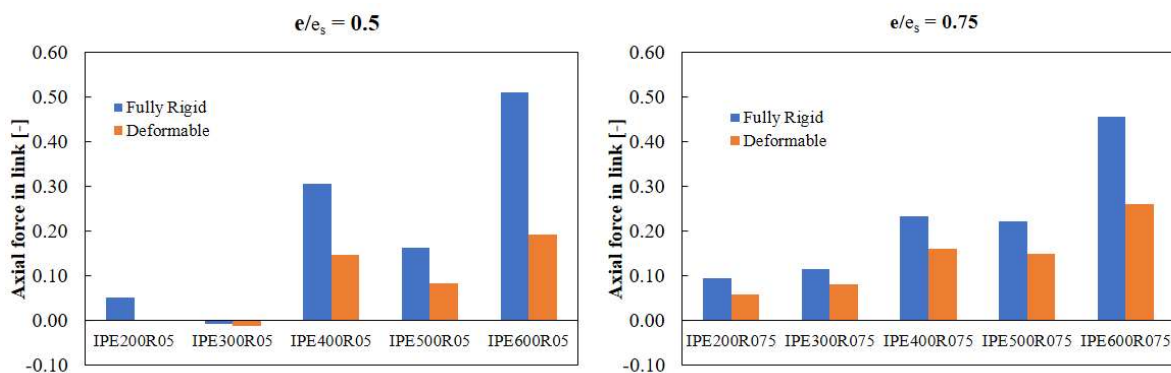


Figure 66. Axial force development considering fully rigid and deformable boundary conditions

All assemblies showed significant increase in axial forces in both the compression and tension sides of the curve when fully rigid boundary conditions are imposed instead of deformable springs. Unlike FEP assemblies that mostly remain in compression until a plastic rotation of 0.08 rad, most EEP assemblies, especially those with longer links, reached tension. Considering the established fact that tension is more detrimental to the bending resistance, the succeeding analysis of the forces will focus on them instead of compression.

	Fully rigid BC		Deformable BC	
	Maximum axial force	Tension at 0.08 rad	Maximum axial force	Tension at 0.08 rad
IPE200R05	-0.38 (C)	0.05	-0.15 (C)	0 (remains in compression)
IPE300R05	-0.40 (C)	0	-0.18 (C)	0 (remains in compression)
IPE400R05	0.31 (T)	0.31	0.15 (T)	0.15
IPE500R05	-0.30 (C)	0.16	-0.10 (C)	0.08
IPE600R05	0.51 (T)	0.51	0.19 (T)	0.19
IPE200R075	-0.42 (C)	0.10	-0.14 (C)	0 (remains in compression)
IPE300R075	-0.40 (C)	0.12	-0.17 (C)	0.08
IPE400R075	-0.31 (C)	0.23	0.16 (T)	0.16
IPE500R075	-0.31 (C)	0.22	0.15 (T)	0.15
IPE600R075	0.46 (T)	0.46	0.26 (T)	0.26
IPE200R1	0.33 (T)	0.33	0.20 (T)	0.20
IPE300R1	-0.39 (C)	0.24	0.18 (T)	0.18
IPE400R1	0.33 (T)	0.33	0.24 (T)	0.24
IPE500R1	0.33 (T)	0.33	0.24 (T)	0.24
IPE600R1	0.31 (T)	0.31	0.26 (T)	0.26



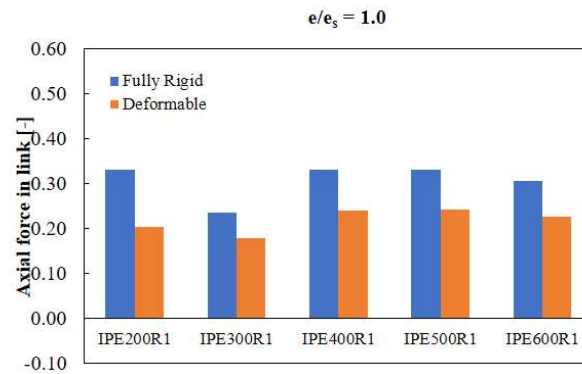


Figure 67. Axial force in links at 0.08 rad link rotation

The values presented above are the axial forces at 0.08 rad, which in most cases are in significant tension. There is an average decrease of 37% in tensile forces when the same model with initially fully rigid restraints is analyzed considering deformable springs. The decrease is more significant for shorter links with an average of 50% for $0.5e_s$, 33% for $0.75e_s$ and 30% for e_s . Therefore, it remains valid for EEP that considering the deformability of the frame to which the link is connected greatly reduces the axial demand on links.

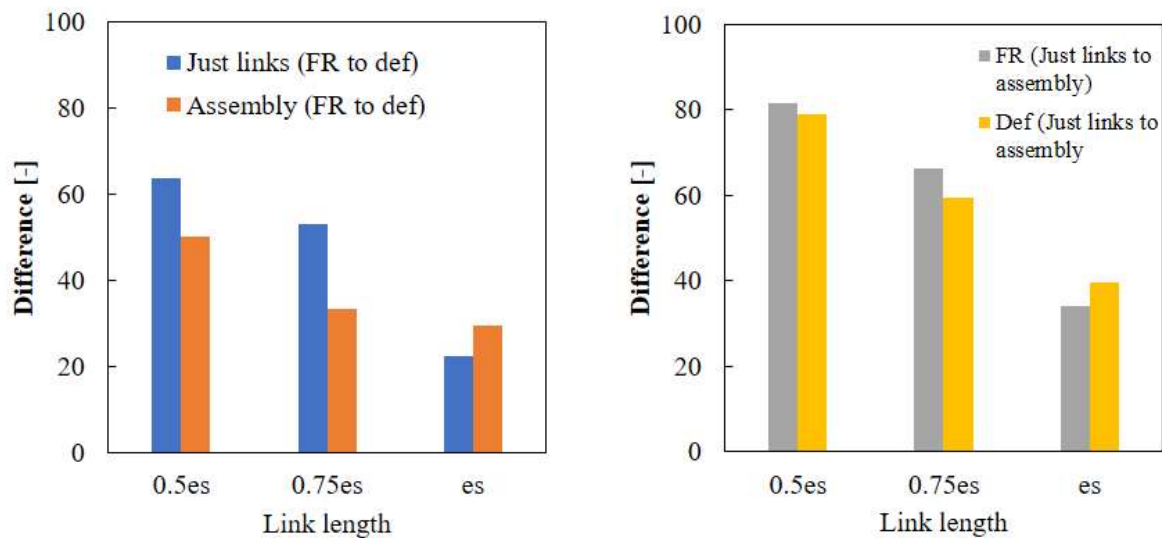
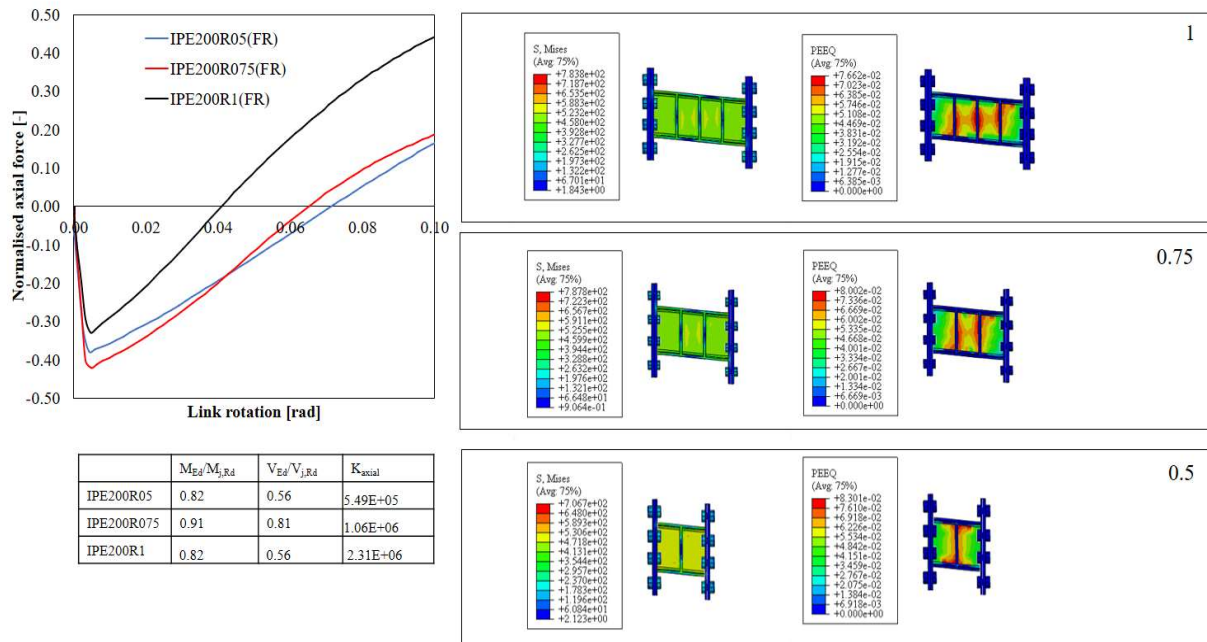


Figure 68. Average change in axial force for different cases

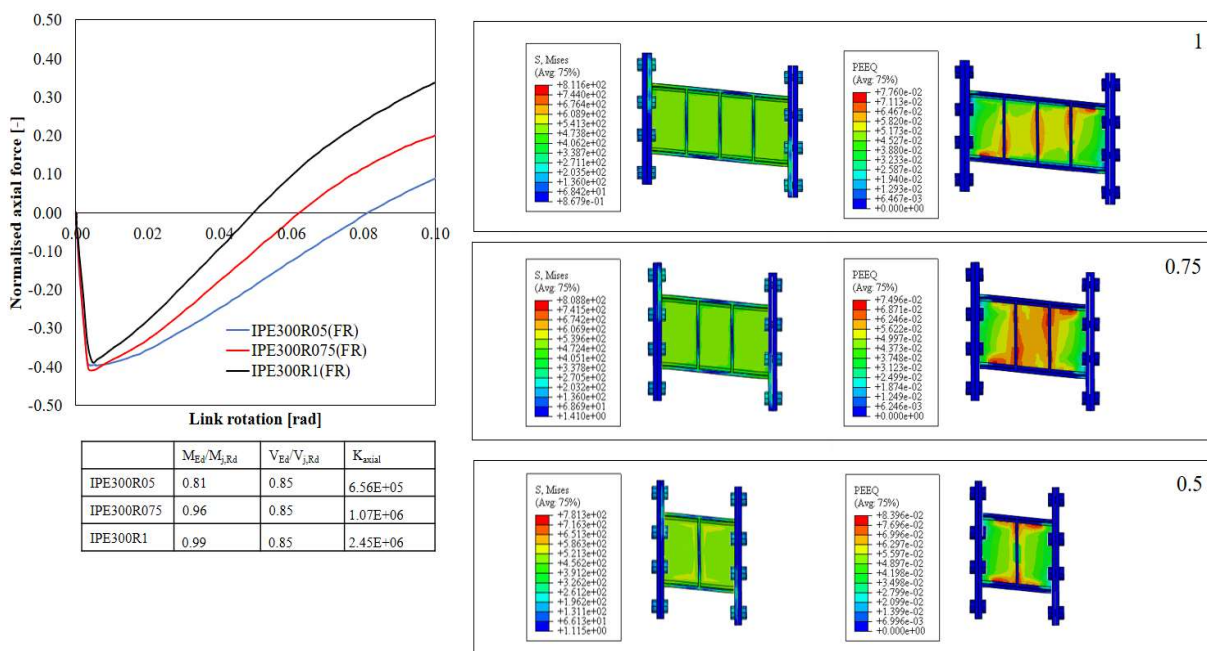
Results from the same depth of links with varying length ratios

Shown below are the superimposed graphs of links with the same depth but with varying lengths, strength, and stiffness. Using the results from FEPs regarding the effect of each parameter, the trend of the graphs is in agreement with prior results.

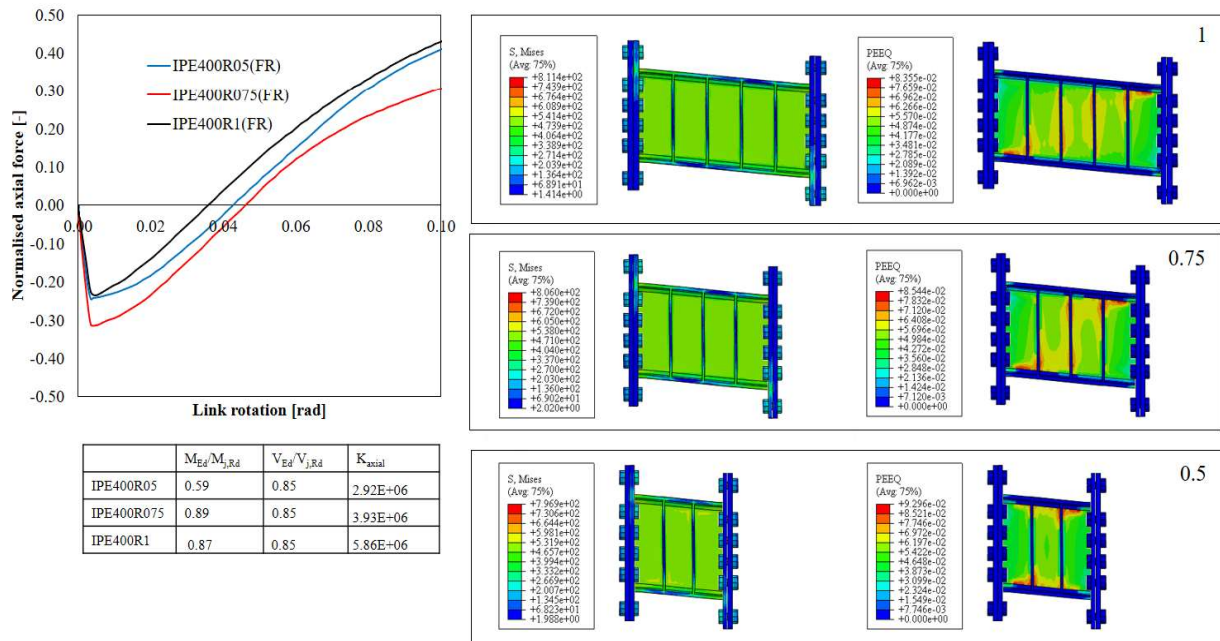
IPE200



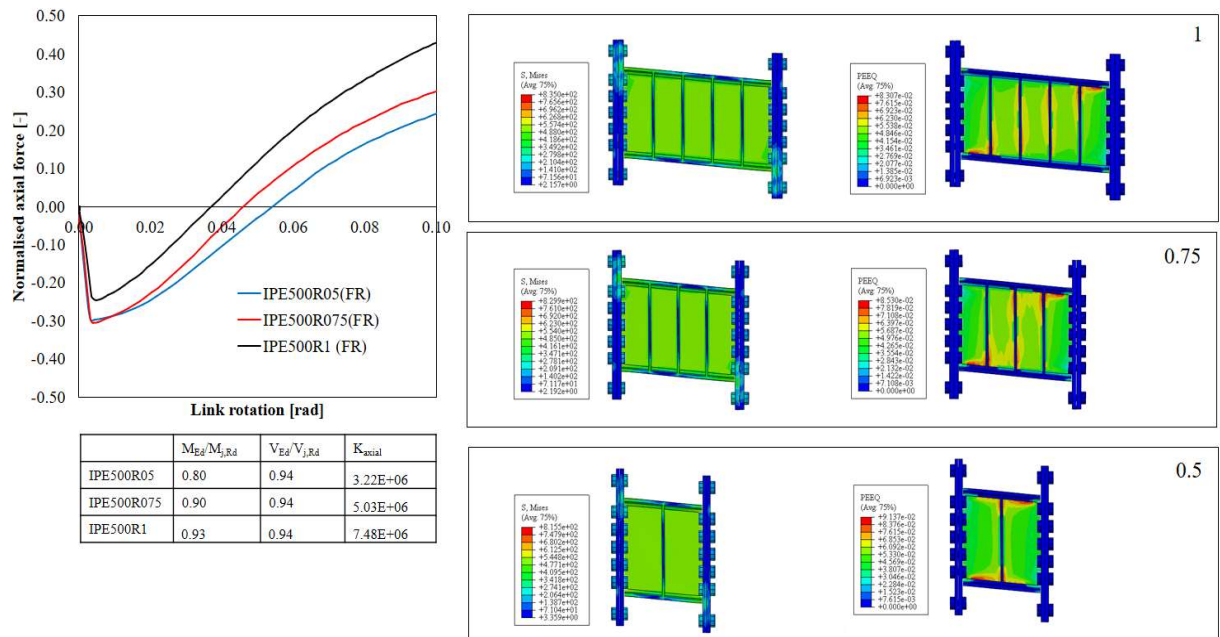
IPE300



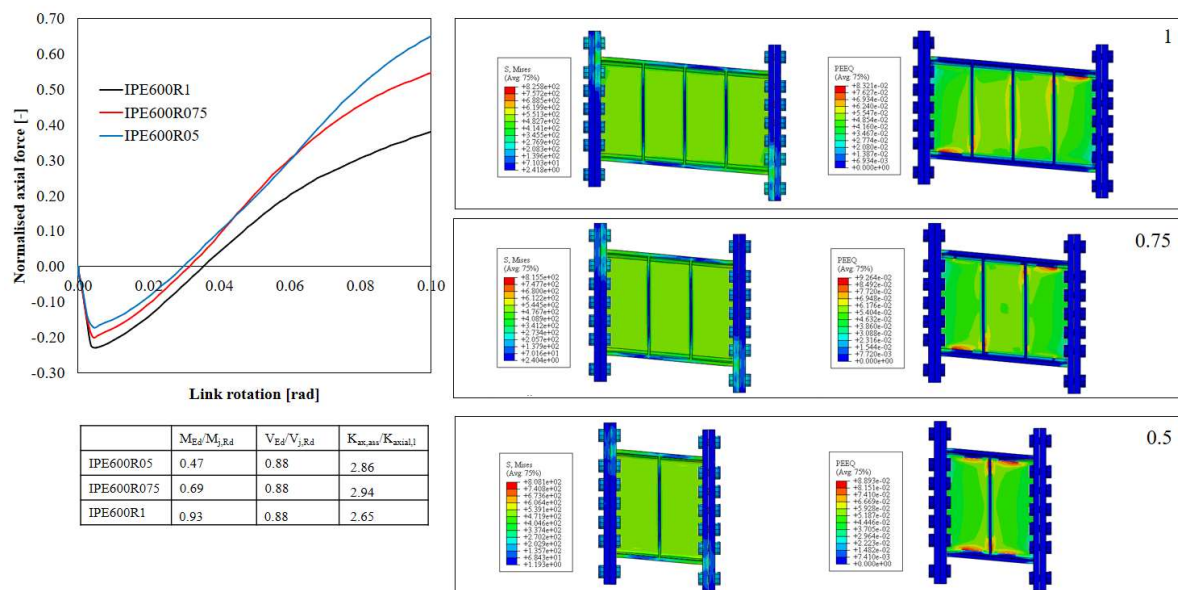
IPE400



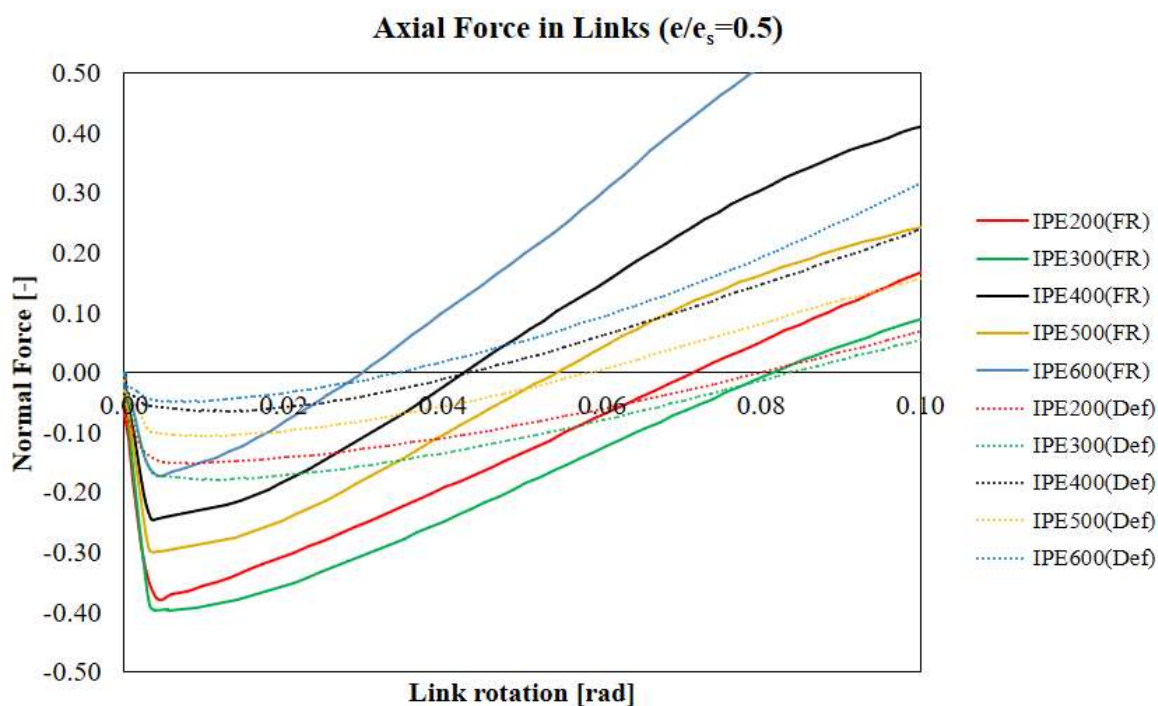
IPE500



IPE600

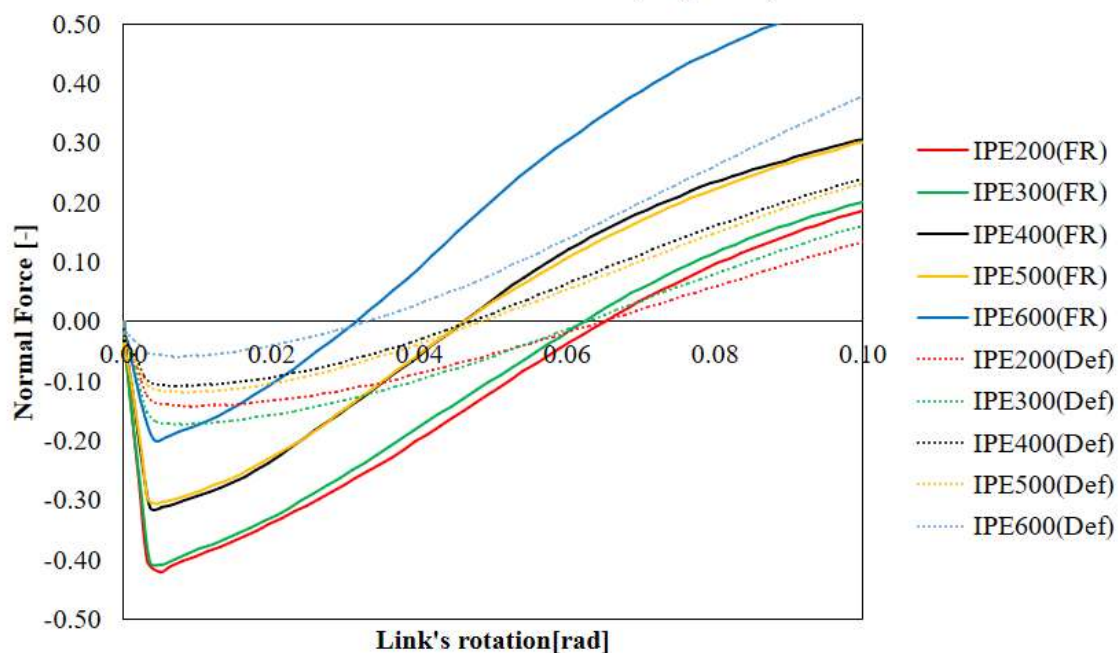


Result from the same length ratios but varying link depths



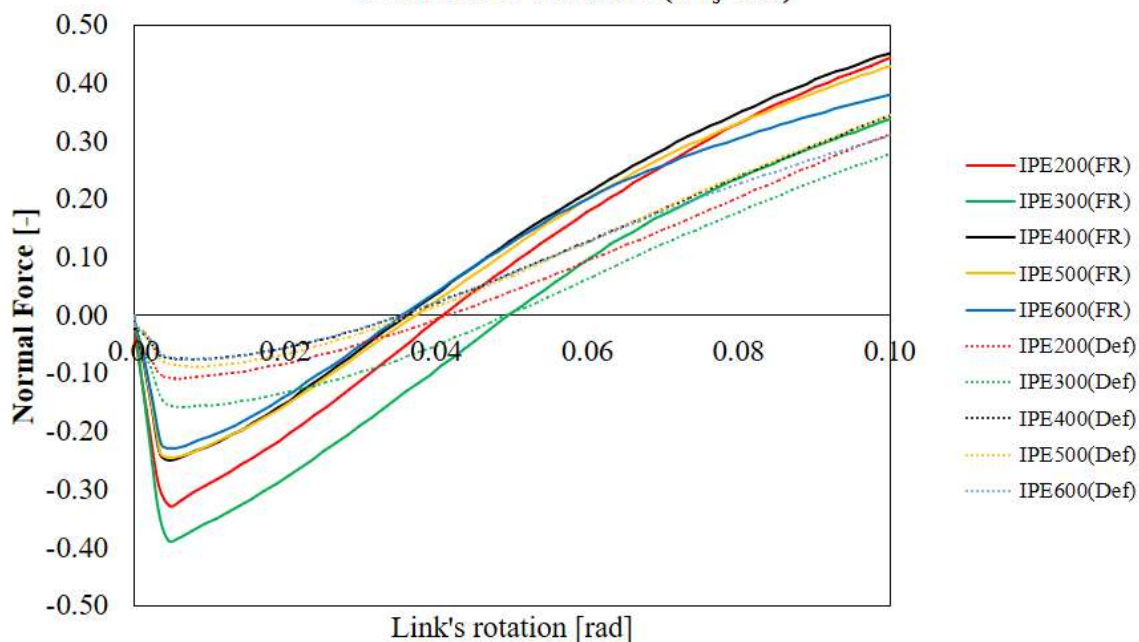
	IPE200	IPE300	IPE400	IPE500	IPE600
M	0.82	0.81	0.59	0.80	0.47
$K_{ax,assembly}/K_{ax,link}$	0.36	0.39	1.28	1.15	2.86

Axial Force in Links ($e/e_s=0.75$)



	IPE200	IPE300	IPE400	IPE500	IPE600
M	0.95	0.96	0.89	0.90	0.69
$K_{ax,assembly}/K_{ax,link}$	0.74	0.60	1.73	1.89	2.94

Axial Force in Links ($e/e_s=1.0$)

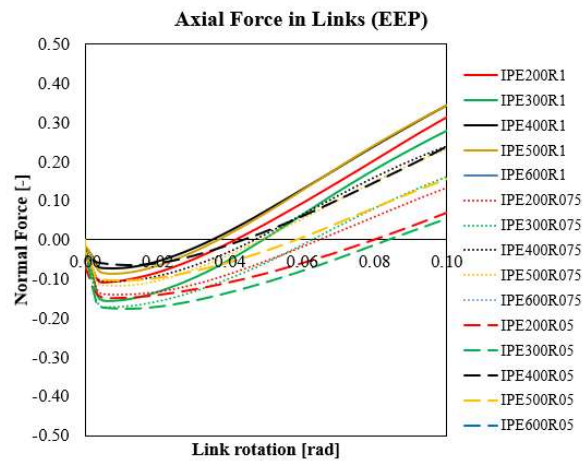
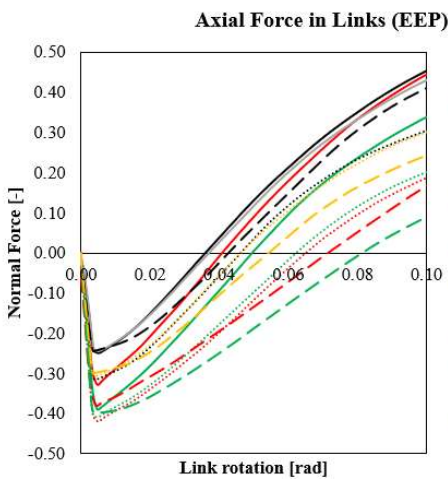
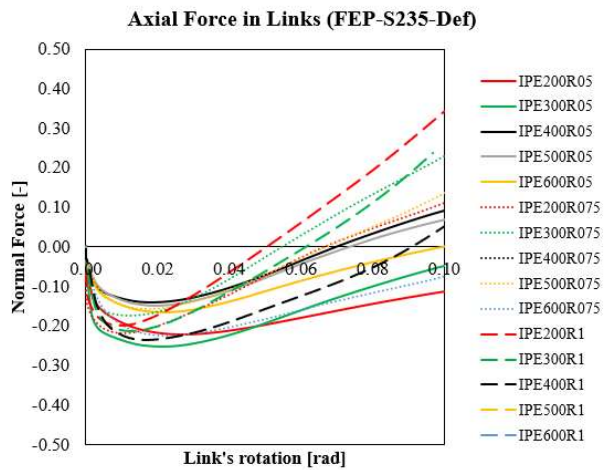
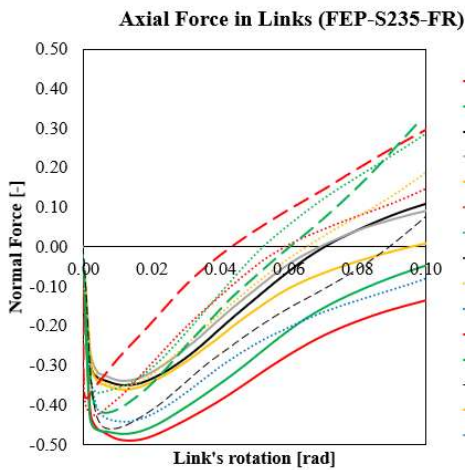
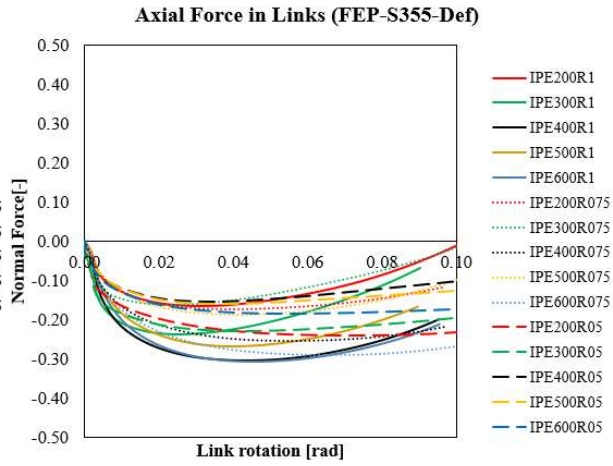
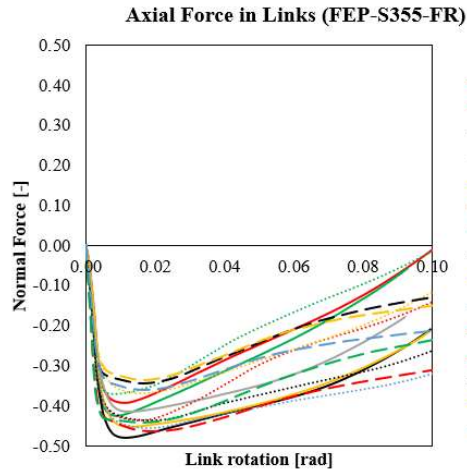


	IPE200	IPE300	IPE400	IPE500	IPE600
M	0.82	0.99	0.87	0.93	0.93
$K_{ax,assembly}/K_{ax,link}$	1.62	1.37	2.58	2.67	2.65

Comparison of axial force in FEP-S355, FEP-S235 and EEP assemblies

Fully rigid BC

Deformable BC



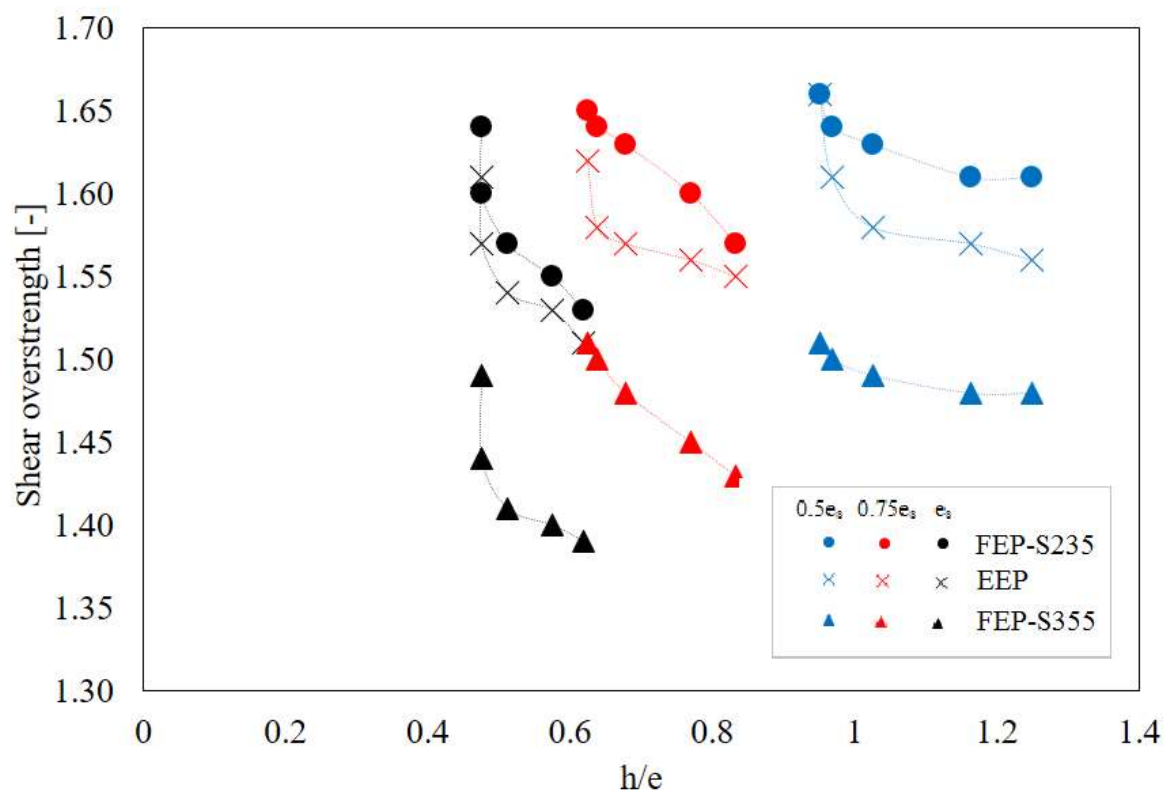


Figure 69. Comparison of shear overstrength for FEP-S355, FEP-S235 and EEP assemblies

The superimposed graphs above demonstrate the evolution of axial force in FEP (with S235 and S355 steel grade for links) and EEP (S355) assemblies, considering both boundary conditions. All FEP-S355 assemblies are still in compression at 0.08 rad of link rotation. Furthermore, the maximum axial force is compression for all analyses performed and with any of the two boundary conditions imposed. Replacing the steel grade of the links with S235, the axial response shows that there are still high compressive forces, but the behavior of the compressive arch changes. The inelastic segment of the compressive arch is now steeper, resulting to the links reaching tension at an earlier stage than FEP-S355. Since the end plates are stronger than the link, no plastic deformation occurs in the end plates and they are not contributing to development of catenary forces. Lastly, the third group of plots show that most EEP assemblies reached tension until 0.08 rad.

It can also be noticed that there is a significant difference in the shear overstrength between FEP and EEP assemblies. Using it to interpret the development of axial forces, an increase in shear overstrength causes a reduction in the compression arch of the links, as demonstrated by EEP assemblies with lower compression and reaching tension at a smaller link rotation. This observation is consistent for both boundary conditions.

CHAPTER VI. FINAL CONCLUSIONS

From the results of analytical and numerical investigations performed in links with FEP and EEP assemblies, the following main conclusions are drawn:

Shear overstrength

- The values of shear overstrength at 0.08 rad are consistently close to 1.5. From literatures, analyses of links alone show that shear overstrength for short links may go beyond 2.0 This shows that considering the connection in the analysis of link could provide a more accurate estimate for the design of elastic members.
- Shear overstrength decreases as profile depth increases. For the same profile, the values are higher for shortest links ($0.5e_s$) and decreases along with the increase of length.
- More compact profiles (HEA and HEB) have higher shear overstrength than narrow flange profiles (IPE)
- A lower shear overstrength corresponds to an increase in compressive arch.

There are several parameters affecting the level of axial force in links.

- Shortest links develop high catenary forces, resulting to large compressive arch and the link staying in compression for larger rotations
- Weaker connections (those designed close to resistance) corresponds to a large compressive arch
- The stiffness of the connection also influences the level of catenary action in the links. Higher stiffness causes an increase in the compressive arch.
- Consequently, the mentioned parameters that cause an increase in the compressive arch also corresponds to lower level tensile force due to catenary forces.
- The imposed boundary conditions that represent the stiffness of the frame has significant effect on the level of axial forces. Higher axial forces develop when the deformability of the frame is not considered (fully rigid BC), while these are lower when deformable springs corresponding to the stiffness of the frame are imposed. This applies to both compressive and tensile forces.
- In terms of the two types of end plate configurations investigated, FEP connections have design limitations. Due to high design forces, they are not applicable for any length of HEB profiles, nor for $0.75e_s$ and e_s of HEA profiles. The link-connection

assemblies remain in compression until or beyond 0.08 rad of link rotation, and the compressive arch is significantly greater compared to EEP. On the other hand, EEP connections have a wider range of application due to larger level arm. The compressive arch is considerably smaller and most of the assemblies analyzed are subjected to tension.

- Tensile forces induce significant reduction of bending resistance. For the same magnitude of axial force, one in tension and the other in compression, the corresponding bending resistance under the presence of a tensile force is lower than the bending resistance for a compressive force.

REFERENCES

- [1] Azad, S. & Topkaya, C., 2017. A review of research on steel eccentrically braced frames. *Journal of Constructional Steel Research*.
- [2] Bosco, M., Marino, E. & Rossi, P., 2014. Proposal of modifications to the design provisions of Eurocode 8 for buildings with split K eccentric braces. *Engineering Structures*, Volume 61, pp. 209-223.
- [3] CEN EN 1993 – 1 – 8, 2005. Eurocode 3: Design of Steel Structures: Part 1 – 8: Design of joints.
- [4] Cerfontaine, F., 2003. *Study of the interaction between bending moment and axial force in bolted joints*. PhD presented at Liege University, s.n.
- [5] Ciutina, A., 2015. Sustainable design of seismic resistant steel and composite building structures, *Habilitation Thesis*. Politehnica University of Timisoara, Romania.
- [6] Clifton, C., Bruneau, M., MacRae, G. L. R. & Fussell, A., 2011. Steel structures damage from the Christchurch earthquake series of 2010 and 2011. *Bulletin of the New Zealand Society for Earthquake Engineering*, 44(4), pp. 297-318.
- [7] Coelho, A. & Bijlaard, F., 2007. Experimental behavior of high strength steel end-plate connections. *Journal of Constructional Steel Research*, Volume 63, pp. 1228-1240.
- [8] da Silva, L. & Coelho, A., 2001. An analytical evaluation of the response of steel joints under bending and axial force. *Computers and Structures*, 79(8), pp. 873-881.
- [9] da Silva, L., de Lima, L. & da S. Vellasco, P., 2004. Behavior of flush end-plate beam-to-column joints under bending and axial force. *Steel and Composite Structures*, 4(2), pp. 77-97.
- [10] D’Aniello, M., 2017. Design for seismic and climate change, *Lecture presented for SUSCOS_M 16/18*, Timisoara, Romania.
- [11] D’Aniello, M., Cassiano, D. & Landolfo, R., 2016. Monotonic and cyclic inelastic tensile response of European preloadable gr10.9 bolt assemblies. *Journal of Constructional Steel Research*, Volume 124, pp. 77-90.
- [12] Del Savio, L. et al., 2009. Generalized component-based model for beam-to-column connections including axial versus moment interaction. *Journal of Constructional Steel Research*, 65(8), pp. 1876-1895.
- [13] Della Corte, G., D’Aniello, M. & Landolfo, R., 2013. Analytical and numerical study of plastic overstrength of shear links. *Journal of Constructional Steel Research*, Volume 82, pp. 19-32.
- [14] Dubina, R., Stratan, A. & Dinu, F., 2008. Dual high-strength steel eccentrically braced frames with removable links. *Earthquake Engineering and Structural Dynamics*, Volume 37, pp. 1703-1720.
- [15] Dusicka, P., Itani, A. & Buckle, I., 2010. Cyclic behavior of shear links of various grades of plate steel. *Journal of Structural Engineering*, 136(4).
- [16] Han, X., 2008. *Eccentrically braced frame design for moderate seismic regions*. Beijing, China, 14th World Conference on Earthquake Engineering.

- [17] Hjelmstad, K. & Popov, E., 1983. Cyclic behavior and design of link beams. *Journal on Structural Engineering*, 109(10), pp. 2387-2403.
- [18] Ioan, A., Stratan, A. & Dubina, D., 2013. Numerical simulation of bolted links removal in eccentrically braced frames. *Pollack Periodica*.
- [19] Ioan, A. et al., 2016. Experiment validation of re-centring capability of eccentrically braced frames with removable links. *Engineering Structures*, Volume 113, pp. 335-346.
- [20] Jaspart, J. & Cerfontaine, F., 2002. *Analytical study of the interaction between bending and axial force in bolted joints*. Proceedings of the Third European Conference on Steel Structures, (EUROSTEEL).
- [21] Ji, X., Wang, Y., Ma, Q. & Okazaki, T., 2016. Cyclic behavior of very short steel shear links. *Journal on Structural Engineering*, 142(2).
- [22] Kasai, K. & Popov, E., 1986. General behavior of WF steel shear link beams. *Journal on Structural Engineering*, 112(2), pp. 362-382.
- [23] Khademi, Y. & Rezaie, M., 2017. Comparison study of CBFs and EBFs bracing in steel structures with nonlinear time history analysis. *Civil Engineering Journal*, 3(11), pp. 1157-1165.
- [24] Malley, J. & Popov, E., 1984. Shear links in eccentrically braced frames. *Journal of Structural Engineering*, 110(9), pp. 2275-2295.
- [25] Mansour, N., Shen, Y., Christopoulos, C. & Tremblay, R., 2008. *Experimental evaluation of nonlinear replaceable links in eccentrically braced frames and moment resisting frames*. Beijing, 14th World Conference on Earthquake Engineering.
- [26] Mazzolani, F., della Corte, G. & D'Aniello, M., 2009. Experimental analysis of steel dissipative bracing systems for seismic upgrading. *Journal of Civil Engineering and Management*, 15(1), pp. 7-19.
- [27] McDaniel, C., Uang, C. & Seible, F., 2003. Cyclic testing of built-up steel shear links for the new bay bridge. *Journal of Structural Engineering*, 129(6), pp. 801-809.
- [28] National Oceanic and Atmospheric Administration, 2014. *The Significant Earthquake Database*. [Online]
Available at: <https://www.ngdc.noaa.gov/nndc/struts/form?t=101650&s=1&d=1>
[Accessed 22 January 2018].
- [29] Popov, E., Kasai, K. & Engelhardt, M., 1987. Advances in design of eccentrically braced frames. *Bulletin of the New Zealand National Society for Earthquake Engineering*, 20(1).
- [30] Popov, E., Ricles, J. & Kasai, K., 1992. *Methodology for optimum EBF link design*. Balkema, Rotterdam, Earthquake Engineering Tenth World Conference.
- [31] Roeder, C. & Popov, E., 1978. Eccentrically Braced Steel Frames for Earthquakes. *J. Structural Division, ASCE*, 104(ST3).
- [32] Stratan, A. & Dubina, D., 2004. Bolted links for eccentrically braced steel frames. *Connections in Steel Structures*, Volume V, pp. 223-332.
- [33] Sumner, E. & Murray, T., 2003. *Experimental investigation of the MRE 1/2 end-plate moment connections*, Virginia, Canada: Virginia Polytechnic Institute and State University.

- [34] Tan, K. & Christopoulos, C., 2016. Development of replaceable cast steel links for eccentrically braced frames. *Journal of Structural Engineering*.
- [35] Vataman, A., Ciutina, A. & Grecea, D., 2016. Numerical analysis of short link steel in eccentrically-brad frames under seismic actions. *Pollack Periodica*, 11(2), pp. 29-42.
- [36] Weynand, K. & Jaspart, J., 2014. *Design of Steel Buildings with worked examples*, Brussels, Belgium: European Convention of Constructional Steelwork.
- [37] Yu, H., Burgess, I., Davison, J. & Plank, R., 2011. Experimental and numerical investigations of the behavior of flush end plate connections at elevated temperatures. *Journal of Structural Engineering*, Volume 137, pp. 80-87.
- [38] Zimbru, L. et al., 2017. *Finite Element Modelling of Detachable Short Link*. Rhodes Island, Greece, 16th ECCOMAS Thematic Conference on Computational Methods in Structural Dynamics and Earthquake Engineering.
- [39] Babu, S. & Sreekumar, S, 2012. A study on the ductility of bolted beam-column connections." *International Journal of Modern Engineering Research*, 2(5), pp. 3517-3521
- [40] BCSA, 2013. *Moment-resisting joints to Eurocode 3*. P398 ed. London: British Constructional Steelwork Association Limited.